MAGNETIC MOMENTS OF VIBRATIONAL STATES IN PLATINUM NUCLEI

by

AUDREY B. BUYRN

S.B., Massachusetts Institute of Technology

(1958)

SUBMITTED IN PARTIAL FULFILLMENT

OF THE REQUIREMENTS FOR THE

DEGREE OF DOCTOR OF

PHILOSOPHY

at the

MASSACHUSETTS INSTITUTE OF TECHNOLOGY

July, 1966

Signature of Author. . . . . .
Department of Physics, July 1966

Certified by. . . . . .
Thesis Supervisor

Accepted by. . . . . .
Chairman, Departmental Committee on
Graduate Students

Magnetic Moments of Vibrational States in Platinum Nuclei

by

Audrey Backman Buyrn

Submitted to the Department of Physics on July 5, 1966 in partial fulfillment of the requirements for the degree of Doctor of Philosophy at the Massachusetts Institute of Technology.

ABSTRACT

The technique of recoilless resonant absorption (the Mossbauer effect) was used to measure the g-factor of the $3/2^-$, 99 KeV state of Pt-195. The source was single line Au-195 in Cu. The absorber was ferromagnetic Pt-Fe alloy (3 at % Pt). The sign of $g(3/2^-)$ was established as negative by polarizing the absorber parallel to the direction of propagation of the gamma rays (perpendicular to the absorber disc plane). $g(3/2^-) = -(0.40 \pm 0.10)$. H_{int} (Pt) = $(1.26 \pm 0.10) \times 10^6$ gauss. Experiments on alloys with higher platinum concentrations established H_{int} (Pt) as very weakly dependent on platinum concentration.

The g-factors of the first 2^+ states of Pt-192, Pt-194, and Pt-196 and the g-factor of the second 2^+ state of Pt-194 were determined from the measurement of the Larmor precession of $\gamma - \gamma$ angular correlations through the 2^+ states. For the Pt-192 and Pt-194 cases, sources of Ir-192 and Ir-194 in Ir-Fe alloy wire (3 at % Ir) were used. It was assumed that the magnetic field at the Pt nucleus in 3 at % Ir Ir-Fe alloy was the same as the field at the Pt nucleus in 3 at % Pt Pt-Fe alloy. The Mossbauer experiments were performed at $\sim 4.2^\circ$ K and the angular correlation experiments done at $\sim 300^\circ$ K. A Curie temperature equal to that of pure iron (769° K) was assumed for the Ir-Fe alloy. A small electromagnet provided an aligning field of about a thousand gauss. For the Pt-196 measurement, a source of carrier free Au-196,-195 diffused into iron wire was used. We found H_{int} (Pt) in this source by using it as a Au-195 in Fe Mossbauer source; the internal field was anomalously low, $(0.85 \pm 0.12) \times 10^6$ gauss. The reasons for this low field most probably can be traced to source preparation.

Pt-192, -194, -196 RESULTS

2^+ Level	Correlation	Experimental Correlation Coefficients	g
Pt-192 316 KeV	4-2-0 (468-316) KeV	$A_2 = 0.096 \pm 0.002$ $A_4 = 0.007 \pm 0.003$	0.31 ± 0.04
Pt-194 328 KeV	0-2-0 (939-328) KeV (1151-328)KeV	$A_2 = 0.23 \pm 0.02$ $A_4 = 0.82 \pm 0.02$ $A_2 = 0.12 \pm 0.02$ $A_4 = 0.66 \pm 0.02$	0.32 ± 0.05
Pt-194 622 KeV	0-2-0 (645-622) KeV	$A_2 = 0.22 \pm 0.02$ $A_4 = 0.88 \pm 0.03$	0.18 ± 0.05
Pt-196 356 KeV	2-2-0 (333-356 KeV)	$A_2 = 0.077 \pm 0.002$ $A_4 = 0.318 \pm 0.003$	0.23 ± 0.05

Spehl et al (SKR-65) has measured g(2^+ of Pt-194) as positive; we established g(2^+)H_{int}(Pt) as negative; therefore H_{int}(Pt) is negative.

Our magnetic moment results indicate that core-particle coupling schemes in simplified form do not predict the correct magnetic moments for the first excited 2^+ states of Pt-194 or Pt-196. Further the only theoretical prediction of the values of the g-factors of the first 2+ plus states is considerably higher than our experimental values. The large difference between the g-factors of the first and second excited 2^+ states of Pt-194 is evidence that the structures of the two states are significantly different.

Mossbauer experiments with the 99 KeV line of Pt-195 using various sources and absorbers gave the following Debye temperatures: θ_D(Pt in Pt):$(238 \pm 20)^oK$. θ_D(Pt in Cu):$(220 \pm 20)^oK$. θ_D(Pt in Be):$(220 \pm 30)^oK$. θ_D(Pt in Ir):$(315 \pm 35)^oK$. θ_D(Pt in Fe):$\sim 275^oK$.

The Mossbauer effect of the $5/2^-$, 129 KeV level of Pt-195 was also looked for; no unambiguous effect was observed. However the expected effect was of the order of our experimental uncertainty.

Thesis Supervisor: Lee Grodzins

Title : Professor of Physics

TABLE OF CONTENTS

TABLE OF CONTENTS

LIST OF TABLES

ACKNOWLEDGMENT

I would like to thank Professor Lee Grodzins, my supervisor, for his advice and encouragement and patience. Professor John Wulff, of the Metallurgy Department, provided invaluable assistance by making the Fe-Pt alloy Mossbauer absorbers and the Fe-Ir alloy wire for the angular correlation sources. I also wish to thank Professor Robert Ogilvie for carrying out the electron beam analysis of the alloys. I am grateful to Mrs. C. E. Buyrn and Miss Helen Engstrand who typed most of this thesis. Finally, I must acknowledge Dr. E. Alan Phillips; the net result of his many contributions is impossible to assess.

I. INTRODUCTION

A combination of Mossbauer effect and angular correlation experiments was used to measure magnetic moments of first and second excited states of several platinum isotopes.

A measurement of the magnetic moment of an excited state is basically a measurement of the hyperfine energy splitting in the presence of a magnetic field. The energy of a magnetic dipole, u , in a magnetic field, H , is:

$$E = -u \cdot H = -g u_N m H \quad \text{where } g = \frac{u}{I}$$

and

$$\Delta E = g u_N H$$

is the quantity measured.

With the Mossbauer effect, which measures the precise energy of a transition, the hyperfine splitting of the ground and the excited level is directly seen: the separation of two lines in the Mossbauer spectrum is

$$\Delta = u_N H \left(a g_O + b g_{ex} \right)$$

where a and b are easily derived numbers depending on the spins of the excited and ground levels, the multipolarity of the transition, and the specific lines considered.

In an angular correlation measurement, the angular distribution of a cascade is observed, and only the intermediate state enters into the result.

The quantity measured is

$$\Delta E = g_{ex} u_N H = \hbar w_L$$

where w_L is the Larmor frequency.

In order to measure w_L directly, it is necessary to have a time resolution τ_o between the cascading γ-rays which is short compared to $1/w_L$. $\tau_o \approx 10^{-9}$ seconds is the effective limit of present electronic time resolution. Therefore for very short lived states, $\tau << 1/w_L$ and $\tau << \tau_o$, it is not possible to observe the full Larmor frequency, but we must be content with observing a small angular precession

$$\Delta\theta = w_L \tau = \frac{g_{ex} u_N H}{h} \tau$$

In order to measure g_{ex} the magnetic field, H, at the nucleus must be known. When H is applied externally, by a magnet, the determination of the magnetic field is simplified: often, to first order, the magnetic field at the nucleus is the magnetic field applied by the magnet. However the largest magnets produce only 80,000 to 150,000 gauss, and they are difficult to work with. More usual are magnets of 15,000 to 45,000 gauss. Although many magnetic moments can be measured with such fields, very small g-factors or very short lived states require stronger fields.

The magnetic field at a nucleus dissolved in iron may be as high as 1,500,000 gauss: 100,000 gauss is a relatively modest internal field. (SW-65). However the measurement of an internal field can be difficult.

Angular correlation is incapable of simultaneously measuring g_{ex} and H ; one always measures their product. On the other hand, the Mossbauer effect can simultaneously measure g_{ex} and H provided the ground state magnetic moment is known and the lines are at least partially resolved. Thus the determination of an internal field by the Mossbauer effect may make possible the measurement of certain g_{ex} by angular correlation.

Each method has its limitations. For the Mossbauer effect they are:

(1) The transition must be to the ground state of a stable or very long lived nucleus ($t_{1/2} \gtrsim 10^6$ years).

(2) The transition must be low in energy: $E \lesssim 150$ KeV.

(3) $g_{ex}H$ must be greater than about 0.25 the observable line width Γ .

Since $\frac{\Gamma\, t_{1/2}}{0.692} = 2\pi$, this puts a limit of about 700×10^{-12} seconds on the half life of the level, if g_{ex} = 1.0 nm and H = 100,000 gauss.

For angular correlation, the condition corresponding to (3) is:

$w\tau$ must be greater than about

(a) .06 for a 4-2-0 correlation

(b) .004 for a 0-2-0 correlation

to measure $\Delta\theta$. This means the half life of the level must be greater than about (a) 84×10^{-12} seconds or (b) 6×10^{-12} seconds, if g_{ex} = 1.0 nm and H = 100,000 gauss.

The states in the even-even platinum isotopes are short-lived and require the integral technique using internal fields. The measurement of H_{int} is done with the 99KeV line of Pt^{195} using the Mossbauer effect.

The integral correlation method measures one parameter, $\Delta\theta$, and the interpretation of the results requires an understanding or a separate measurement of extraneous pertubations. A discussion of the problems that may arise follows:

(1) Non - Equivalent Sites

When impurity atoms are diffused into a host, there is a chance that not all of the atoms will go into equivalent sites. This may cause a spectrum of magnetic fields and electron densities to interact with the impurity nuclei. Both effects will increase the width of the Mossbauer lines making measurement of splittings less accurate. Moreover, if the resolution is poor to begin with, the accurate interpretation of the Mossbauer spectrum requires an accurate knowledge of the line width. Non-unique fields show up in time dependent angular correlation by attenuating the angular precession. The electron density at the nucleus does not affect angular correlation results.

(2) Quadrupole Fields

An electric field gradient may exist at an impurity site, even when the host is cubic. The impurity atom distorts the lattice, and even if it sits at a lattice position its environment may not be cubic. However the electric field gradient is usually very small, particularly if the impurity concentration is low. The quadrupole interaction splits a level into sublevels of $|m|$, which causes a magnetic Mossbauer pattern to become asymmetric. The lines are also broadened. In angular correlation the angular precession is attenuated.

(3) Non-Equivalent Sources

There is the danger that the internal field may not be the same in the Mossbauer and angular correlation samples. H_{INT} may vary with impurity concentration, heat treatment, magnetic and cold-working history, and ambient temperature.

(4) Excited Electronic States

The processes that lead to the excited state, particularly K-capture and internal conversion, disrupt the electron shell and thus affect the magnetic field, electric field gradient, and electron density at the nucleus. Integral correlation has shown that, in a metal, the electron shell returns to normal in about 10^{-12} seconds. (S-65). Therefore, for half lives $\lesssim 10^{-11}$ seconds these effects must be considered.

All of these effects were measurable in a study carried out by M. Deutsch, A. Buyrn, and L. Grodzins of the magnetic moments of excited states of Sn^{118}, Sn^{119}, and Sn^{120}. The 24.4 KeV Mossbauer level of Sn^{119} was used to determine the field at tin in iron, and the moments of the 5^- states of Sn^{118} and Sn^{120} were measured by angular correlation in the same internal field. The paper is reproduced on the following four pages.

In the present work on the platinum isotopes, these effects could not be accurately measured. It is argued in the thesis that they were small.

The energy levels of interest in the isotopes investigated are shown in the following figure.

In the present work, the magnetic field at the platinum nucleus in a Pt-Fe alloy absorber (3 at % Pt) was measured by analysis of the Mossbauer hyperfine spectrum of the 99 KeV line of Pt^{195}. Then Ir-Fe alloy (3 at % Ir) was irradiated with neutrons to make $Ir^{192,194}$ which decays to $Pt^{192,194}$. If it is assumed that the magnetic field at $Pt^{192,194}$ nuclei in an Ir-Fe alloy source is the same as that at Pt^{195} nuclei in a Pt-Fe alloy absorber (1,260,000 gauss), angular correlation can measure the g-factors of the following levels:

Pt^{192}	2^+	316 KeV	$t_{1/2}$ = 35 p sec
Pt^{194}	2^+	328 KeV	$t_{1/2}$ = 35 p sec
Pt^{194}	2^+	622 KeV	$t_{1/2}$ = 57 p sec

In addition, it was possible to measure the g-factor of the level:

Pt^{196}	2^+	356 KeV	$t_{1/2}$ = 30 p sec

with a source of $Au^{195,196}$ diffused into iron. The magnetic field at the platinum nucleus in this source was directly measured by the Pt^{195} Mossbauer effect.

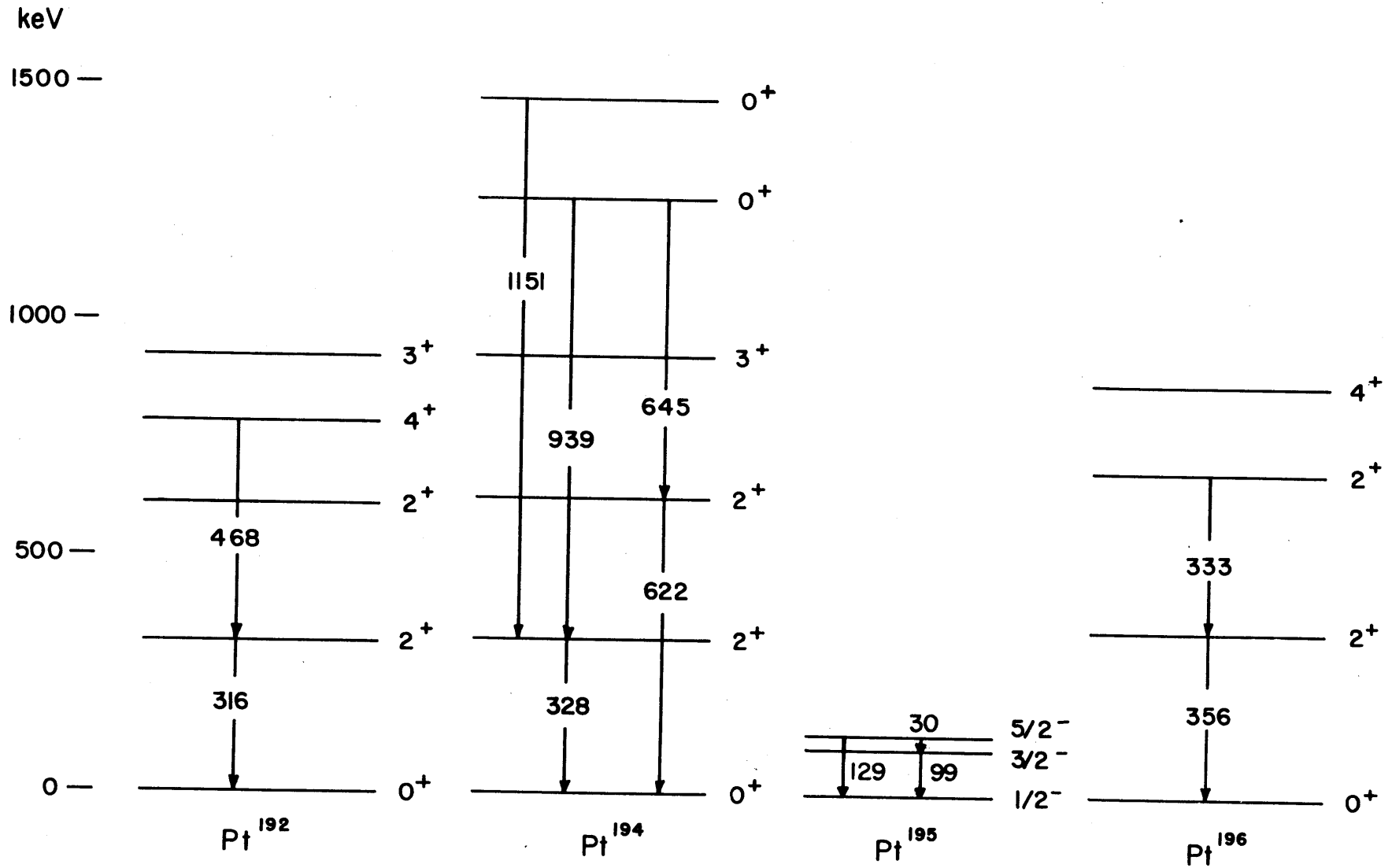
keV
1500
1000
500
0
3+
4+
2+
2+
0+
468
316
0+
0+
3+
2+
2+
0+
1151
939
328
645
622
Pt 192
Pt 194
30
129
99
5/2-
3/2-
1/2-
Pt 195
4+
2+
2+
0+
333
356
Pt 196

Figure 3

Magnetic Moments of 5^- States in Sn^{118} and Sn^{120}

M. Deutsch, A. Buyrn and L. Grodzins

Laboratory for Nuclear Science,

Massachusetts Institute of Technology,

Cambridge, Massachusetts, USA

The magnetic moments of the 5^- states in Sn^{118} and Sn^{120}, at 2.32 and 2.30 MeV respectively, have been determined by precessing gamma ray-gamma ray angular correlations in an external as well as an internal magnetic field. The pertinent parts of the decay scheme are shown in fig 1. In the first experiment aqueous solution sources were used. The techniques and equipment have been described previously. The angular correlations were first shown to be unperturbed over three mean lives by measuring the anisotropy as a function of delay time. The precession of the correlation as a function of time in an external field of 28 kOe was then determined. The g- factors of the 5^- states were found to be

$$g = -0.06 \pm 0.01$$

in both cases. The low value of $g \cdot H$ made more precise measurements difficult.

In the second experiment, carrier free sources of Sb^{118} from $In(\alpha,n)$ and $Sb^{119,120}$ from Sn(d,n) and Sn(d,2n) were diffused into 6 mil thick pure iron foils. The internal field at the tin nuclei was determined by measuring the Mössbauer hyperfine spectrum of the 24.4 KeV transition in Sn^{119} fed from Sb^{119}. One such spectrum is shown in fig. 2a. The internal field, determined from the splitting and the measured value of the ground state magnetic moment, is 78.5 ± 3.0 kOe. This value, which agrees with that determined from the isomeric Sn^{119} diffused in iron, may

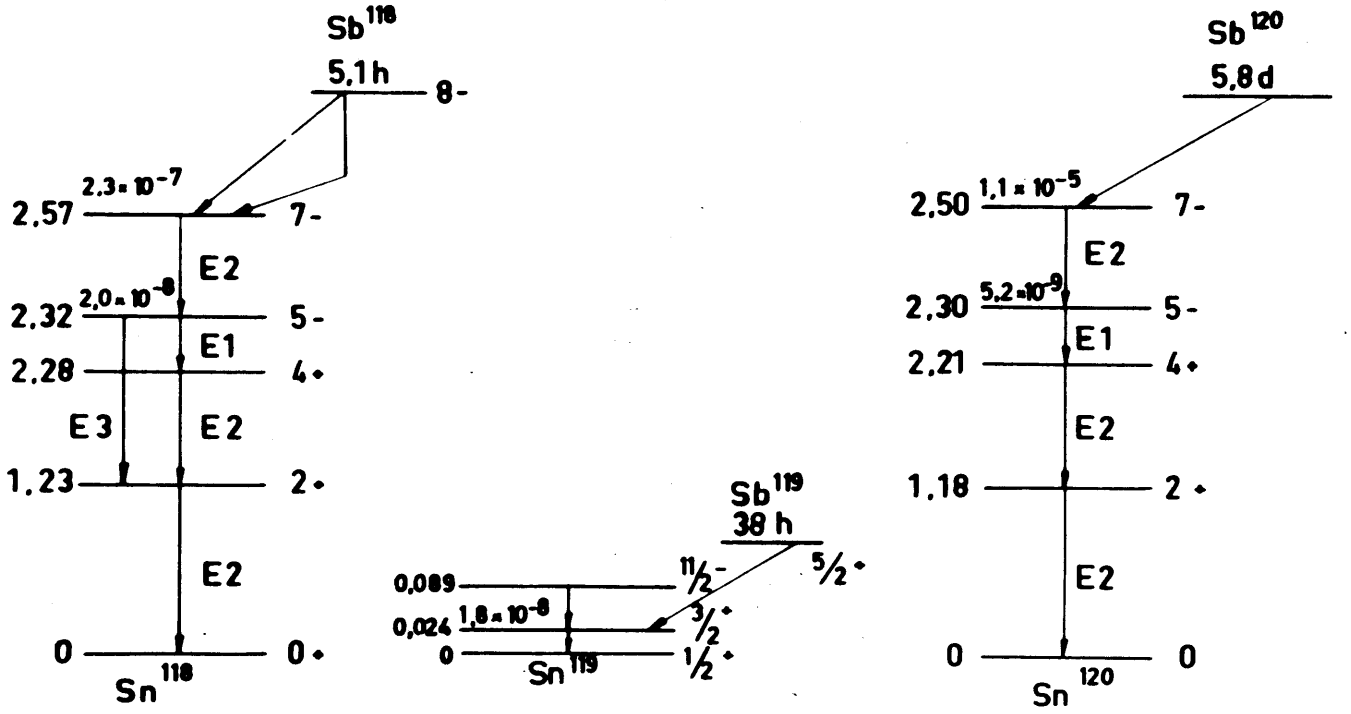

Fig. 1. Decay schemes of Sb^{118}, Sb^{119} and Sb^{120} from Bolotin. Phys. Rev. 124 (1961) 213 and Nuclear Data Sheets. Energies are in MeV.

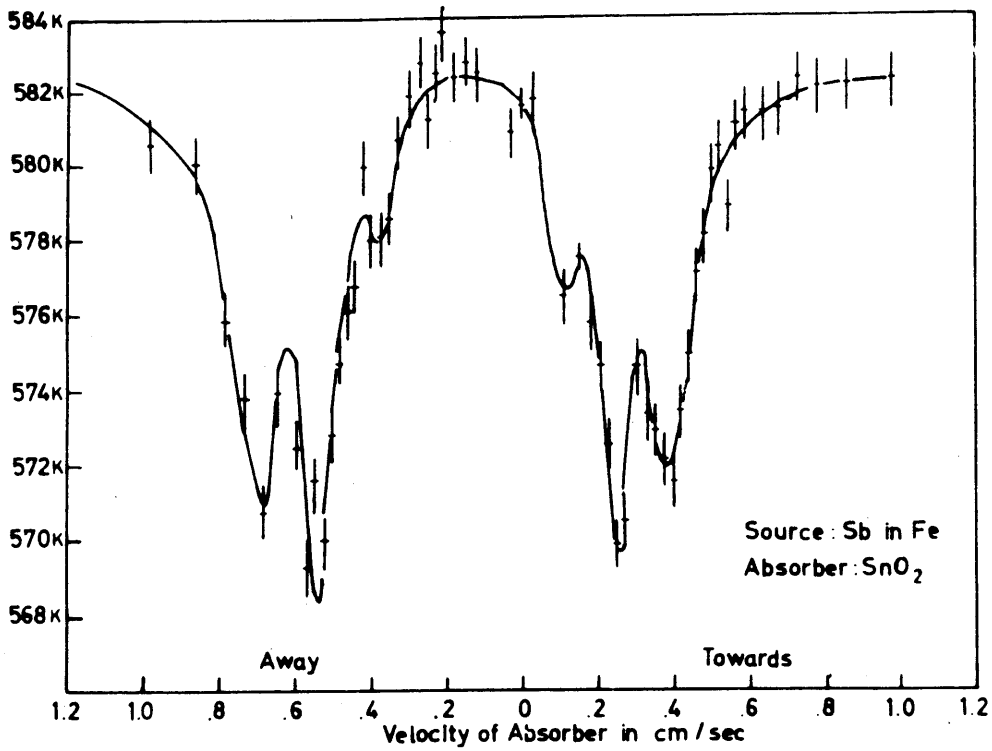

Fig. 2a. Mössbauer hyperfine splitting pattern. The source polarized perpendicular to the photon momentum.

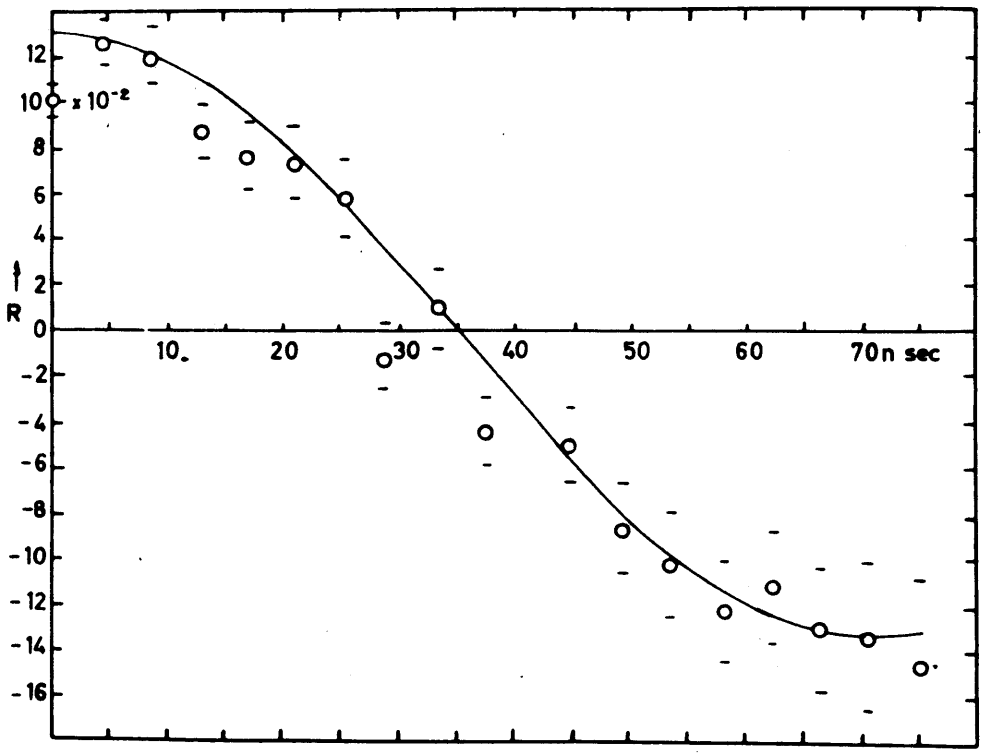

Fig. 2b. Typical curve of $R = 2\,\dfrac{W(\pi) - W(\frac{1}{2}\pi)}{W(\pi) + W(\frac{1}{2}\pi)}$ versus delay time for Sb^{118m} in iron.

be compared with the value of 190 kOe found by Pipkin* for the internal field at the Sb nucleus when Sb is dissused in iron. The electronic states of tin in iron must reach equilibrium after internal conversion and K-capture in a time less than 10^{-8} sec.

The source of $Sb^{119-120}$ diffused in Fe was placed across the poles of an Alnico "C" magnet so that the magnetic field was perpendicular to the angular correlation plane. The correlation was determined as a function of time; one such result is shown in fig. 2b. The g-factors for the 5^- states were determined to be

$$2.34 \text{ MeV}, 5^- \text{ state in } Sn^{118} \qquad g = -0.060 \pm 0.005,$$
$$2.30 \text{ MeV}, 5^- \text{ state in } Sn^{120} \qquad g = -0.056 \pm 0.005.$$

These values agree surprisingly well with that predicted using the shell model assignments of $|h_{\frac{11}{2}}\, s_{\frac{1}{2}}|\, 5^-\rangle$ for the two neutrons.

Finally, the lack of attenuation of the angular precession indicates that no major perturbation on the correlation due to internal quadrupole fields or non-unique magnetic fields are present at the tin nucleus in iron. The widths of the Mossbauer Hyperfine lines (1.5 times greater than theoretical) must be due to isomer shifts.

---

* (PSW-63). More recently, B. N. Samoilov et al have reported H_{int} (Sb in Fe) as 250 kOe. (Post deadline paper given at Ninth International Conference on Low Temperature Physics, Columbus, Ohio, September 1964.)

II. Pt^{195}

A. Background: The Mossbauer Effect

In 1961 Rudolph Mossbauer was awarded the Nobel Prize in physics for his discovery that, if a nucleus is bound in a crystal, nuclear gamma ray emission may take place with the entire crystal absorbing the recoil momentum. Thus no phonons are excited in the crystal. The probability for this Mossbauer effect, or recoilless gamma ray emission, is given by the factor

$$f = \exp\left[- \frac{3E_\gamma^{\,2}}{4Mc^2 k \theta_D} \left(1 + \frac{4T^2}{\theta_D^{\,2}} \cdot \int_0^{\theta_D/T} \frac{x\,dx}{e^x - 1} \right) \right]$$

where θ_D, to first approximation is the Debye temperature of the crystal. E_γ is the energy of the gamma ray, M the mass of the nucleus, and T the temperature. For such emission the mean energy of the gamma ray is exactly the energy of the nuclear transition; its shape is Lorentzian ($\frac{1}{1 + \alpha x^2}$), and its line width is determined by the lifetime of the nuclear level. Nuclear resonant absorption and scattering, without recoil, also take place, with the same line shape and width. The literature on the Mossbauer effect is extensive and detailed; several comprehensive references are listed in a special section in the Bibliography. The following pages are intended to be only a brief survey of the topics important in this work.

The f-factor is strongly dependent on temperature, and is appreciable ($\gtrsim$ 1%) at room temperature only for very low energy transitions such as the 14 KeV line of Fe^{57} and the 24 KeV line of Sn^{119}. However at $4^\circ K$, the Mossbauer effect can be observed for gamma rays as high as 150 KeV in energy. In practice, the Mossbauer effect is observed by resonantly absorbing or scattering the recoilless gamma rays. This requires that source and absorber

be the same isotopic species and that the transition terminate on the ground state of a stable or very long lived nucleus ($\gtrsim 10^6$ years). By moving the source relative to the absorber - applying a Doppler shift - the emission line may be shifted off resonance. The observed curve of absorption versus velocity has a Lorentzian shape, but its width is twice that of the emission or absorption line.

The cross-section for resonant absorption is

$$\sigma_{abs}(E) = \sigma_o \frac{\Gamma^2 F}{4(E_\gamma - E_r)^2 + \Gamma^2}$$

where

$$\sigma_o = \frac{2I_{ex} + 1}{2I_{gr} + 1} 2\pi\lambda^2,$$

λ is the wavelength of the gamma ray, Γ is the full width of the level, F is the fraction of deexcitations that go by way of the gamma ray, and E_r is the mean energy of the transition. From this, the Mossbauer "mean free path" may be written

$$1/\lambda_{Moss} = \pi\lambda^2 \frac{2I_{ex} + 1}{2I_{gr} + 1} \frac{B}{1 + \alpha} f \rho$$

where B is the branching ratio from the excited level, α is the internal conversion coefficient, ρ the isotopic density, and f the recoilless fraction. The maximum absorption as a function of thickness of absorber is plotted in Figure 4. The absorption is not purely exponential because both emission and absorption lines have a width: the wings of the emission line are absorbed less strongly than the center. This effect increases the width of the observed line, and for thick absorbers ($\gtrsim \lambda_{Moss}$), also distorts the shape.

Nuclear Environment

The energy of a nuclear level can be measurably affected by the environment of the nucleus. These effects may be separated into multipole

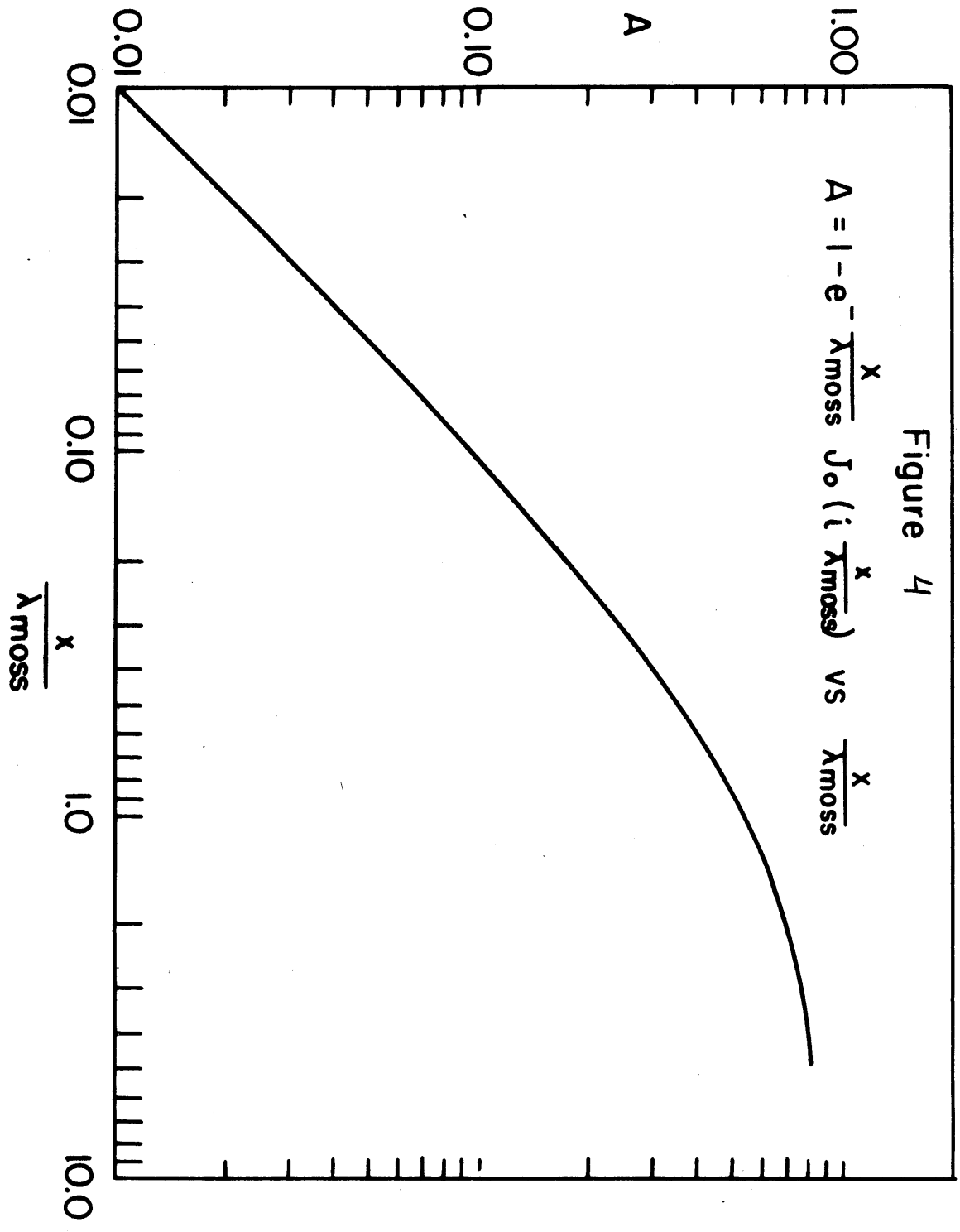

Figure 4

$A = 1 - e^{-\frac{x}{\lambda_{moss}}} J_0\left(i\frac{x}{\lambda_{moss}}\right)$ vs $\frac{x}{\lambda_{moss}}$

order, of which only electric monopole, magnetic dipole, and electric quadrupole are important. The effect of temperature and gravitational potential - relativistic effects - have also been observed.

1. The Electric Monopole Interaction: The Isomer Shift

If the charge radii of the ground and excited states of the nucleus differ, the energy of the transition will depend on the electron density at the nucleus. Therefore, if source and absorber are different compounds, or are imbedded in different hosts, the maximum of the absorption curve will be displaced from zero velocity. The expression for this isomer shift is

$$\delta = \frac{2\pi}{5} Z e^2 \left(R_{ex}^2 - R_{gr}^2 \right) \left(|\psi(o)|_a^2 - |\psi(o)|_s^2 \right)$$

where R_{ex} and R_{gr} are the charge radii of the excited and ground states, and $|\psi(o)|^2$ is the total electron density at the center of the nucleus in the source (s), and absorber (a).

2. Electric Quadrupole Interaction

The energy of interaction between a nuclear electric quadrupole moment Q, and an axially symmetric electric field gradient eq is

$$E = \frac{e^2 Qq}{4} \quad \frac{3m^2 - I(I+1)}{I(2I-1)}$$

where I is the spin of the nuclear level and m is its component along the axial direction. This interaction splits the nuclear level into sublevels depending on the absolute value of m, and hence splits the transition. For the case of an $I = 3/2$ to $I = 1/2$ transition, the first level is split into two, separated by

$$\Delta E = \frac{e^2 Qq}{2}$$

The second is unsplit; therefore the observed absorption curve is split in two. The electric field gradient is zero in cubic lattices.

3. Magnetic Dipole Interaction

The energy of interaction between a nuclear magnetic dipole moment, u, and a magnetic field H, is given by:

$$E = -u \cdot H = -gHmu_n$$

where g, the nuclear gyromagnetic ratio equals $^{u}/I$, and m is the component of I along H. The nuclear level is thus split into 2I + 1 sublevels. Figures 5 and 6 show the transitions between states of I = 3/2 and I = 1/2 in the presence of a magnetic field. Figure 7 is a schematic drawing of the absorption curve for the case of an unsplit absorber and a split source, or vice versa. However the 3:2:1:1:2:3 intensity ratio will hold for the case of a split absorber and unsplit source only if the thickness of the absorber for the most intense line is less than about $1/4\ \lambda_{Moss}$. The magnetic field may be supplied either by an external magnet or an internal ferromagnetic field.

Magnetic Splitting of an MI Transition Between $I = 3/2$ and $I = 1/2$

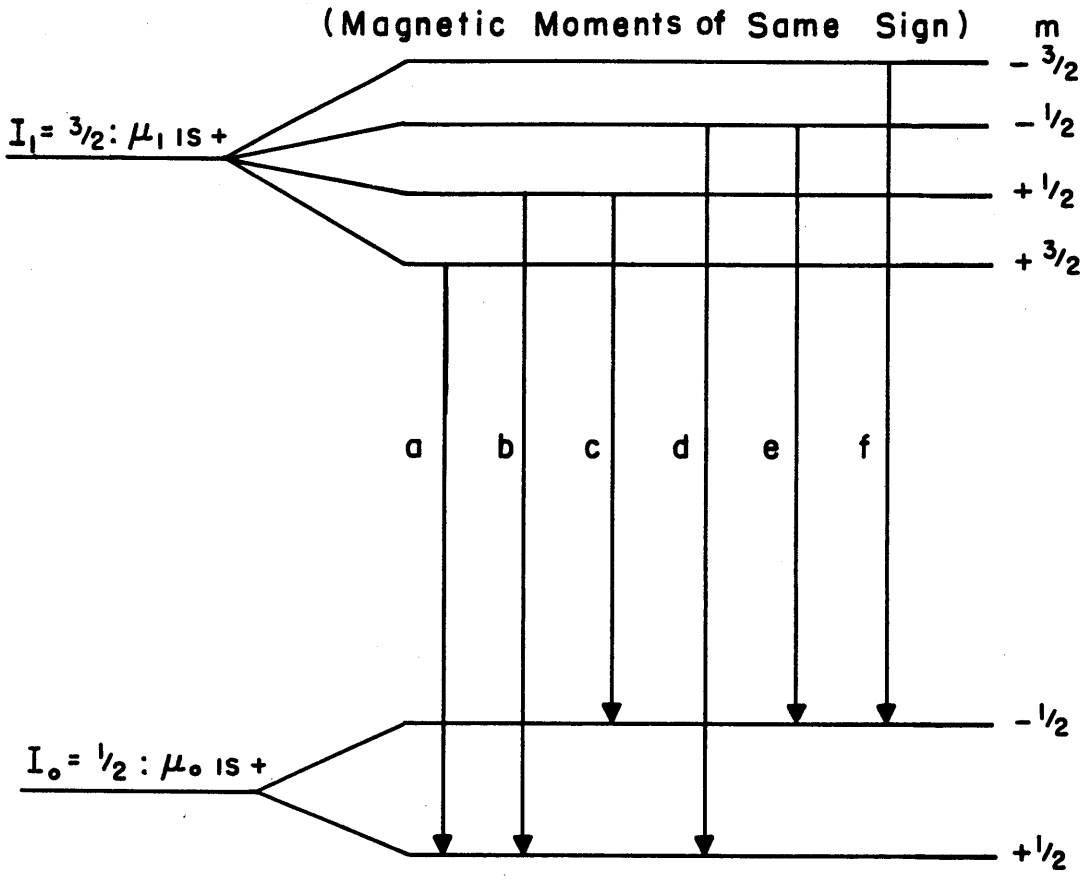

Line	Δm	Strength	Magnetic Energy
a	-1	3	$1/2(-3g_1 + g_o)H$
b	0	2	$1/2(-g_1 + g_o)H$
c	-1	1	$1/2(-g_1 - g_o)H$
d	+1	1	$1/2(+g_1 + g_o)H$
e	0	2	$1/2(+g_1 - g_o)H$
f	+1	3	$1/2(+3g_1 - g_o)H$

FIGURE 5

FIGURE 6

Magnetic Splitting of an M1 Transition
Between $I = 3/2$ and $I = 1/2$
(Magnetic Moments of Opposite Sign)

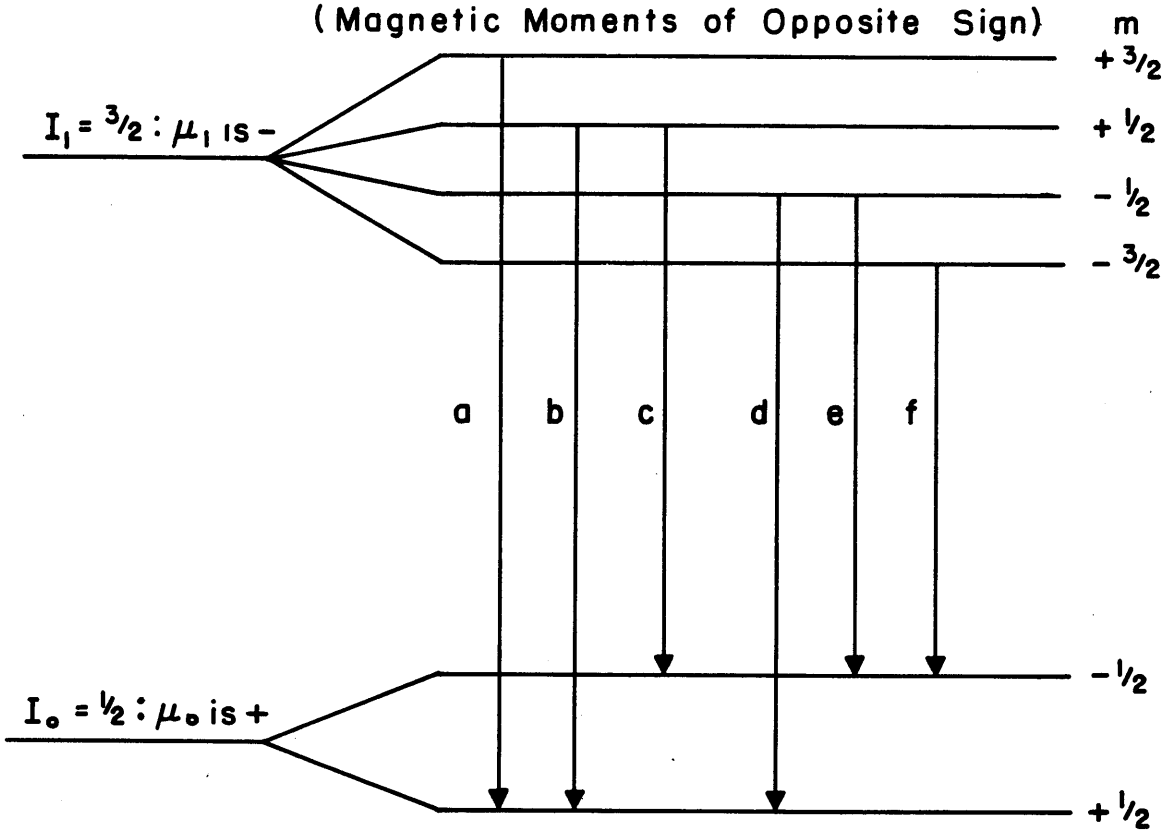

Line	Δm	Strength	Magnetic Energy⊗
a	-1	3	$\frac{1}{2}(3g_1 + g_o)H$
b	0	2	$\frac{1}{2}(g_1 + g_o)H$
c	-1	1	$\frac{1}{2}(g_1 - g_o)H$
d	1	1	$\frac{1}{2}(-g_1 + g_o)H$
e	0	2	$\frac{1}{2}(-g_1 - g_o)H$
f	1	3	$\frac{1}{2}(-3g_1 - g_o)H$

⊗ $g = \left|\frac{\mu}{I}\right|$

Figure 7

SCHEMATIC DRAWING OF MOSSBAUER ABSORPTION SPECTRUM
FOR THE CASE OF A SPLIT SOURCE
AND AN UNSPLIT ABSORBER (or Vice Versa)

$I_1 = 3/2$ μ is negative

$I_o = 1/2$ μ is positive

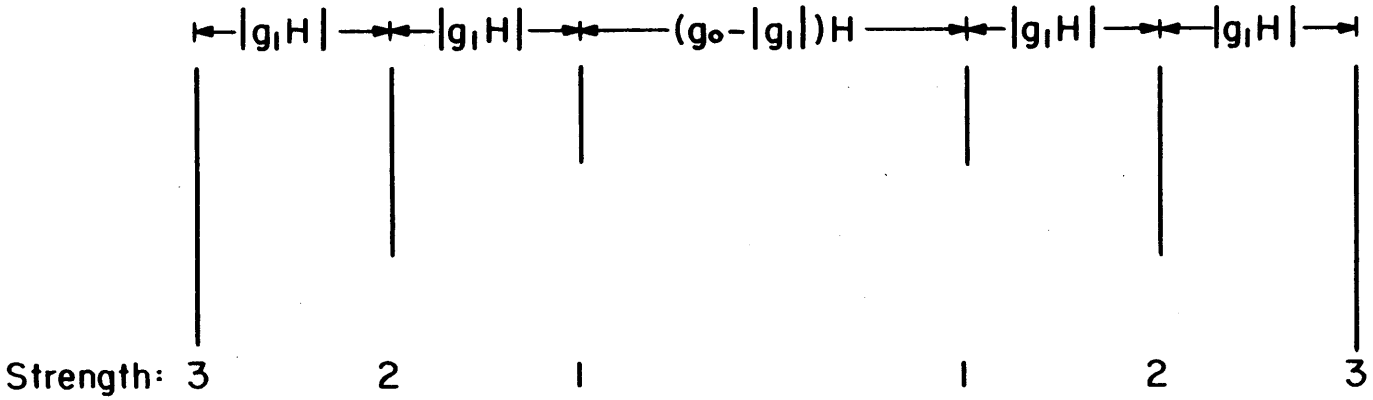

B. EXPERIMENTAL TECHNIQUES

1. Mossbauer Effect Apparatus

Two systems were used. The first, described in Section A, had a constant velocity mechanical drive. The second, described briefly in Section B, had a constant acceleration electronic drive.

A. Mechanical Drive System

A schematic drawing of the mechanical system is given in Figure 8. For the lower speeds, 0.05 to 1.4 cm/sec, a 1/8 hp Bodine motor (DC shunt wound, 1750 rpm, with 6:1 gear reduction) was used. The higher speeds, 0.12 to 4.0 cm/sec, were taken with a 1/2 hp direct drive Bodine motor. A belt drive connected the motor and a constant velocity cam of 1/8 inch throw. With the high speed motor a one inch pulley was used; with the low speed motor a two inch pulley was used. The pulley on the cam shaft was twelve inches in diameter. The cam pushed a rod which was about thirty inches long, and the source was taped to the end of this rod. Nylon tape was stuck on the cam follower, providing a low friction surface which reduced wear of the cam.

Source and absorber were held on the ends of stainless steel tubes of ten mils wall thickness. The source tube was 3/8 inch in diameter; the absorber tube 3/4 inch. The absorber was 3/4 inch under the source. 1 3/8 inches below the source was the first of three beryllium windows of the Dewar. The counter was about five inches below the source. The geometry of source, absorber, and counter was such that all detected gamma rays passed through the absorber.

The detector was a 1 3/4 inch by 3/4 inch thick NaI(Tl) scintillation counter. 30 mils of cadmium was placed directly on the counter to reduce pileup of the 67 KeV Pt K X-ray. For the weaker Au^{195} in Ir source, 15 mils

of tin was used. In all experiments, the counting rate at 129 KeV from X-ray pileup was less than 5%. This was calculated by assuming a resolving time of one microsecond.

The dewar, purchased from Andonian Associates, Inc., held liquid helium for twelve to eighteen hours, depending on factors which were never completely understood by this author. With liquid nitrogen in both resevoirs, liquid nitrogen survived in the inner resevoir for at least four days. A bellows arrangement permitted operation with any pressure in the center tube of the dewar, although a pressure of about one-half atmosphere of helium was used to insure good heat transfer.

The drive system was mounted on the top of a hydraulic lift and the dewar suspended from the movable platform. The dewar was filled with liquid helium in the raised position from a can of liquid helium raised on a second lift. Three carbon resistors attached at various heights to a rod inserted in the liquid helium resevoir monitored the level of liquid helium.

Electronics

Figure 9 gives a block diagram of the electronics. Pulses from the counter were fed through a preamplifier to a Franklin amplifier (model 358) with differential discriminator. The counts were recorded in two gated scalars. The scalars were gated by photoelectric relays mounted on the drive platform. An occulting disk, slightly more than half a circle to eliminate end point effects, was mounted on the cam shaft. Thus one scalar recorded counts while the source approached the absorber; the other recorded while the source moved away from the absorber. The same gating signals activated two other scalars which recorded timing pulses. When 10,000 timing pulses, usually at 60 cps, were recorded, the corresponding data scalar was stopped. When both channels had stopped, the data was typed out by an IBM typewriter connected to

a serial converter. Then the relay control circuit changed the speed of the motor and restarted the counting. After a period of hours, a long data tape had been produced; each entry corresponded to counts received at a single speed. In order to get the final data, it was necessary to add up all the corresponding entries.

The voltage applied to the armature of the motor determined the speed. This voltage was controlled by a stepping switch which permitted the selection of any number of speeds up to one hundred. The lower speeds, up to about 1.0 cm/sec, were determined from the throw of the cam by timing several revolutions of the cam with a stopwatch. For the high speeds, a Strobotac was used to time the revolutions of the cam.

The up-down speed correspondence was tested by comparing the number of timing pulses registered during the first two half cycles at a particular speed. Counting always started as the cam follower moved down. These two numbers were typed out on the data tape. Except at the lowest speeds, speed up equalled speed down to about 5%.

The uniformity of the motion over half a cycle was checked by observing the Mossbauer absorption spectrum of iron vs Co^{57} in stainless steel. The broadening of the iron lines indicated that the speed was constant over half a cycle to about 5%.

B. Electronic Drive System

The electronic drive system belonged to Norman Blum, and is described in detail in his thesis(B-64). A loudspeaker was used to move the source at constant acceleration. A triangular wave from an audio oscillator drove a power amplifier with feedback so that the velocity of the source was proportional to the voltage of the triangular wave. This voltage

also provided the multichannel analyzer with the address in which counts were to be stored. Counts from the Mossbauer gamma ray were stored in one half of the MCA, and counts from a non-resonant portion of the spectrum were stored in the other half for normalization. The final Mossbauer velocity spectra were obtained by dividing the data in the first half by the data in the second point by point. The velocity scale was calibrated by the resonances of Fe^{57}.

It was also possible to address the multichannel analyzer with a sawtooth signal of the same frequency and phase as the triangular velocity wave, with the analyzer operating in the time mode.

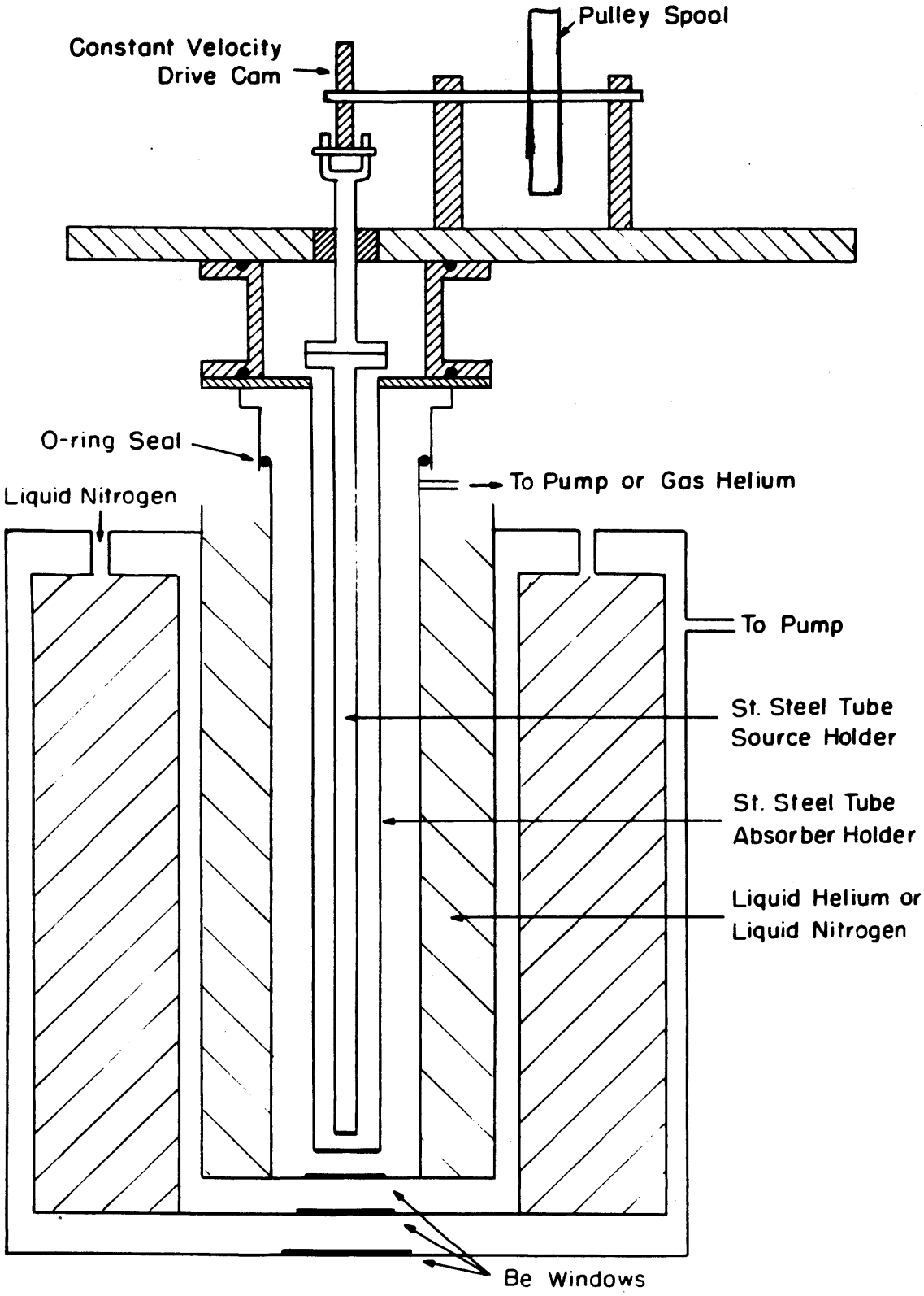

SCHEMATIC OF THE APPARATUS

Figure 8

(NOT TO SCALE)

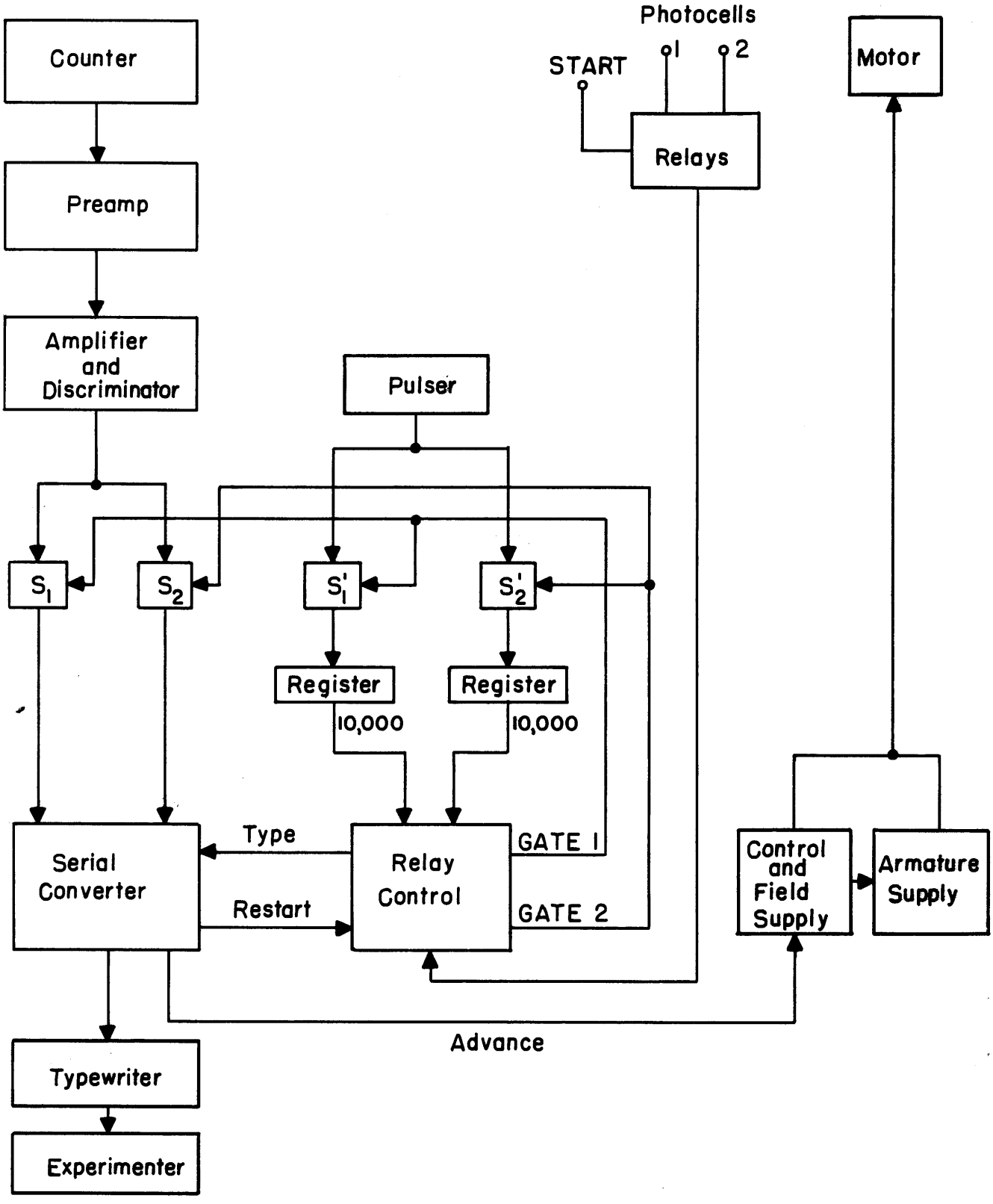

Figure

BLOCK DIAGRAM of ELECTRONICS

2. Source Preparation

Figure 10 shows the level scheme of Pt^{195}. It is seen that the 99KeV and 129KeV levels are fed both by 192 day Au^{195} and 4.1 day Pt^{195m}. Four types of sources were made: Au^{195} in Cu, Au^{195} in Be, Au^{195} in Ir and Pt^{195m} in Pt. A $Au^{195,196}$ in Fe source is discussed in Section III.

The first two sources were made by Mr. Irwin Gruvermann of the New England Nuclear Corporation. Carrier free Au^{195} was electroplated onto the copper or beryllium disk. The copper source was annealed for 8 hours at 1000°C in H_2; the beryllium source for 8 hours at 1000°C in H_2. The Au^{195} of both sources was free of any contaminating activity. (Figure 11).

Several attempts were made to diffuse carrier free Au^{195} into iridium. However the melting point of iridium is so high (2454°C) that gold cannot diffuse into its lattice at the comparatively low temperature of 1050°C. Gold melts at 1063°C. After one hour at 1050°C in a hydrogen atmosphere more than 95% of the Au^{195} had evaporated and none had gone into the iridium foil. A similar result was obtained with an annealing temperature of 950°C. In contrast, Harris (H-65) diffused Au^{195} into platinum (mpl774°C) at 1000°C.

A Au^{195} in Ir source was made at the M. I. T. cyclotron by a 13 hour, 50 microampere 28 MeV alpha bombardment of 1.5 mil natural iridium foil. In the first attempt the iridium was soft soldered to the

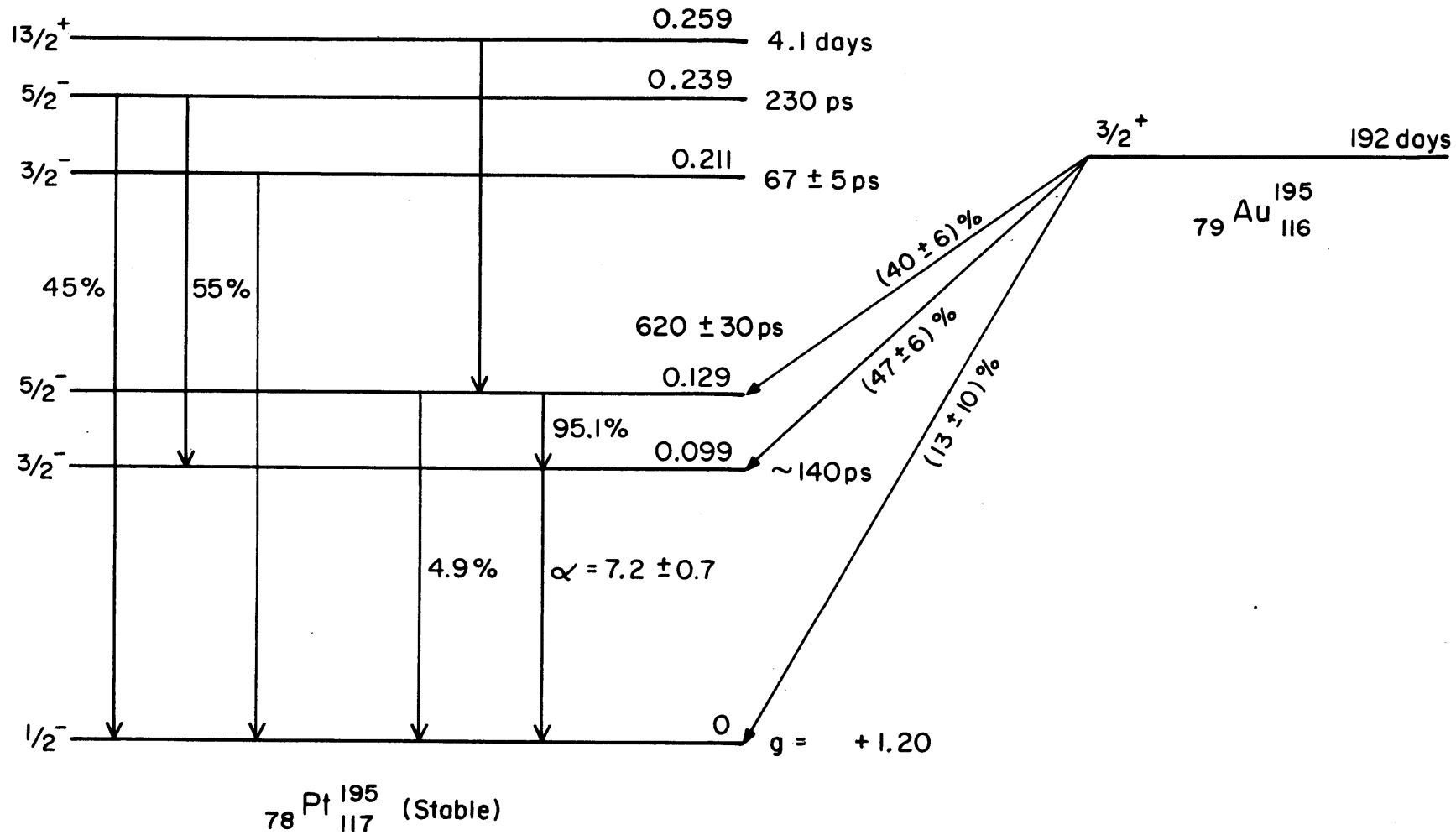

Figure 10

Au^{195} DECAY SCHEME

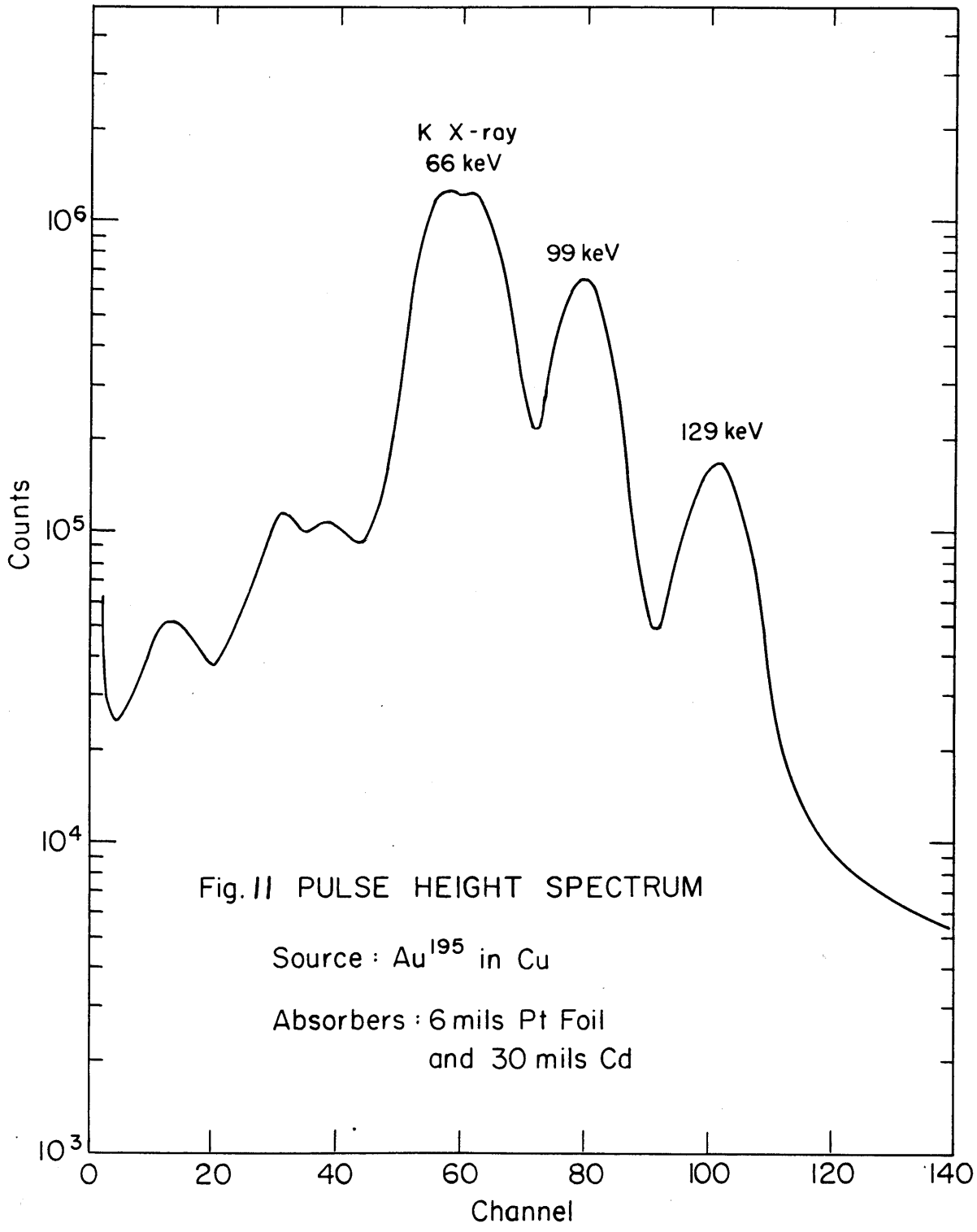

Fig. 11 PULSE HEIGHT SPECTRUM

Source : Au^{195} in Cu

Absorbers : 6 mils Pt Foil
and 30 mils Cd

copper target holder and vaporized because of poor heat conduction. In the second try the foil was silver soldered to the holder and held up very well under bombardment. To remove the foil, copper holder and silver solder were dissolved in boiling aqua regia. The source was then annealed for two hours at 1000°C in vacuum and furnace cooled. About 200uC of Au^{195} was made.

With the exception of 192 day Au^{195} and 74 day Ir^{192} from $Ir^{191}(\alpha,He^3)Ir^{192}$, a most unlikely reaction (WH-49), the longest lived product of alpha bombardment on iridium should be 6 day Au^{196}. However the source contained long lived high energy activity which has tentatively been ascribed to 40 day Ag^{105} from $(\alpha,2n)$ on rhodium impurity and 71 day Co^{58} from (α,np) on iron impurity. This contamination is serious. As long as eight months after bombardment it produced a 50% background under the 129 KeV peak for running conditions of 11.2 mils platinum absorber and 15 mils tin semi-critical absorber. (Figure 12).

The Pt^{195m} in Pt source was produced at the M. I. T. Reactor by a neutron irradiation of platinum powder enriched to 57% in Pt^{194}. The desired reaction is $Pt^{194}(n,\gamma)Pt^{195m}$: σ =1.2 barns. 3 day Pt^{191}, 4.4 day Pt^{193}, 18 hour Pt^{197}, and 30 minute Pt^{199} which decays to 3.15 day Au^{199} are also produced. Of these contaminating activities, only Au^{199} was produced in sufficient amounts to interfere with the observation of the Pt^{195} lines. Therefore the Au^{199} activity was separated from the platinum activities by extraction into ethyl acetate (L-61). Platinum was precipitated as $(NH_4)_2$ Pt Cl_6 by the addition of solid NH_4 Cl to a cold (0°C) solution of H_2 Pt Cl_6. The $(NH_4)_2$ Pt Cl_6 was dried, then heated to produce spongy platinum. One source was used in this form. For another source, the spongy platinum was converted to normal metallic platinum by melting it by a gas-oxygen flame. The resulting small sphere of platinum

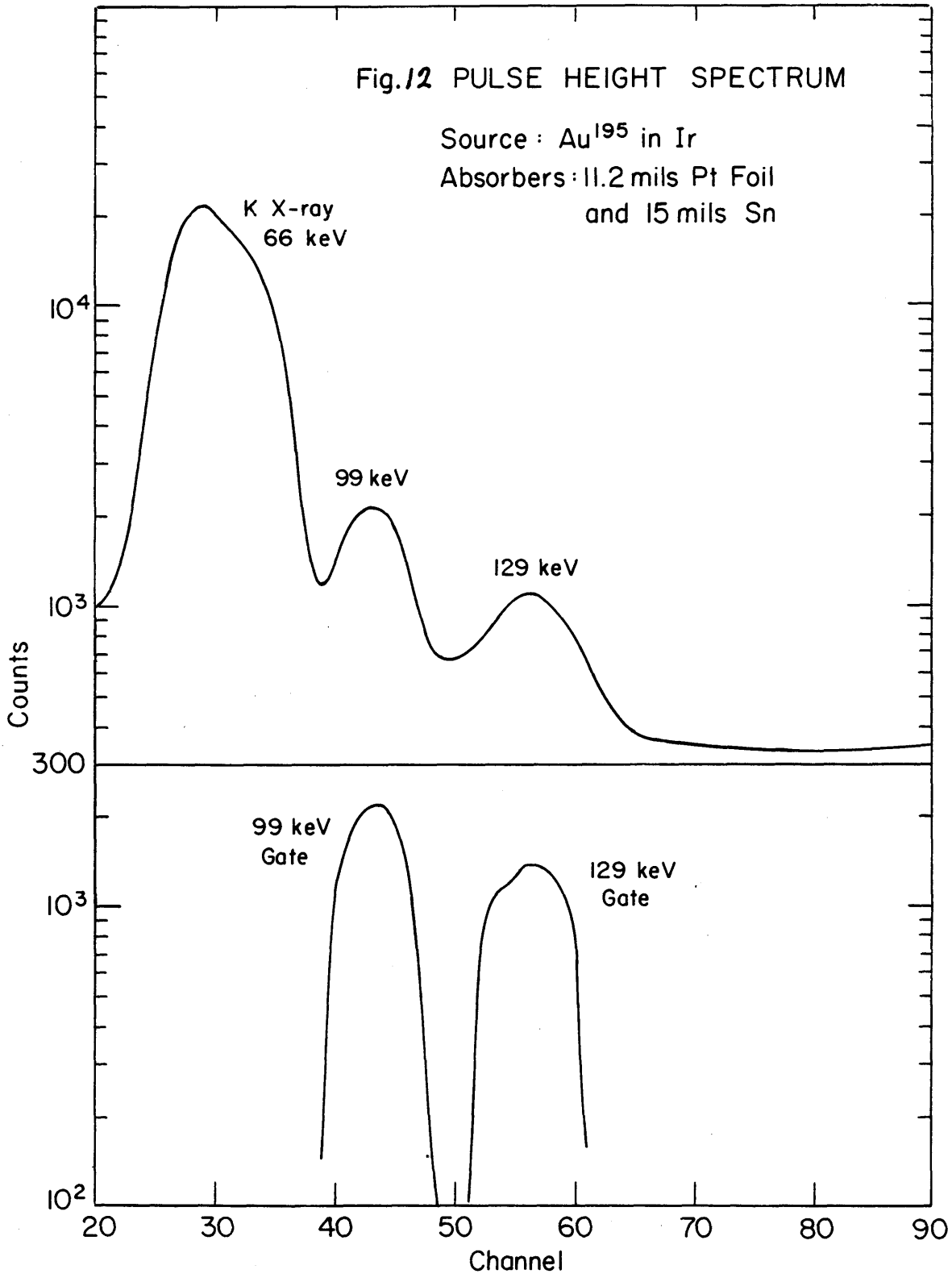
Fig. 12 PULSE HEIGHT SPECTRUM
Source : Au195 in Ir
Absorbers : 11.2 mils Pt Foil
and 15 mils Sn
K X-ray
66 keV
99 keV
129 keV
99 keV
Gate
129 keV
Gate
Counts
10⁴
10³
300
10³
10²
20
30
40
50
60
70
80
90
Channel

was hammered to two mils thickness and then annealed for one-half hour at 1000°C.

Only two Pt^{195m} sources were made. In neither was the gold decontamination or yield of platinum satisfactory, and this approach was shelved because the Au^{195} in Iridium source seemed more promising. However, it should be possible, with practice, to get very good decontamination and yield.

3. Absorber Preparation

The Pt-Fe alloy absorbers were made by Prof. John Wulff of the M.I.T. Department of Metallurgy. Five absorbers were made, ranging in composition from $Pt_{0.03}Fe_{0.97}$ to $Pt_{0.50}Fe_{0.50}$.

The alloys were prepared by melting together iron and platinum wire in a water cooled copper hearth argon arc furnace. The samples were remelted several times until no gross segregation could be found metallographically. Table I presents the relevant history of each sample. Analysis for homogeneity was performed on the alloys using the electron microbeam probe technique; no concentration gradients, precipitates, or inclusions were detected. The Mossbauer spectra of these absorbers were obtained for sample temperatures near $4.2^{\circ}K$. At this temperature, all the samples were probably in the bcc α phase. (BDFS-57).

TABLE I

	Wt % Pt	at % Pt	Thickness of Pt (mils)	No. of remelts; arc heat-treated finally.	Treatment before maching and grinding.	Heat Treatment in purified Helium
1	8	3	3.5	4	Pressed hot to disc shape	1300°C for 1 hr. Slow cooled
2	27	10	2.4	15	Pressed hot to disc shape	1300°C for 1 hr. and slow cooled
3	54	25	4.9	15	Pressed cold to disc shape	800°C for 1 hr. in He and quenched
4	60	30	5.4	15	Pressed cold to disc shape	1000°C for 1 hr. furnace cooled
5	78	50	12.0	50	Pressed hot to disc shape	800°C for 1 hr. in He and quenched

C. DIAMAGNETIC ENVIRONMENTS

1. Introduction

The levels of Pt^{195} fed from the decay of 192 day[1] Au^{195}, 4.1 day[2] Pt^{195m}, and observed in Coulomb Excitation[3], and particle reactions[4], are shown in Figure 10. The first two excited states, at 99 and 129 KeV, should both be Mossbauer levels. The transition energies are low enough to yield sizeable f-factors at $4^{\circ}K$ (Figure 13). The half lives imply narrow but not too narrow lines: about 6.5×10^{-6} ev or 2.0 cm/sec for the 99 KeV transition, and about 1.45×10^{-6} ev or 0.34 cm/sec for the 129 KeV transition. However, the 129 KeV effect will be difficult to observe because only 4.9% of the deexcitations of the 129 KeV level go by way of the 129 KeV branch. The cross section for resonant absorption is thus reduced by a factor of 20 (Section II-A), and the mean free path correspondingly increased. Figure 14 shows the Mossbauer mean free path at $4^{\circ}K$ for both transitions as a function of the Debye temperature of the absorber. Internal conversion coefficients of 7.2 for the 99 KeV line (HRB-K-65) and 1.79 for the 129 KeV line (McGS-59) were assumed.

Source preparation is discussed in Section II-B, and Figures 11 and 12 show pulse height spectra obtained with sources of Au^{195} in Cu and Au^{195} in Ir respectively. Figures 15 and 16 show several Mossbauer spectra for the 99 KeV transition. The principal results on the 99 KeV transition are given in Table 2.

1. GMKB-64; HRB-K-65; NS-65
2. de-SHS-52
3. McGS-59; BGH-65; BDGHP-65
4. M-65

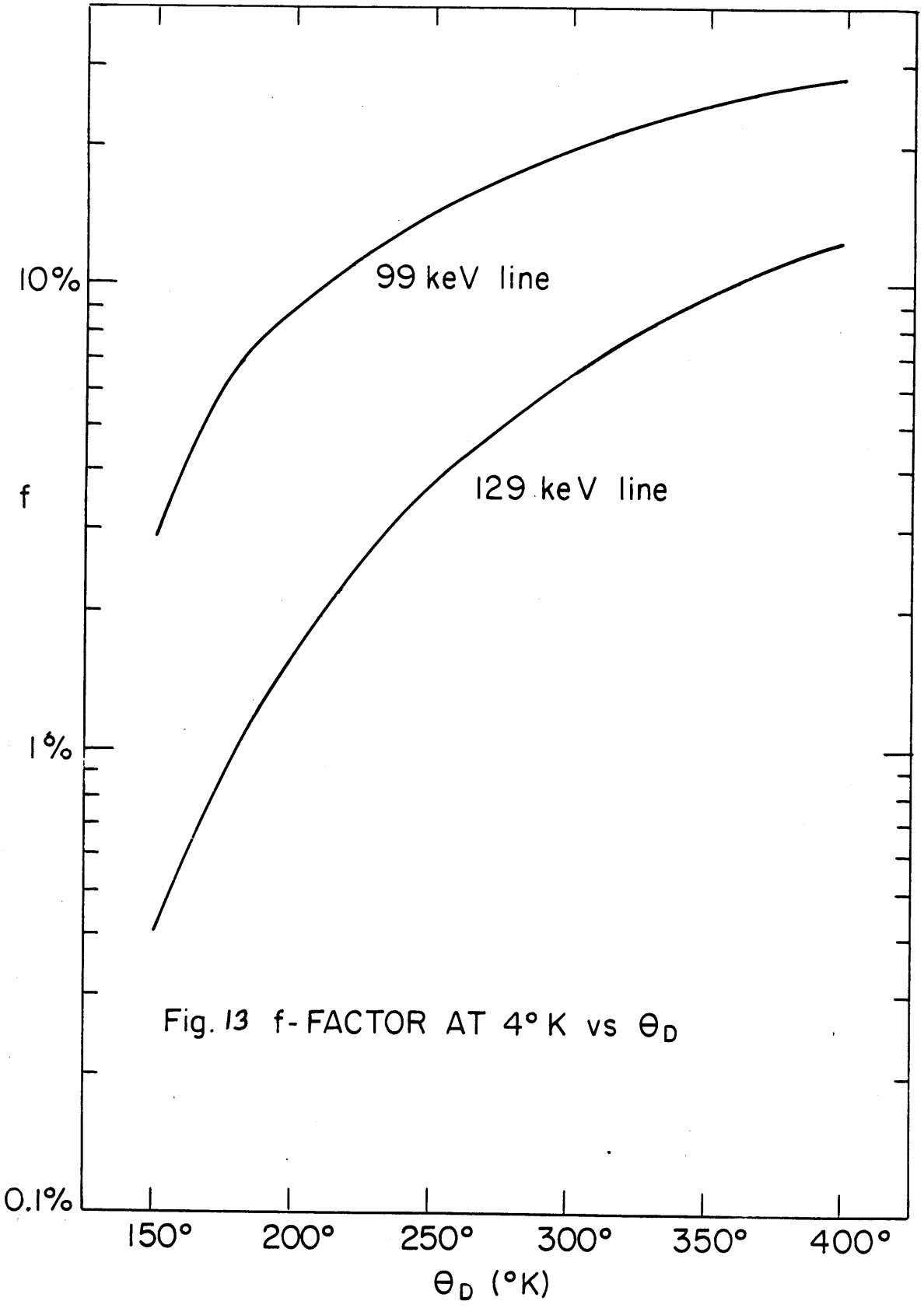

Fig. 13 f-FACTOR AT 4° K vs Θ_D

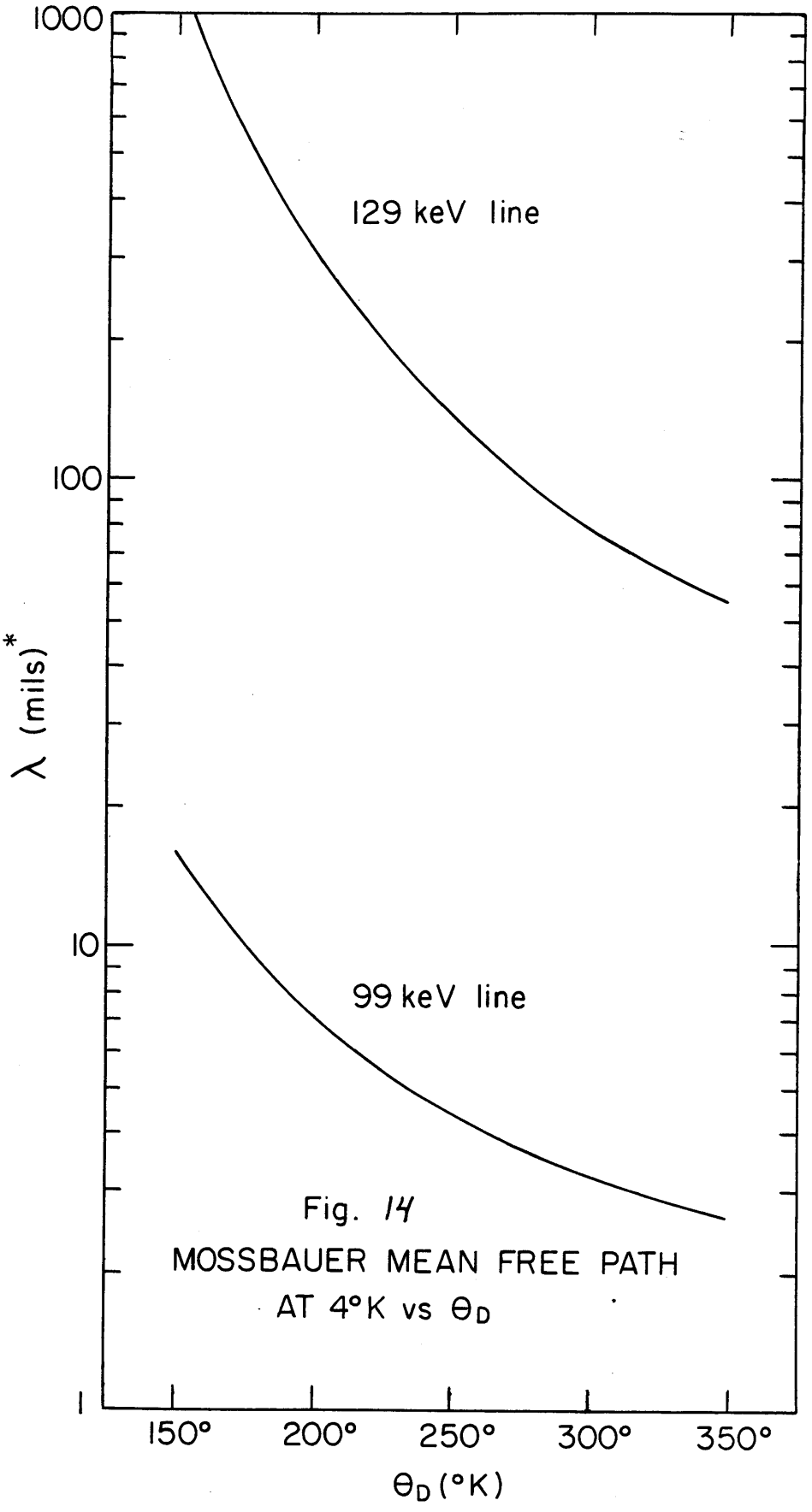

Fig. 14
MOSSBAUER MEAN FREE PATH
AT 4°K vs Θ_D

* Pt metal. 1 mil of Pt metal is the equivalent of 54.5 mg/cm^2 of Pt.

FIGURE 15

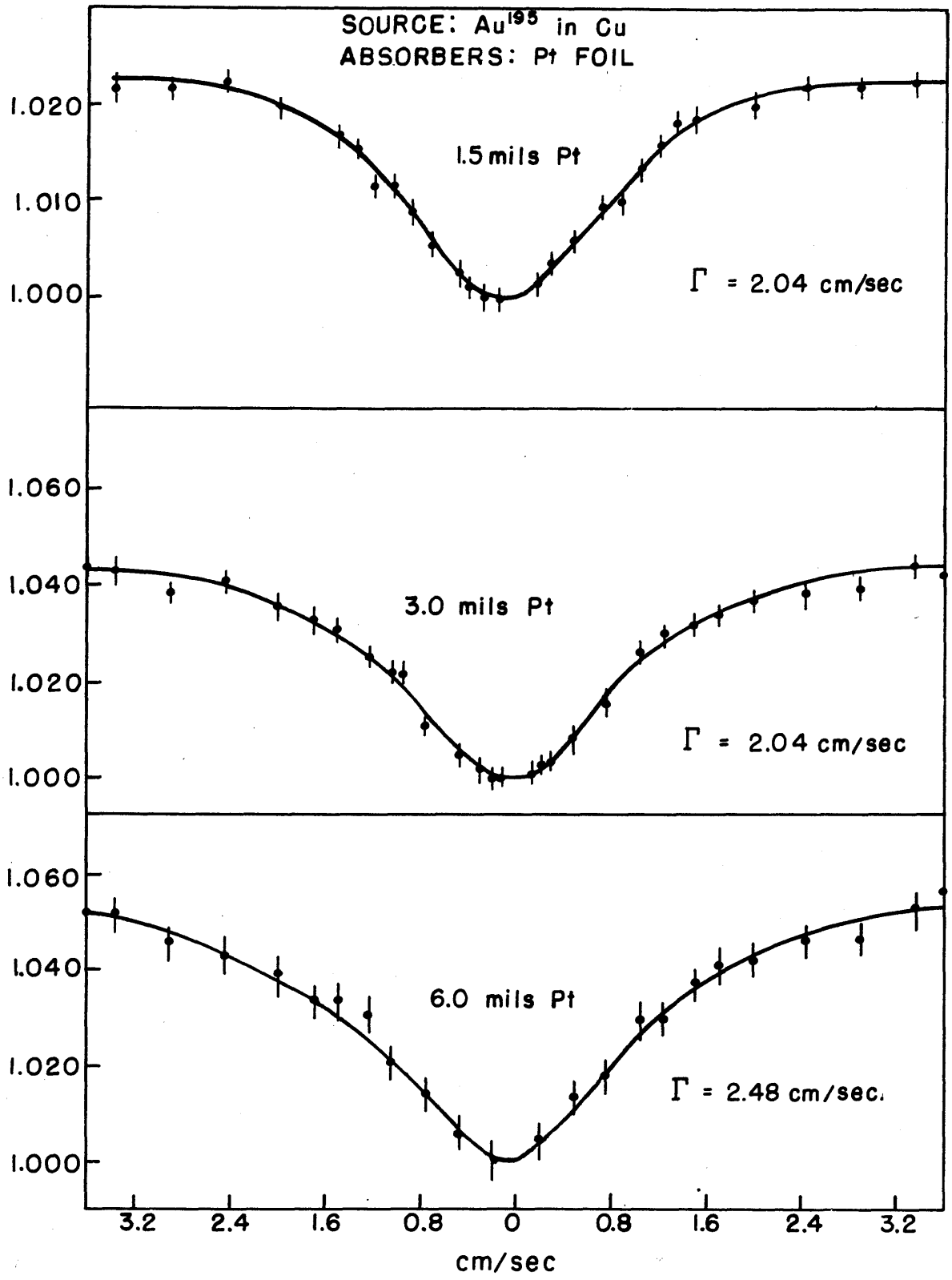
SOURCE: Au^{195} in Cu
ABSORBERS: Pt FOIL
1.020
1.010
1.000
1.5 mils Pt
Γ = 2.04 cm/sec
1.060
1.040
1.020
1.000
3.0 mils Pt
Γ = 2.04 cm/sec
1.060
1.040
1.020
1.000
6.0 mils Pt
Γ = 2.48 cm/sec.
3.2
2.4
1.6
0.8
0
0.8
1.6
2.4
3.2
cm/sec

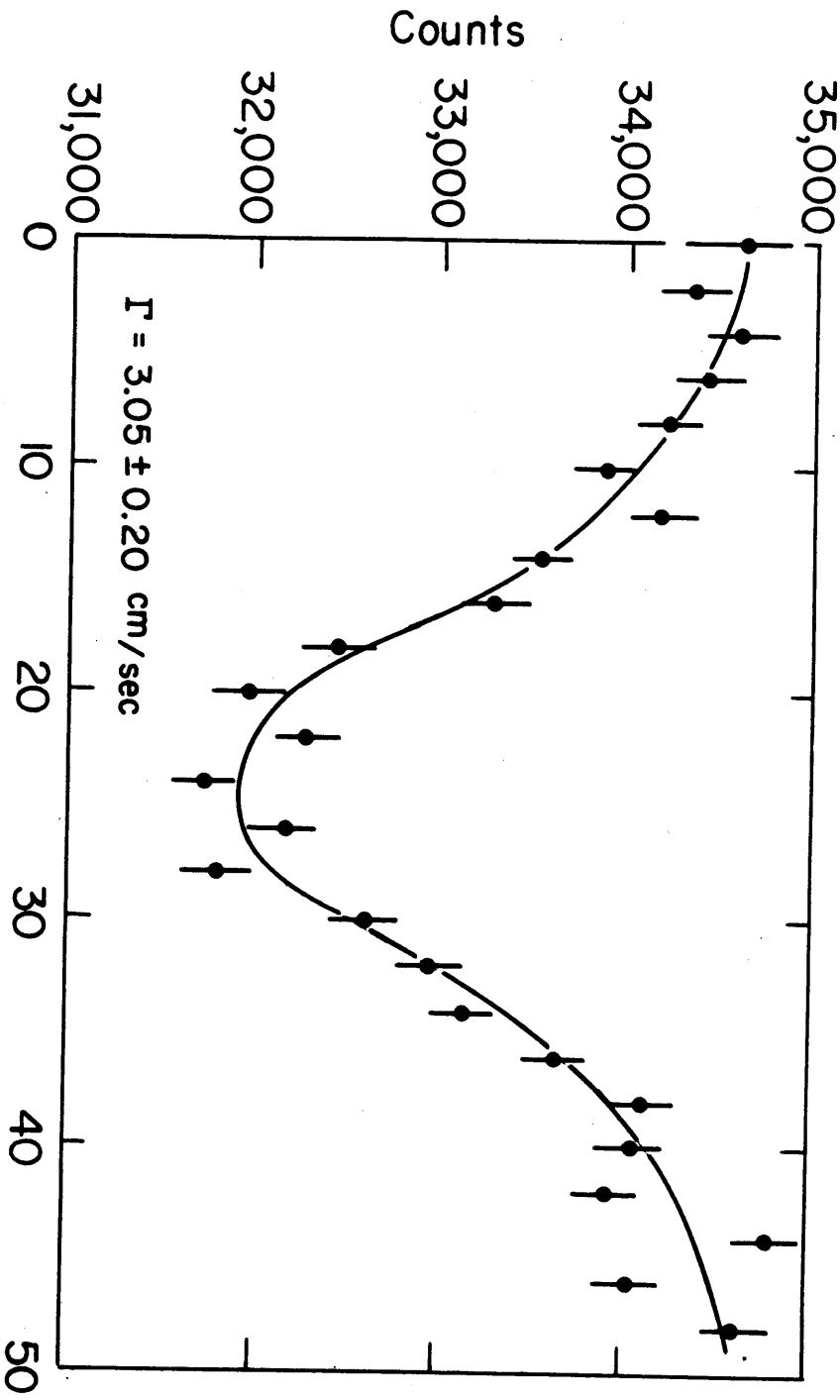

Fig. 16 Au^{195} in Ir vs 11.2 mils Pt Foil

TABLE 2

Principal results of Mössbauer experiments on the 99 KeV line of Pt^{195} in diamagnetic environments. All runs were taken at 4.2°K except runs 4 and 11 which were taken at 78°K. 1.0 cm/sec = 3.3×10^{-6} ev. or 798 Mc/sec.

Run No.	Source	Absorber	Semi-Critical Absorber	Isomer Shift (cm/sec)	Γ (cm/sec)	$\frac{N(\infty)-N(0)}{N(\infty)}$	Bkg. Under Peak	Corrected Effect
1.	Au^{195} in Cu	1.5 mils Pt foil	15 mils Sn	< .05	2.04 ± .10	2.4%	3%	2.5% ± 0.2%
2.	"	3.0 mils Pt foil	30 mils Cd	< .05	2.04 ± .10	4.4%	6%	4.7% ± 0.3%
3.	"	6.0 mils Pt foil	30 mils Cd	< .05	2.48 ± .10	5.7%	8%	6.2% ± 0.3%
4.	"	6.0 mils Pt foil	30 mils Cd	---	-------	~ 0.7%	8%	~0.8% ± 0.2%
5.	"	K_2PtCl_6 Eq. 1.8 mils Pt foil	30 mils Cd	< .05	2.00 ± .10	2.0%	5%	2.1% ± 0.2%
6.	"	PtO_2 Eq. 3.0 mils Pt foil	30 mils Cd	< .05	2.00 ± .10	4.2%	6%	4.5% ± 0.3%
7.	Au^{195} in Be	6.0 mils Pt foil	30 mils Cd	---	2.5 cm/sec	5.5%	8%	6.0% ± 0.8%
8.	Pt^{195m} in Pt	6.0 mils Pt foil	30 mils Cd	---	-------	~ 3%	~50%	~ 6%
9.	Au^{195} in Ir	6.0 mils Pt foil	none	< .05	2.48 ± 0.10	9.1%	25%	12.1% ± 1.0%
10.	Au^{195} in Ir	11.2 mils Pt foil	15 mils Sn	< .05	3.05 ± 0.15	8.9%	25%	11.9% ± 1.0%
11.	Au^{195} in Ir	5.6 mils Pt foil	15 mils Sn	< .05	2.0 ± .1	2.2%	15%	2.6% ± 0.3%

2. Discussion of Results

A least squares fit to the results of Runs 1, 2, 3, 9, and 10 of Table 2 gives Γ (full width at half maximum) extrapolated to zero absorber thickness as 1.81±0.15 cm/sec. This makes τ_{mean} for the 99 KeV level 219±18 p sec ($t_{1/2}$=152±12 p sec) in agreement with the direct electronic measurement, $\tau \approx$ 200 psec (B-60), and with the Mossbauer result of 246±28 p sec of Harris et al (HB-KR-65). See Figure 17.

No quadrupole effect was observed. Platinum, copper, iridium and K_2PtCl_6 are all cubic. Beryllium is hexagonal, but the data, although poor, indicated no quadrupole broadening. However, a eq of 10^{-6} volts, which is a large quadrupole interaction, would separate the m=±1/2 and the m=±3/2 sublevels by only 0.15 cm/sec. Thus it is clear that the 99 KeV line is too broad to detect small or even moderately large quadrupole interactions.

The isomer shift in all cases was less than 0.10 cm/sec or 3.3×10^{-7} ev. However, this limit is not very informative, because it is of the order of the <u>largest</u> isomer shifts observed for other Mossbauer isotopes. For example, the largest Te^{125} isomer shift known is that for Te^{125m} in TeO_2 vs Na_2TeO_4 : 1.9×10^{-7} ev. (B-62). A much better value of a 99 KeV line isomer shift could be obtained by measuring the difference in counting rate at $v=+\frac{\Gamma}{2\sqrt{3}}$ and $v=-\frac{\Gamma}{2\sqrt{3}}$, the points of maximum slope on a Lorentzian curve.

Table 3 lists Debye temperatures deduced from our results. θ_D (Pt in Pt) was obtained from Runs 1, 2, 3, 9, and 10 of Table 2 by looking at the effect and the line width as a function of absorber thickness. (M-61). The ratio of the effects in Runs 3 and 4 served as a rough confirmation. A resonance scattering experiment in which the

Table 3

Debye Temperatures for Pt^{195} in Various Hosts

Host	Θ_D (°K)	Θ_D (°K) of Host from Specific Heat Data	Θ_{eff} (°K) by * Lipkin Theory
Pt	$238^\circ \pm 20^\circ$	240°	240°
Cu	$220^\circ \pm 20^\circ$	343°	198°
Be	$220^\circ \pm 30^\circ$	1160°	250°
Ir	$315^\circ \pm 35^\circ$	420°	420°
Fe (3 at % Pt Fe-Pt alloy)	$\sim 275^\circ$	467°	250°

$$^{*}\Theta_{eff} = \sqrt{\frac{M_{Host}}{M_{Imp}}}\,\Theta_{Host}$$

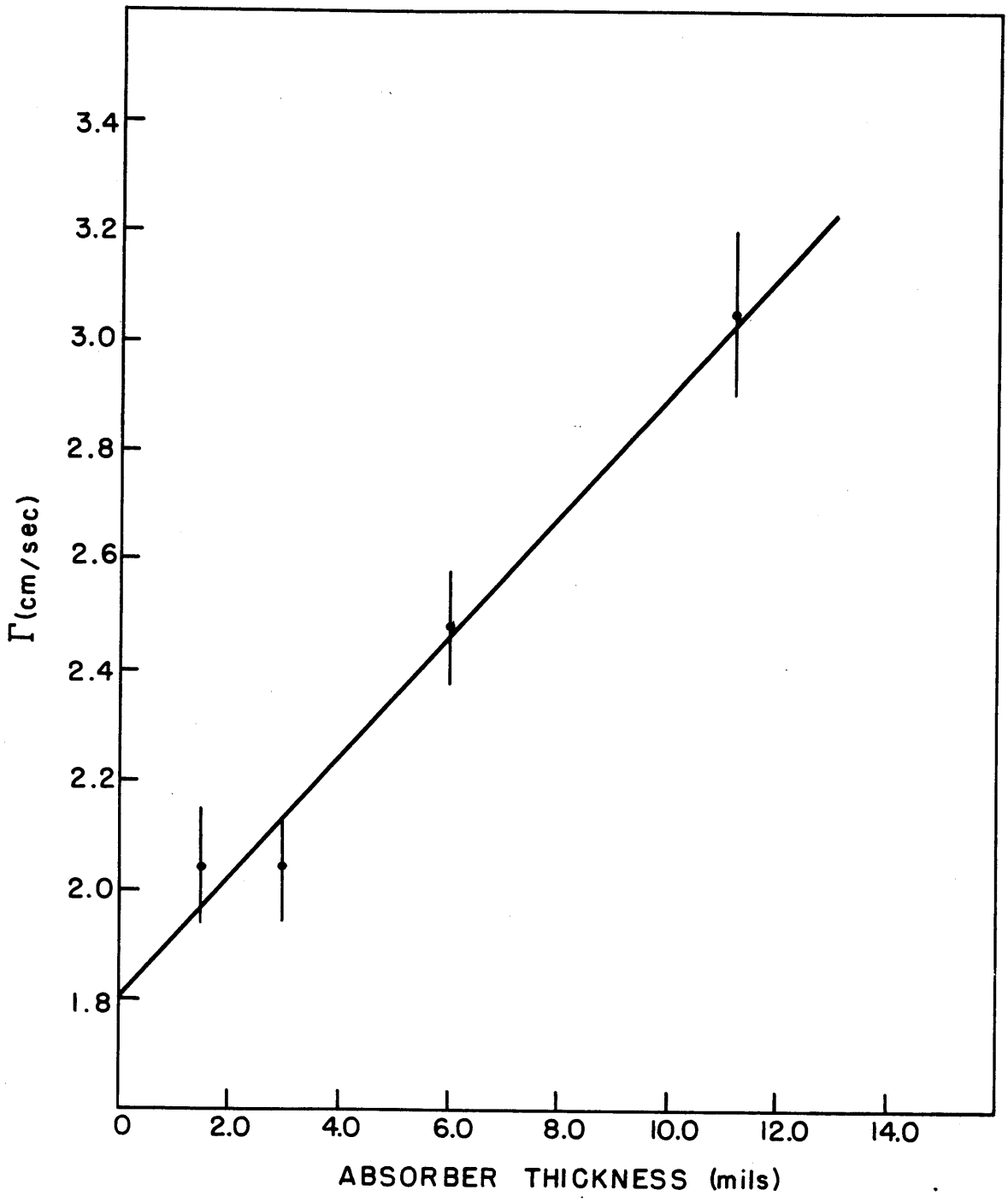
3.4
3.2
3.0
2.8
2.6
2.4
2.2
2.0
1.8
Γ(cm/sec)
0
2.0
4.0
6.0
8.0
10.0
12.0
14.0
ABSORBER THICKNESS (mils)

FIGURE 17

temperature of the Au^{195} in Cu source and the platinum absorber were varied together from 10°K to 80°K (Figure 18) indicated a somewhat higher value. 238°K is in good agreement with the specific heat value of 240°K (G-63) and the Mossbauer result of (234 ± 6)°K obtained by Harris et al (HB-KR-65). θ_D (Pt in Cu) was obtained from Runs 1, 2, and 3 from the variation of effect with absorber thickness (M-61). θ_D (Pt in Be) was calculated from the ratio of the effects of Runs 3 and 7, and θ_D (Pt in Ir) from a comparison of the effects of Runs 3 and 9. The f-factor for Pt^{195} in Cu and the observed absorption by the 3 at% Pt Fe-Pt alloy absorber (Figure 21) gave the Mossbauer "mean free path" and thus the Debye temperature of the absorber. (See Figures 4 and 14).

These Debye temperatures support the prediction of Lipkin (L-63) of an effective Debye temperature $\theta_{eff} = \sqrt{\frac{m_{host}}{m_{imp}}}\ \theta_{host}$ for an impurity atom bound with the same force constant as the host atoms. The more general theory of Kagan and Iosilevskii (KI-62,63) gives Lipkin's results in the limits of $m_{host} << m_{imp}$ or $m_{host} >> m_{imp}$, but does not simplify when $m_{host} \sim m_{imp}$.

Fig. 18

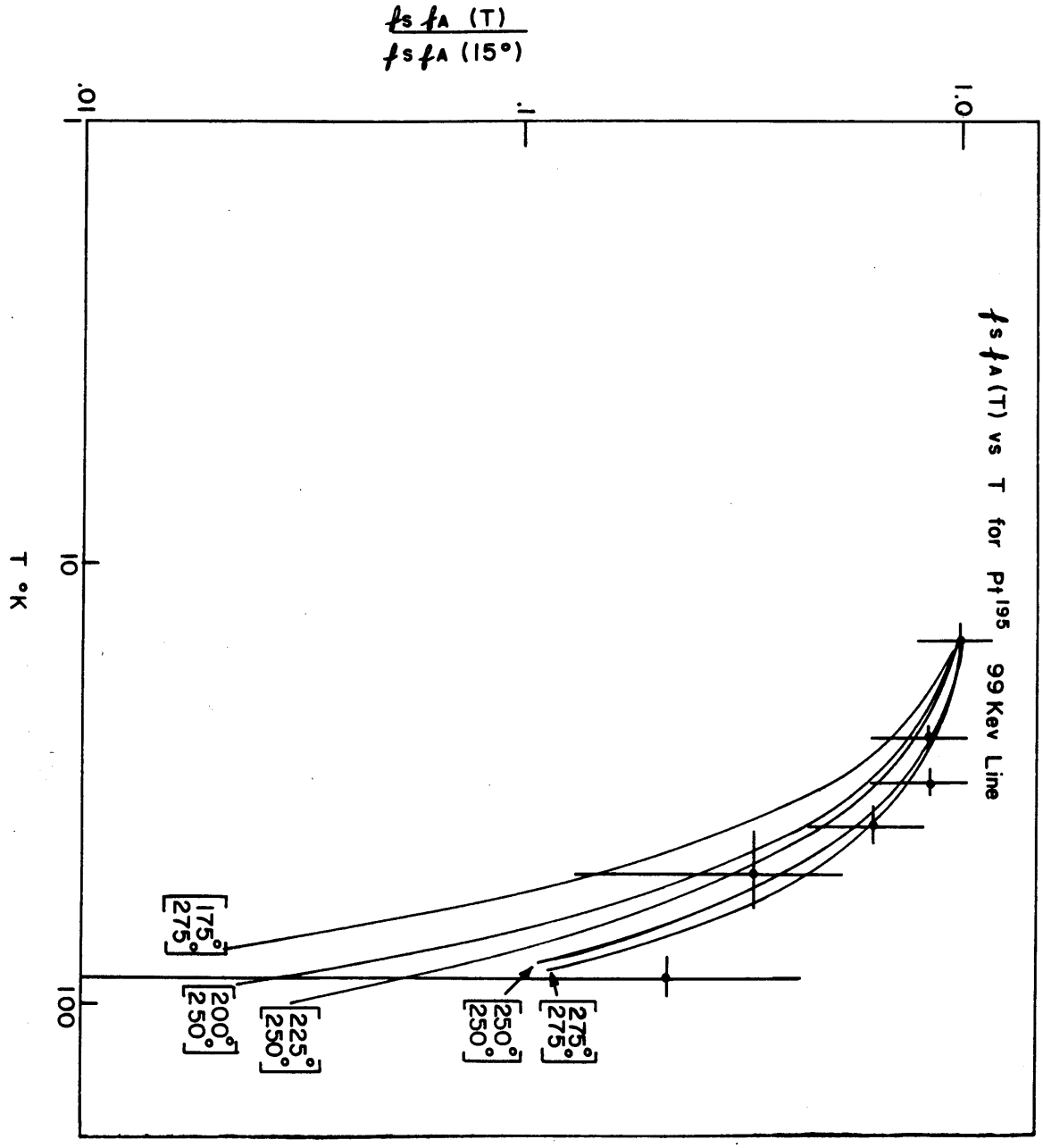
$\frac{f_S f_A (T)}{f_S f_A (15°)}$
.01
1
1.0
10
100
T °K
$f_S f_A$ (T) vs T for Pt^{195} 99 Kev Line
[175° 275°]
[200° 250°]
[225° 250°]
[250° 250°]
[275° 275°]

3. Predictions for the 129 KeV Line

The absorption expected for the 129 KeV transition may be deduced from the Debye temperatures in Table 3. From Figure 13, we see that the recoilless fraction at 4.2°K from sources of Au^{195} in Cu and Au^{195} in Ir should be 2.4±0.7 and 7.3±2.0% respectively. The absorption by natural platinum is, however, small for practical absorber thicknesses. From Figure 14, we see that the Mossbauer "mean free path" (for 53% maximum resonance absorption) is 162±40 mils or 8.8±2.2 gm/cm^2. The mean free path is so long because only a small fraction, (2.0±0.5)/41, of the deexcitations of the 129 KeV level go by way of the 129 KeV branch.(GMKB-64). Since the mean free path for electronic absorption at 129 KeV is only about 7.5 mils, (S-65), this severely limits the thickness of practical absorbers. The most efficient absorber thickness is about 15 mils.

Several experiments on the 129 KeV transition, carried out prior to the new value of the branching ratio (GMKB-64), used absorbers of 10.0 and 11.2 mil thickness. With the Au^{195} in Cu source the expected effect is 0.14%. With the Au^{195} in Ir source, with about 50% background under the 129 KeV peak (Figure 12), the expected effect is 0.25%. Figure 19 presents two of the five significant runs. The results are inconclusive. The observed effect is statistically less than the predicted value. However, if we take the smaller limits for θ_D and for the branching ratio, then the lack of effect could be accounted for. These results are consistent with those obtained by Harris et al on the 129 KeV transition. (HRB-K-65).

It is clear that it will be extremely difficult to see the 129 KeV line Mossbauer effect, and to measure the magnetic moment of the 129 KeV level by splitting the Mossbauer line will be more difficult still. A magnetic field, for an E2 $5/2^-$ to $1/2^-$ transition, splits the Mossbauer line into ten lines.

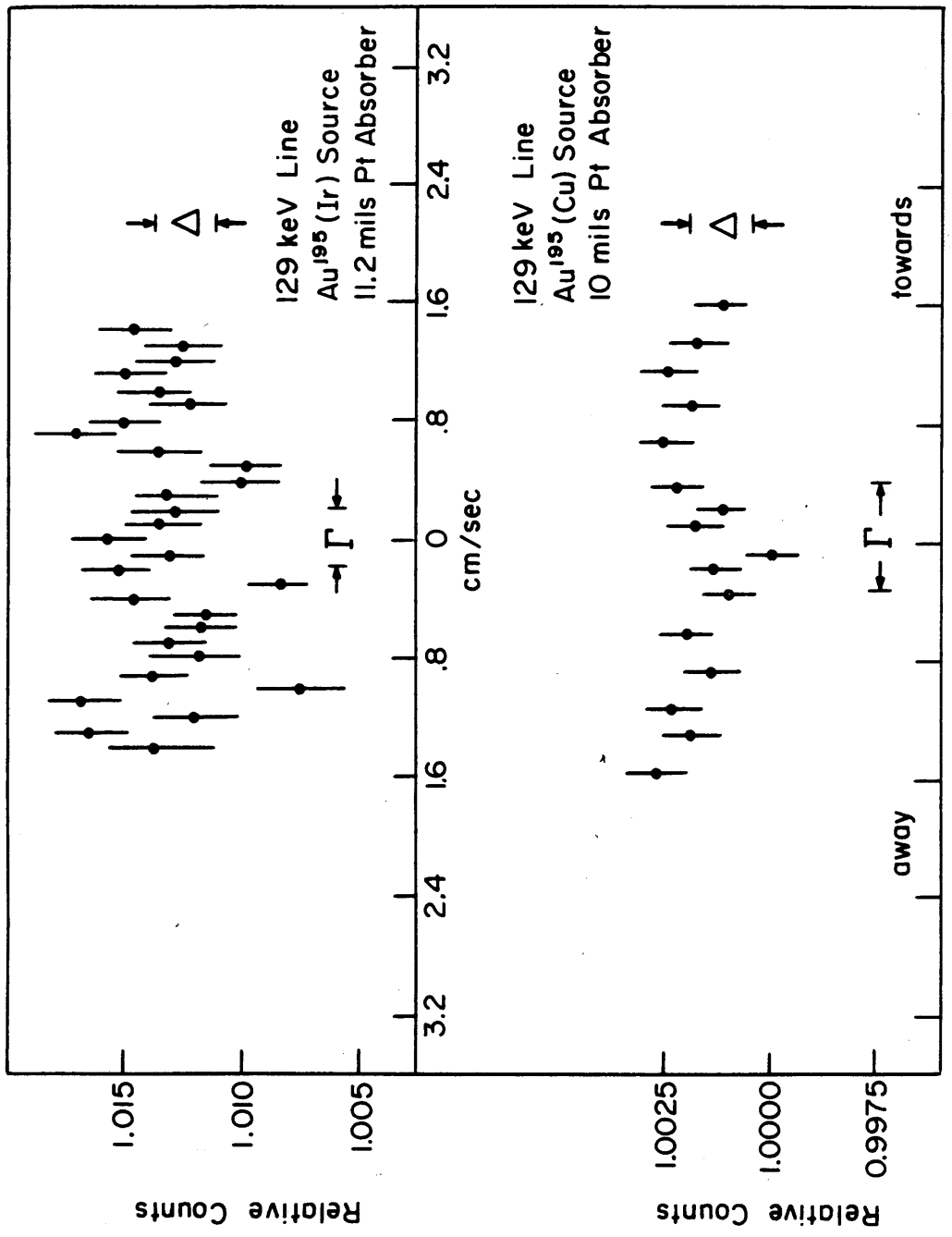
129 keV Line
Au195 (Ir) Source
11.2 mils Pt Absorber
129 keV Line
Au195 (Cu) Source
10 mils Pt Absorber
Relative Counts
1.015
1.010
1.005
1.0025
1.0000
0.9975
3.2
2.4
1.6
.8
0
.4
.8
1.2
cm/sec
away
towards

Figure 19

The two most intense of these each has a weight 1/6 of the total. The exact Mossbauer line pattern to be expected depends on the sign and magnitude of the magnetic moment of the $5/2^-$ level relative to that of the $1/2^-$ (ground) level. The magnetic moment of the ground state is +.6005 nm (PY-51), and theory (see Section IV) suggests a large positive moment for the $5/2^-$ level. Let us assume an unsplit source and a split absorber (or vice-versa). If u_2, the magnetic moment of the $5/2^-$ level, is positive and less than u_o, the ground state moment, the intensity pattern is 1:2:3:4:5:5:4:3:2:1, with the 5-5 separation $(g_o - 5g_2)H$, and the distance between the other adjacent lines, g_2H. For an H_{INT} of 1.23×10^6 gauss (Section II-D-3), g_oH is 1.08 cm/sec or 3.2 Γ, where Γ is the full width at half maximum of the Mossbauer line. For $u_2 < 0.5u_o$, the spectrum will consist of two well resolved lines, and the size of the effect will be reduced, for the same thickness of platinum, by only a factor of about two from the unsplit case. As u_2 increases, the resolution decreases. As u_2 increases beyond u_o, the intensity pattern changes as lines cross, and structure begins to emerge. At $u_2 = 1.0$ nm, close to the theoretical prediction, the spectrum will principally consist of three partially resolved lines, each of weight 8/30, separated from each other by 1.07 Γ. In general, the resolution is better for negative u_2. If u_2 is negative and $|u_2| < 1.67u_o$, the intensity pattern will be 5:4:3:2:1:1:2:3:4:5, with the 1-1 separation $(g_o - 3|g_2|)H$, and the distance between the other adjacent lines, g_2H. For $|u_2| < u_o$, the pattern will consist of two lines well resolved; as $|u_2|$ increases beyond u_o, individual lines will begin to emerge.

If the Mossbauer mean free path were much shorter, the 129 KeV line could easily provide an extremely accurate value of H_{INT}, and a good value for u_2 down to about $|u_2| \geq 0.2$ nm.

The only hope of observing the Mossbauer effect of the 129 KeV line in transmission lies with a strong Au^{195} in Ir source, or with another source

of comparable Debye temperature. If such a source had no background under the 129 KeV peak, and was at least five times as strong as our Au^{195} in Ir source (Section II-B-2), it might even be possible to measure the magnetic moment. Fortunately, the low Pt Fe-Pt alloy absorbers have a higher Debye temperature than platinum metal. (Table 3 and B-K,HR-65). Several approaches are possible:

1. Get extra pure iridium foil, low in iron and rhodium ($\lesssim$ 25 ppm) and subject it to a 3,000 u-amp hour alpha bombardment.

2. Electroplate Au^{195} onto iridium foil and then either plate or evaporate a layer of iridium over the source. Try to diffuse the gold into the iridium at a high temperature: 1200°C or 1400°C or higher.

3. Find a host more receptive to gold than iridium which will still give a high θ_{eff}. Following Lipkin's Rule (L-63), and taking Debye temperatures from the American Institute of Physics Handbook (G-63), we find that the only elements with melting points below 2400°C and θ_{eff}'s for gold above 275°K are:

Chromium $\theta_D = 630°K$ $\theta_{eff} = 326°K$ mp = 1890°C

Rhodium $\theta_D = 480°K$ $\theta_{eff} = 348°K$ mp = 1985°C

Both are cubic.

4. Make a Pt^{195m} source of high specific activity at Oak Ridge and diffuse platinum (mp = 1774°C) into iridium.

Of these four methods, the third is the simplest to try. An annealing temperature of 1050°C should be used.

D. FERROMAGNETIC ENVIRONMENTS

1. Results

Mossbauer absorption spectra were taken for five alloy absorbers ranging in composition from $Fe_{0.97}Pt_{0.03}$ to $Fe_{0.50}Pt_{0.50}$. The source in all cases was single line Au^{195} in Cu. The curves are shown in Figure 21 and the results are summarized in Table 4. The spectra are similar, showing a double line pattern with a splitting nearly independent of composition. The splitting is dominated by the large g value of the ground state, +1.20 nm (PY-51), so that the value of $H_{INT}(Pt)$ can be determined with greater precision than can the value of g_1.

2. The Sign of g_1

g_1 was determined as negative by megnetizing the absorber parallel to the propagation direction of the gamma rays (perpendicular to the absorber disc plane) with an external field of 45,000 gauss. This external field, although large, is much smaller than the internal field, which was found to be 1,260,000 gauss. Thus it aligned the domains without appreciably affecting the magnitude of the field at the nucleus. This longitudinal polarization eliminates the $\Delta m=0$ transitions. Figure 22 shows the Mossbauer spectrum obtained when the external field was applied.

Figure 23 gives the line pattern for all relative values of g_1 and g_o for an M1 transition between levels of spins I=3/2 and I=1/2. Since g_o is positive, the intensity pattern for g_1 negative is:

without external field	3:2:1:1:2:3
with external field	3:0:1:1:0:3

for all values of g_1/g_o .

FIG. 21

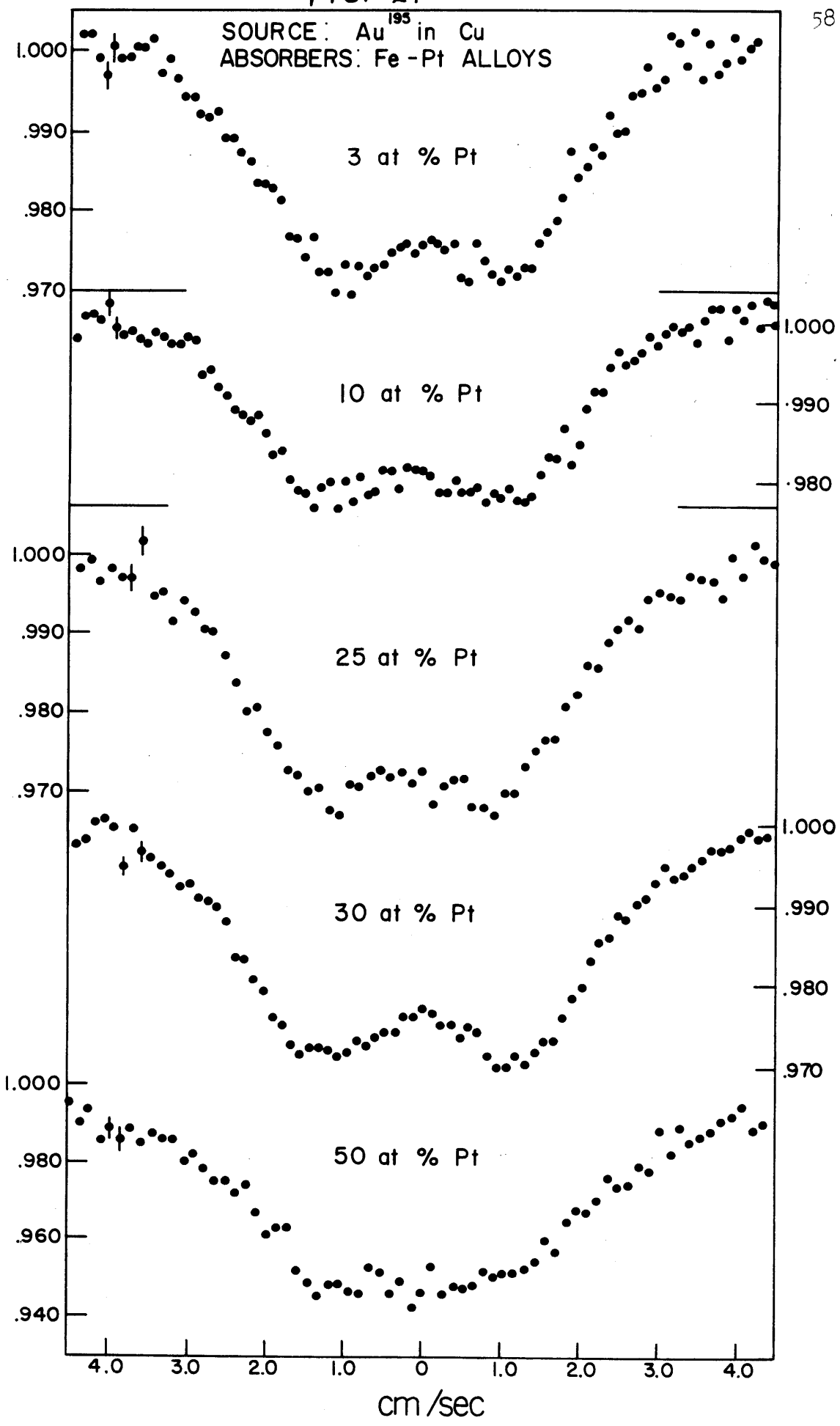
SOURCE: Au 195 in Cu
ABSORBERS: Fe - Pt ALLOYS
3 at % Pt
10 at % Pt
25 at % Pt
30 at % Pt
50 at % Pt
1.000
.990
.980
.970
.960
.940
4.0
3.0
2.0
1.0
0
1.0
2.0
3.0
4.0
cm/sec

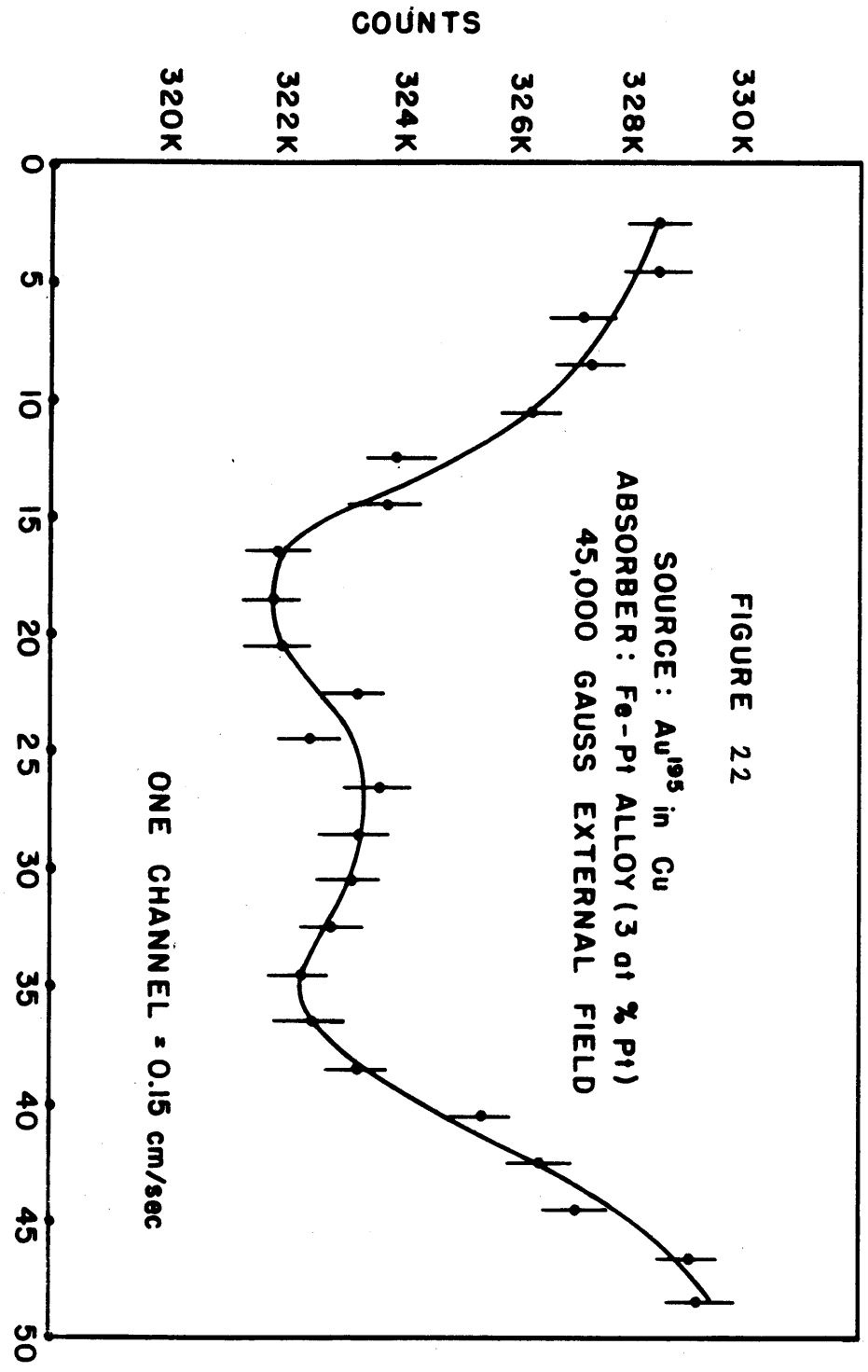
COUNTS
330K
328K
326K
324K
322K
320K
0
5
10
15
20
25
30
35
40
45
50
CHANNEL
SOURCE: Au^{195} in Cu
ABSORBER: Fe-Pt ALLOY (3 at % Pt)
45,000 GAUSS EXTERNAL FIELD
ONE CHANNEL = 0.15 cm/sec

FIGURE 22

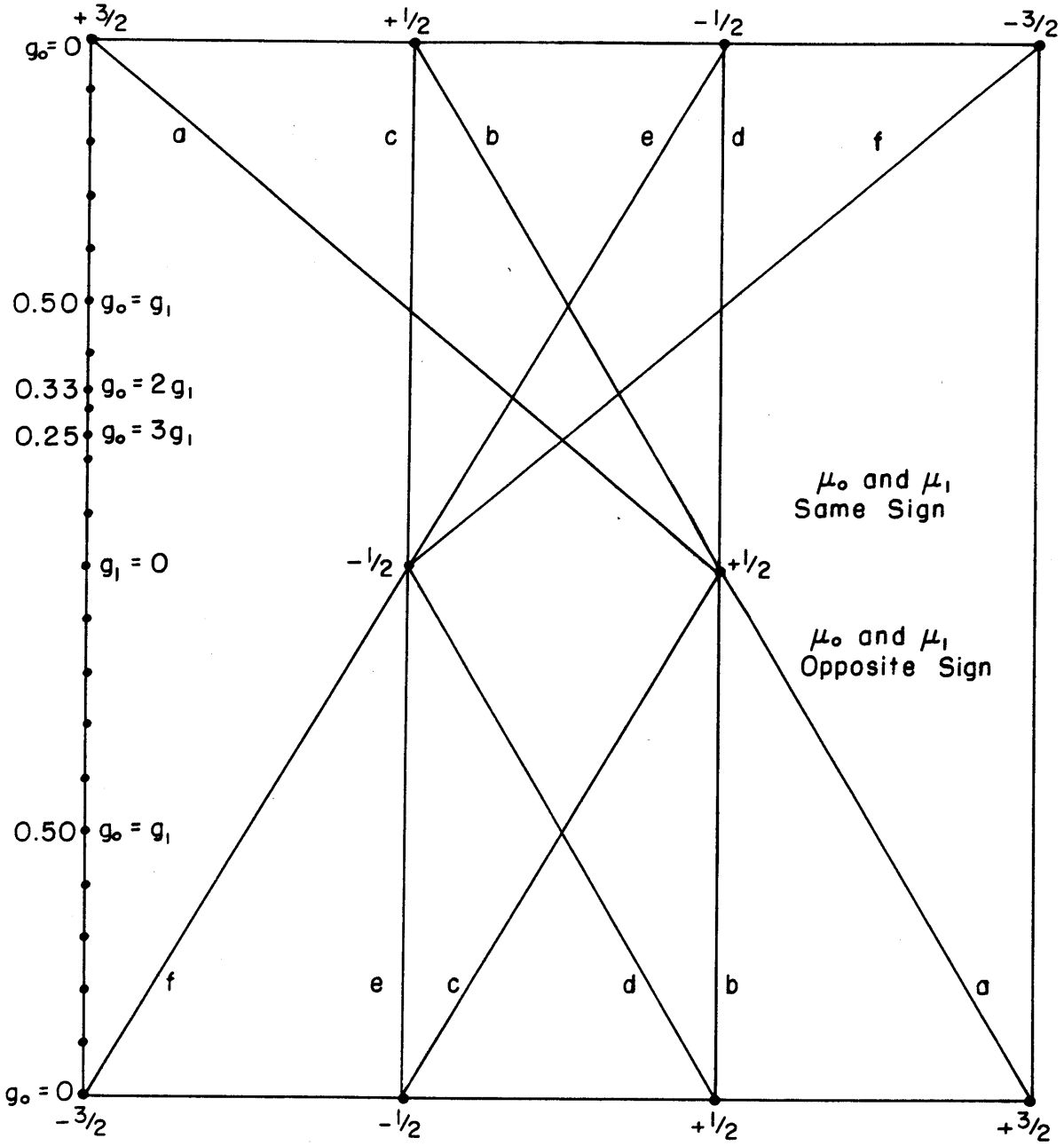

FIGURE 23

Line	Intensity
a	3
b	2
c	1
d	1
e	2
f	3

For g_1 positive, the intensity patterns are:

$g_1 < g_o/2$ or $g_1 < 0.6$nm	without external field	1:2:3:3:2:1
	with external field	1:0:3:3:0:1
$g_o/2 < g_1 < g_o$ or 0.6nm $< g_1 <$ 1.2nm	without external field	1:3:2:2:3:1
	with external field	1:3:0:0:3:1
$g_1 > g_o$ or $g_1 >$ 1.2nm	without external field	3:1:2:2:1:3
	with external field	3:1:0:0:1:3

Thus if g_1 is negative the application of an external field will remove lines b and e and increase the apparent splitting of the double line pattern. If g_1 is positive the removal of lines b and e will decrease the apparent splitting if g_1 is smaller than $g_o/2$, but increase it if g_1 is greater than $g_o/2$. Since polarization by the 45,000 gauss external field increased the apparent splitting by about 18%, the gyromagnetic ratio of the 99 KeV, $3/2^-$ state is either negative, or positive and greater than 0.6 nm. The large positive values of g_1 are ruled out when the curves of Figure 21-1 and Figure 22 are compared with computer simulated six and four line curves. For g_1 greater than +0.6nm, no value of H_{INT}(Pt) could be found that would give a fit to both experimental curves.

3. The Magnitudes of g_1 and $H_{INT}(Pt)$

Using the fact that g_1 is negative, six line spectra were simulated by computer for various values of $H_{INT}(Pt)$ and g_1. The simulated spectra were compared with the 3 at% Pt alloy curve of Figure 21 to determine the values of $H_{INT}(Pt)$ and g_1. Particular note was taken of two features of the curves: the apparent splitting, Δ, and the resolution, R. The latter was defined, for convenience, as the ratio $\frac{N(0)-N(min)}{N(4\ cm/sec)-N(min)}$. Figures 24 and 25 show how Δ and R vary with $H_{INT}(Pt)$ and g_1 for line widths of 1.88 cm/sec and 2.00 cm/sec. The smaller width was calculated from Figure 17 and the thickness of the absorber (Table 4). It is a minimum line width corresponding to a Debye temperature for the alloy absorber equal to that of platinum metal: i.e. about 240°K. The larger width corresponds to a Mossbauer mean free path for the alloy of the equivalent of 2.5 mils of platinum, or a Debye temperature of about 350°K (Figure 14). A third feature of the spectra was also considered: the apparent full width at half maximum, referred to 4.0 cm/sec. However, this parameter was harder to determine experimentally and was less sensitive than the splitting and the resolution to variations in g_1 and $H_{INT}(Pt)$. Consequently, less weight was given to it. From these considerations, we obtained the following numbers:

$$H_{INT}(Pt) = (1.26 \pm 0.10) \times 10^6 \text{ gauss}$$

$$g_1 = -(0.40 \pm 0.10) \text{ nm}$$

The values of $H_{INT}(Pt)$ for the other alloys are listed in Table 4. They were determined by assuming the above value for g_1.

The Mossbauer absorption spectrum for Sample 5, $Pt_{0.50}Fe_{0.50}$, has a much poorer resolution than the others, but the same full width. There are a variety of causes that could be responsible for this. Line broadening, and

TABLE 4

Mossbauer Results With Alloy Absorbers

Source: Au^{195} in Cu

$T \sim 4.2^{o}K$

Absorber	Thickness of Platinum (mg/cm^2)*	Δ (cm/sec)**	Resolution %	H_{INT}(Pt) 10^6 Gauss
$Pt_{0.03}Fe_{0.97}$	191	2.10±0.10	16±2	1.26 ± 0.10
$Pt_{0.10}Fe_{0.90}$	131	2.12±0.10	15±2	1.26± 0.10
$Pt_{0.25}Fe_{0.75}$	268	2.05±0.10	16±2	1.24 ± 0.10
$Pt_{0.30}Fe_{0.70}$	295	2.32±0.15	19±3	1.38 ± 0.12
$Pt_{0.50}Fe_{0.50}$	655	---	---	~1.1

* 54.5 mg/cm^2 of platinum is the equivalent of 1.0 mils of platinum metal

** 1.0 cm/sec = 3.3×10^{-6} ev

change in intensity pattern because of the thick sample certainly contribute, although not enough to account for the low resolution. A quadrupole broadening is unlikely (see below), but a spectrum of magnetic fields arising from non-equivalent sites is a possibility. In any case, the width of the curve demands a high magnetic field.

A quadrupole interaction will split a level of spin 3/2 into two sublevels of $m=\pm 3/2$ and $m=\pm 1/2$ with a separation of $\Delta E_Q = e^2Qq/2$ where Q is the quadrupole moment of the nucleus and eq is the electric field gradient at the nucleus. eq is assumed here to be axially symmetric. If a magnetic interaction is also present, and if the electric field symmetry axis does not have a unique direction with respect to the magnetic field, the quadrupole interaction will broaden the Mossbauer magnetic spectrum. We define a quantity γ: (P-56)

$$\gamma = \frac{e^2Qq}{6g(3/2)H}$$

$6g(3/2)H$ for the 99 KeV level of Pt^{195} is 9.4×10^{-6} ev. For a quadrupole moment of one barn and an electric field gradient of 10^{18} volts/cm^2, e^2Qq is 10^{-6} ev and γ is 0.11. For this value of γ, the broadening of each line in the 6 line magnetic spectrum would be about 0.12 cm/sec (P-56). Since the line width is about 2 cm/sec, this effect would be almost indetectable. Moreover, an eq of 10^{18} volts/cm^2 is a larger field gradient than one expects to find in a cubic alloy of low impurity concentration such as $Pt_{0.03}Fe_{0.97}$. For example, eq in hexagonal osmium metal has been measured as $(3.5 \pm 0.5) \times 10^{17}$ volts/cm^2. (GC-66). Therefore no reasonable quadrupole interaction could be detected, nor could it affect the values of g_1 and H_{INT} deduced from our spectra.

Benczer-Koller et al (B-KHR-65) have also used the Mossbauer effect to investigate the g-factor of the 99 KeV $3/2^-$ state of Pt^{195}. Using Fe-Pt alloys as absorbers, they obtained velocity spectra similar to ours, but with a greater width and apparent splitting. For example, their 10 at% Pt absorber gave an apparent splitting of (2.58 ± 0.27) cm/sec. They did not fit their data with a unique set of g_1 and $H_{INT}(Pt)$, but took the Ho and Phillips (HP-65) calorimetric determination of the hyperfine field at Pt in a 3 at% Pt alloy: 1.39×10^6 gauss. With this number, they found $-0.6 \leq g_1 \leq -0.45$. Their large apparent splitting suggests that the internal field in their alloy was larger than the internal field in our alloy. Since they did not supply the details of the fabrication of their alloys, one cannot even speculate as to how the method of preparation, especially the heat treatment, might affect the internal field.

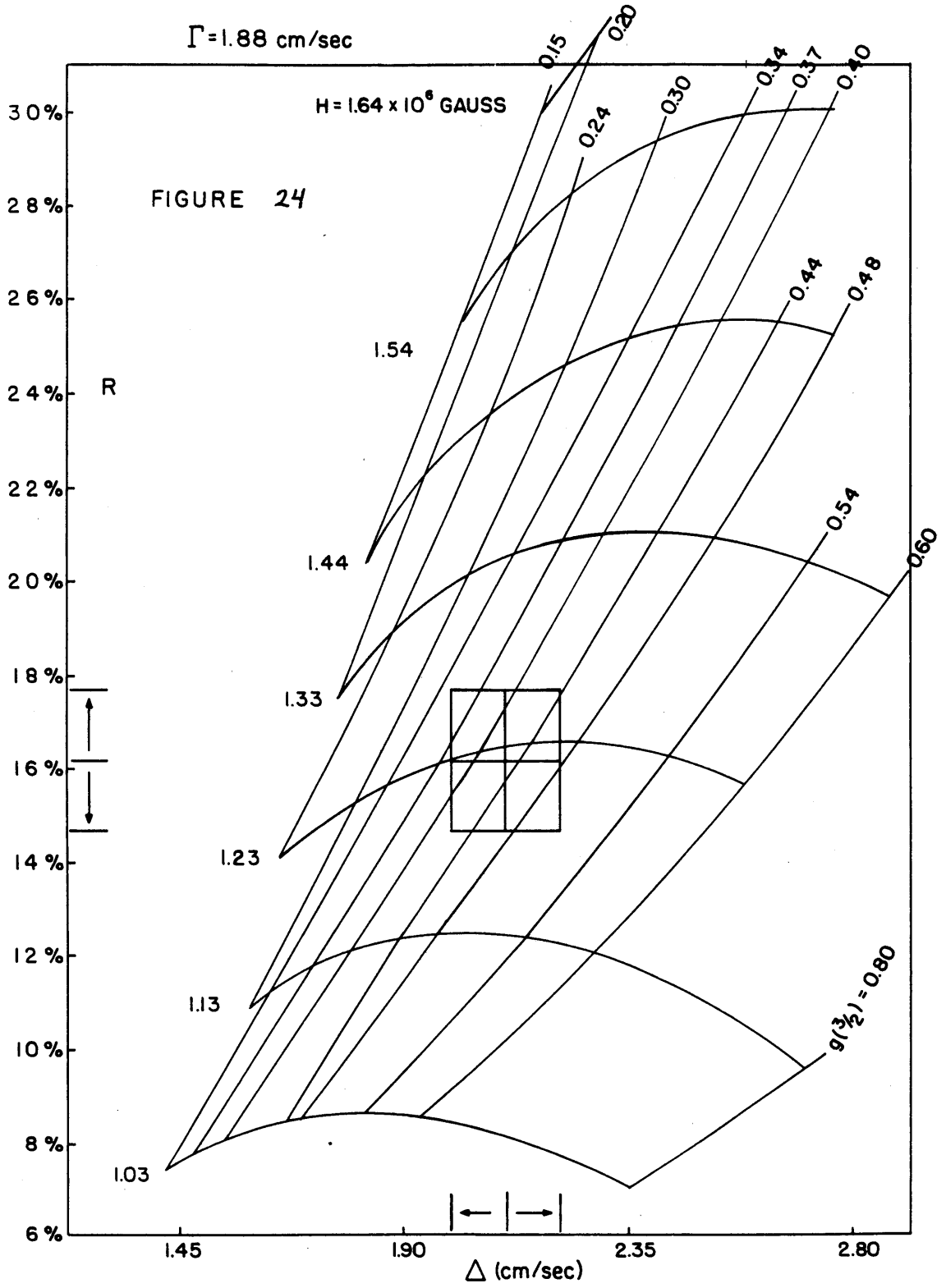
Γ = 1.88 cm/sec
H = 1.64 x 10⁶ GAUSS
0.15
0.20
0.24
0.30
0.34
0.37
0.40
0.44
0.48
0.54
0.60
g(3/2) = 0.80
1.54
1.44
1.33
1.23
1.13
1.03
R
30%
28%
26%
24%
22%
20%
18%
16%
14%
12%
10%
8%
6%
1.45
1.90
2.35
2.80
Δ (cm/sec)

FIGURE 24

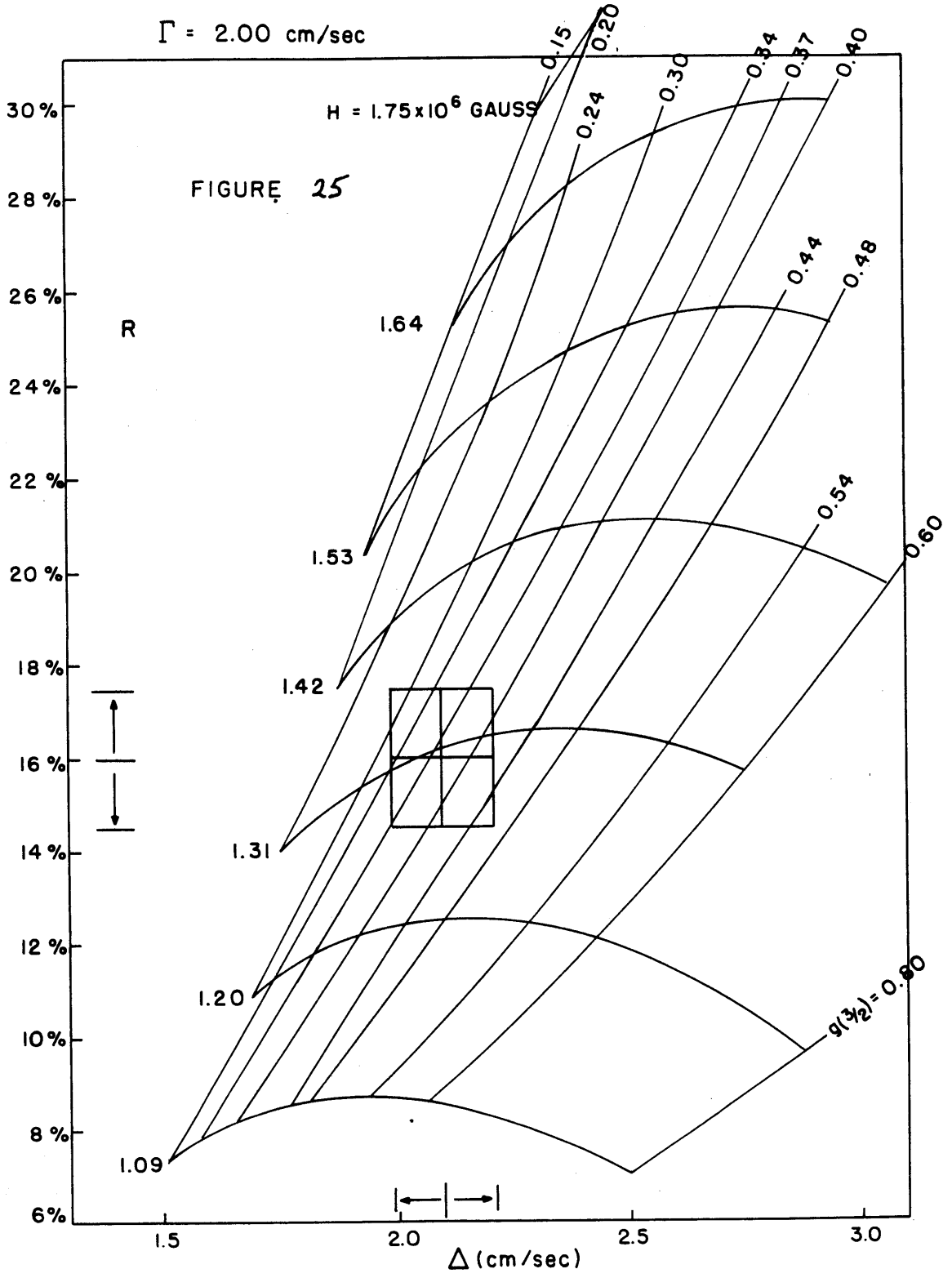
Γ = 2.00 cm/sec
H = 1.75x10^6 GAUSS
FIGURE 25
R
30%
28%
26%
24%
22%
20%
18%
16%
14%
12%
10%
8%
6%
1.5
2.0
2.5
3.0
Δ (cm/sec)
0.15
0.20
0.24
0.30
0.34
0.37
0.40
0.44
0.48
0.54
0.60
g(3/2)= 0.80
1.64
1.53
1.42
1.31
1.20
1.09

Fig. 26

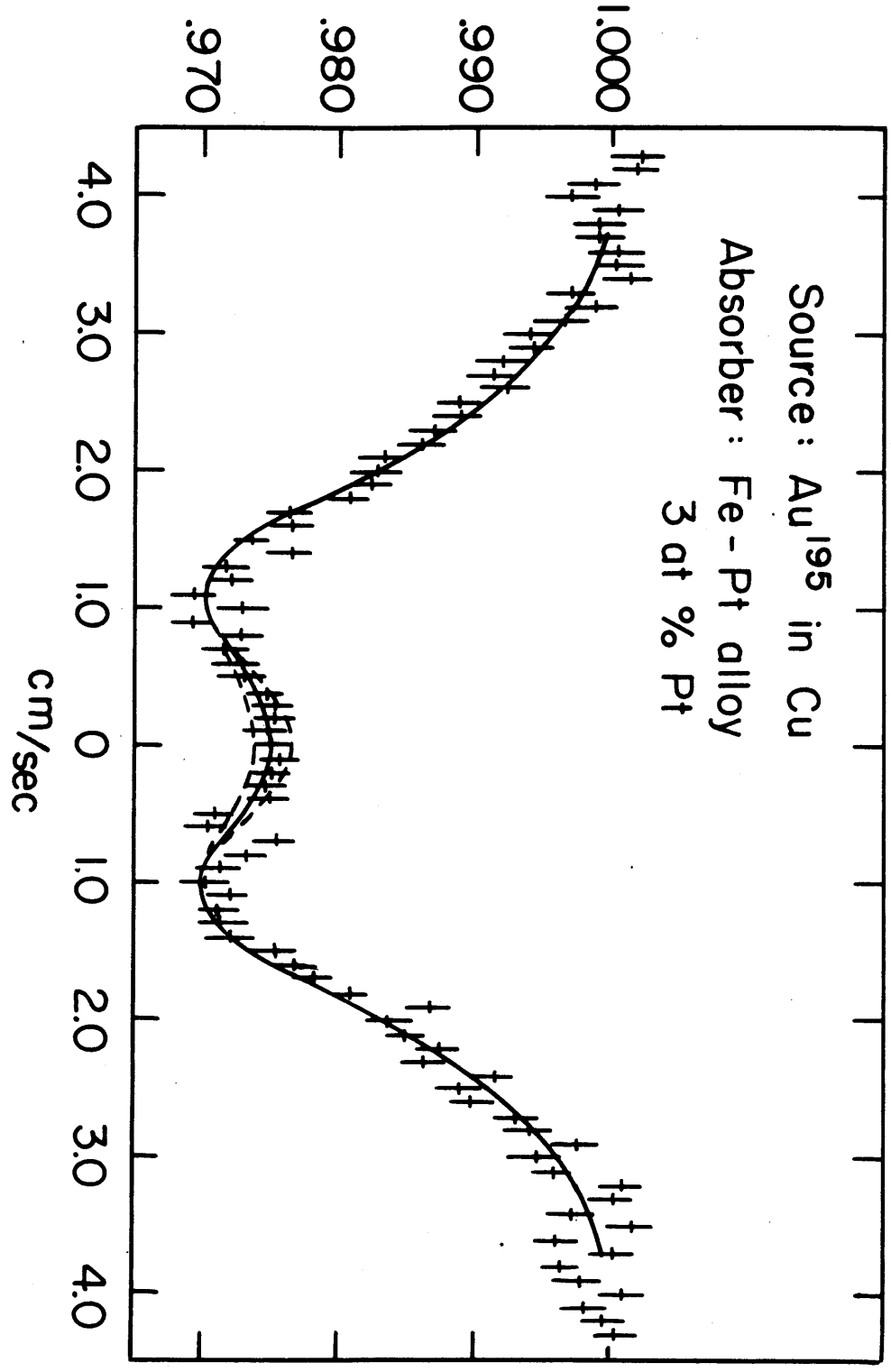
1.000
.990
.980
.970
Source: Au^{195} in Cu
Absorber: Fe-Pt alloy
3 at % Pt
4.0
3.0
2.0
1.0
0
1.0
2.0
3.0
4.0
cm/sec

4. Discussion of $H_{INT}(Pt)$ Results

In Section III-G, $H_{INT}(Pt)$ is shown to be negative. The magnitude and sign of $H_{INT}(Pt)$ observed in these alloys fit in well with internal fields measured for neighboring elements dissolved in iron (Table 5). Accurate theoretical calculations for these fields have not been done, but several mechanisms have been proposed that are in large part borne out by experiment. The dominant contributions to $H_{INT}(Pt)$ in iron comes from the polarization of the conduction electrons by the ferromagnetic iron due to s-d exchange coupling, and from core polarization due to a localized 5d moment on the platinum atoms. A rough estimate can be made of the contributions of these two mechanisms. Neutron diffraction results on Co-Pt and Fe-Pd alloys suggest that the localized moment on the Pt atom in Fe-Pt alloys over a wide range of alloy composition is about $0.3u_B$.(CWK-65). From Knight shift experiments[1] on Pt the hyperfine field per spin from core polarization is about -2.4×10^6 gauss per spin; thus the CP contribution to the internal field at the platinum nucleus is of the order of -0.35×10^6 gauss. For a negative conduction electron spin density at the Pt sites (SW-65), the hyperfine field is -34×10^6 gauss per spin (CJY-64); thus 0.05 unpaired conduction electrons are sufficient to account for the remaining -0.91×10^6 gauss contribution to $H_{INT}(Pt)$.

Fallot (F-38) has measured the magnetization of Fe-Pt alloys and plotted the average atomic moment versus platinum concentration. We have superposed our internal field results on his curve in Figure 27. Our points follow his curve up to 25 at% Pt; then the magnetization falls, but the internal field remains high.

1. (CJY-64)

TABLE 5

Internal Fields at the Nuclei of Several Elements Dissolved in Iron*

Solute Atom	Internal Field (gauss)
Os	$\lvert(1.145 \pm 0.025) \times 10^6\rvert$**
	$\lvert 1.40 \quad 10^6\rvert$
Ir	$-(1.35 \pm 0.30) \quad 10^6$
Pt	$\lvert 1.39 \quad 10^6\rvert$
	$-(1.26 \pm 0.10) \quad 10^6$ (THIS WORK)
Au	$-(1.42 \pm 0.18) \quad 10^6$
	$\lvert(1.35 \pm 0.05)\rvert \quad 10^6$
Hg	$-(0.98 \pm 0.28) \quad 10^6$

* Taken from the article and compilation of Shirley and Westenbarger (SW-65)

** Taken from the article and compilation of Shirley (S-66)

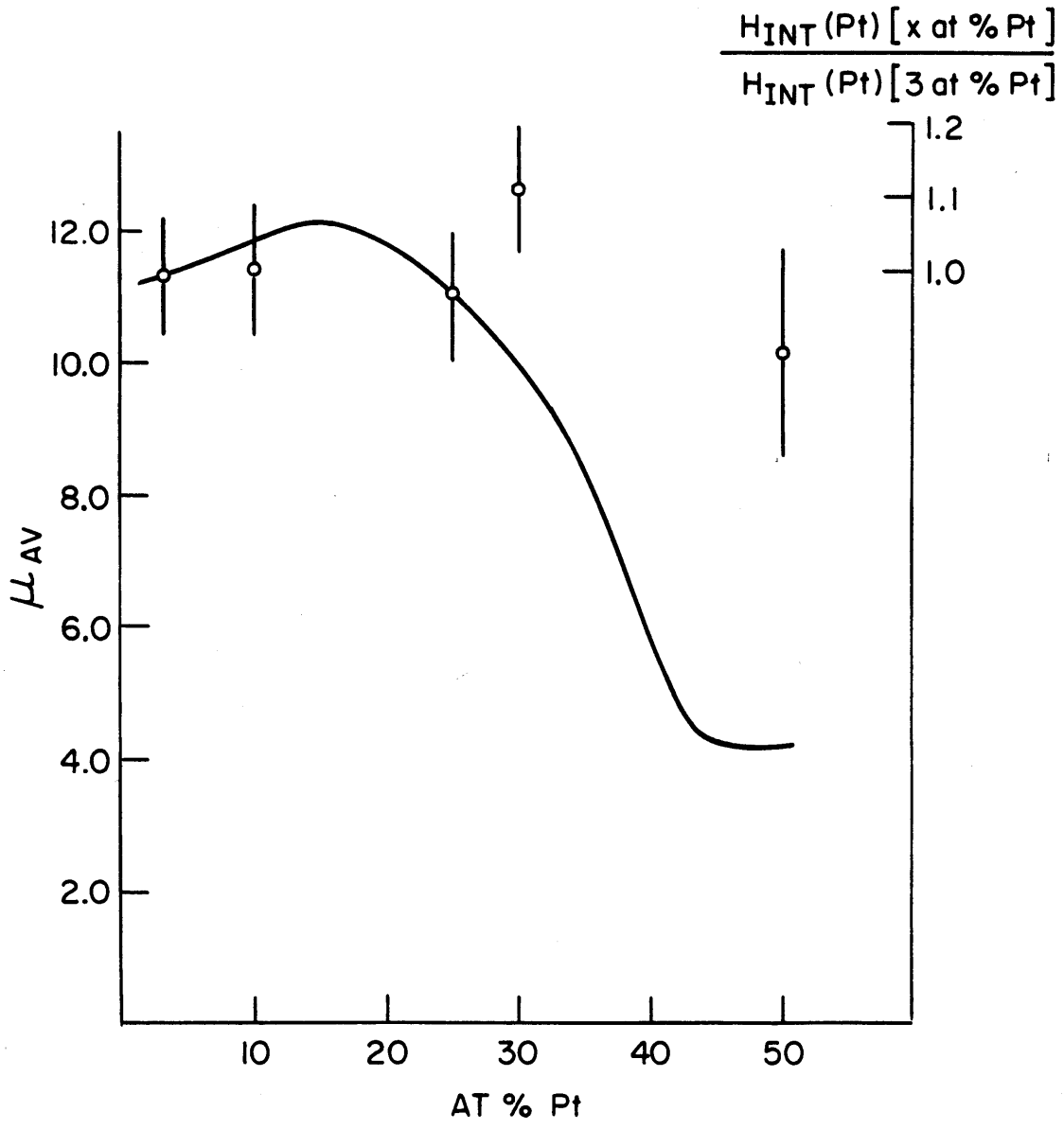
$\frac{H_{INT}(Pt)[x \text{ at \% Pt}]}{H_{INT}(Pt)[3 \text{ at \% Pt}]}$
1.2
1.1
1.0
12.0
10.0
8.0
6.0
4.0
2.0
μ_{AV}
10
20
30
40
50
AT % Pt

Figure 27

III. Pt^{192}, Pt^{194} and Pt^{196}

A. Background: Angular Correlation

The gamma ray distribution from a state $I > 1/2$ will in general be anistropic if the m state populations, m_I, are unequal. Various methods exist for preparing oriented nuclei which then yield non-isotropic radiation (GTH-65). One such method is to observe the direction of emission of a previous radiation. Specifically, let us consider the case of a gamma-gamma cascade. (The literature is extensive and detailed review articles are available (S-65; KMS-64). The following pages present merely a brief survey).

A nucleus in the state I_A goes to the state I_B with the emission of γ_1, then to the state I_C by the emission of γ_2. If we call the direction of emission of γ_1 the z - axis, the state I_B may have an unequal population of m_z - states. In that case the intensity of γ_2 depends on the angle it makes with the z - axis. Experimentally, γ_1 and γ_2 are detected by two counters, and are proved to have come from the same nucleus by being detected in coincidence. The angular distribution, or correlation, of γ_2 with respect to the direction of emission of γ_1 can be written:

$$W(\theta) = 1 + A_2P_2(\cos\theta) + A_4P_4(\cos\theta) + \ldots A_{2\nu}P_{2\nu}(\cos\theta)$$

where 2ν is given by the smallest of the three quantities $2I_B$, $2L(\gamma_1)$ and $2L(\gamma_2)$. Usually P_4 is the highest term because of the rarity of octupole cascades. The coefficients A_2 and A_4 depend on the five parameters I_A, I_B, I_C, L_1 and L_2. If the multipolarity of one or both of the gamma rays is not pure, interference terms may radically change the value of A_2 and A_4 for even a small admixture. (FIG 28; AW-58; C-58).

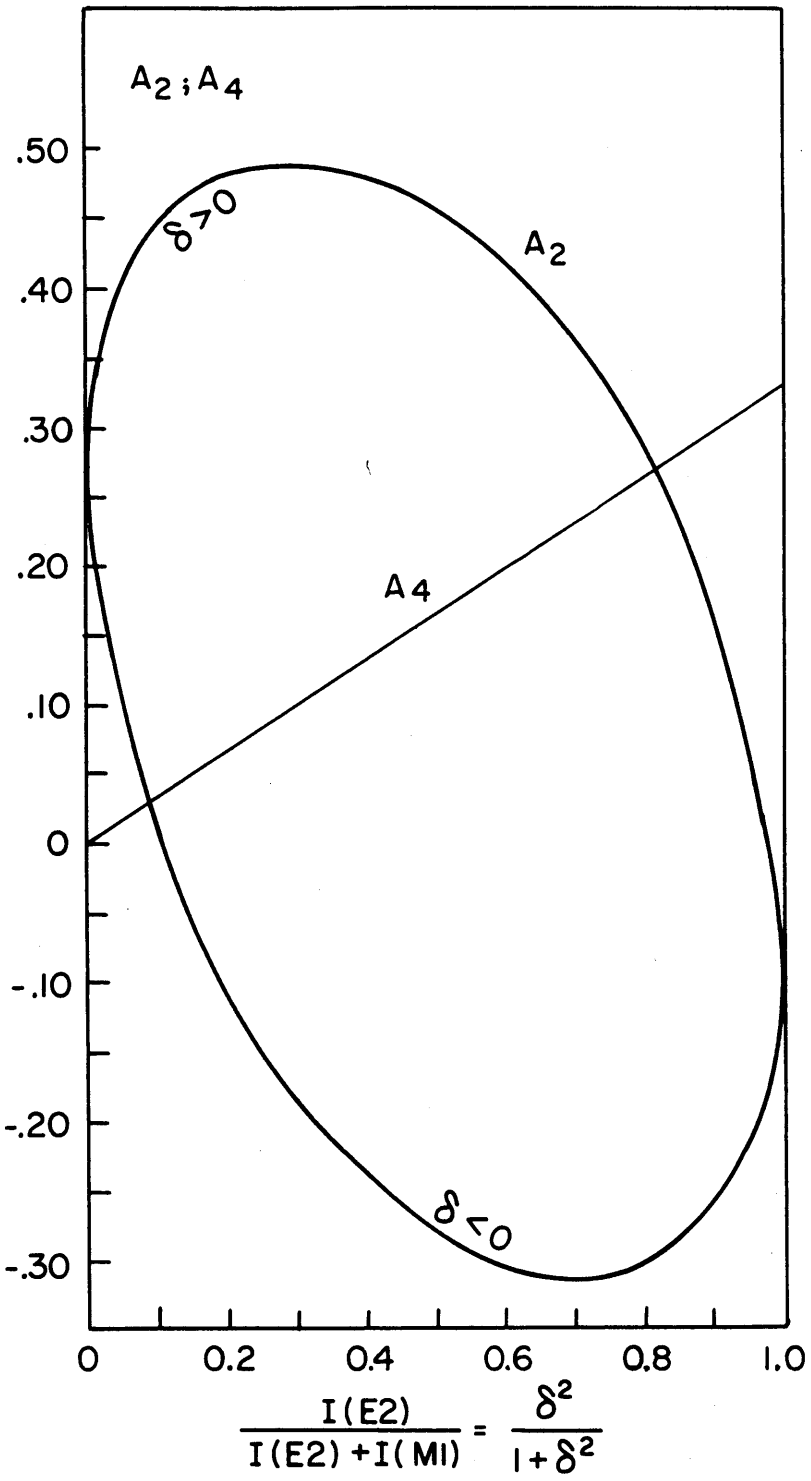

Figure 28

CORRELATION COEFFICIENTS FOR A MIXED 2-2-0 CORRELATION

[2(MI ; E2)2(E2)0]

Measurement of coincidences at three angles uniquely determines A_2 and A_4. For example:

$$A_2 = \frac{50W(180^\circ) + 40W(135^\circ) - 90W(90^\circ)}{7W(180^\circ) + 56W(135^\circ) + 42W(90^\circ)}$$

$$A_4 = \frac{48W(180^\circ) - 96W(135^\circ) + 48W(90^\circ)}{7W(180^\circ) + 56W(135^\circ) + 42W(90^\circ)}$$

Figure 29 shows the theoretical angular correlations for the 4 - 2 - 0 and 0 - 2 - 0 cascades. The 0 - 2 - 0 case is the most anisotropic $\gamma - \gamma$ correlation observed so far.

Perturbed Angular Correlations

The above discussion assumes that the m - state population of the intermediate level does not change during its lifetime. If, however, a magnetic field with a component perpendicular to the direction of γ_1 is applied, the m - state population becomes time dependent. The nuclear spin I_B precesses about the direction of the magnetic field with the Larmor frequency:

$$W = \frac{g\, u_N\, H}{\hbar}$$

where g is the gyromagnetic ratio of the intermediate level. The angular correlation also rotates, and if the intermediate level lives long enough, this rotation can be used to measure the magnetic interaction.

The angular correlation without an applied magnetic field is conveniently written:

$$W(\theta, H = 0) = b_o + b_2 \cos 2\theta + b_4 \cos 4\theta$$

where

$$b_o = 9/64\, A_4 + 1/4\, A_2 + 1$$
$$b_2 = 5/16\, A_4 + 3/4\, A_2$$
$$b_4 = 35/64\, A_4$$

Fig. 29

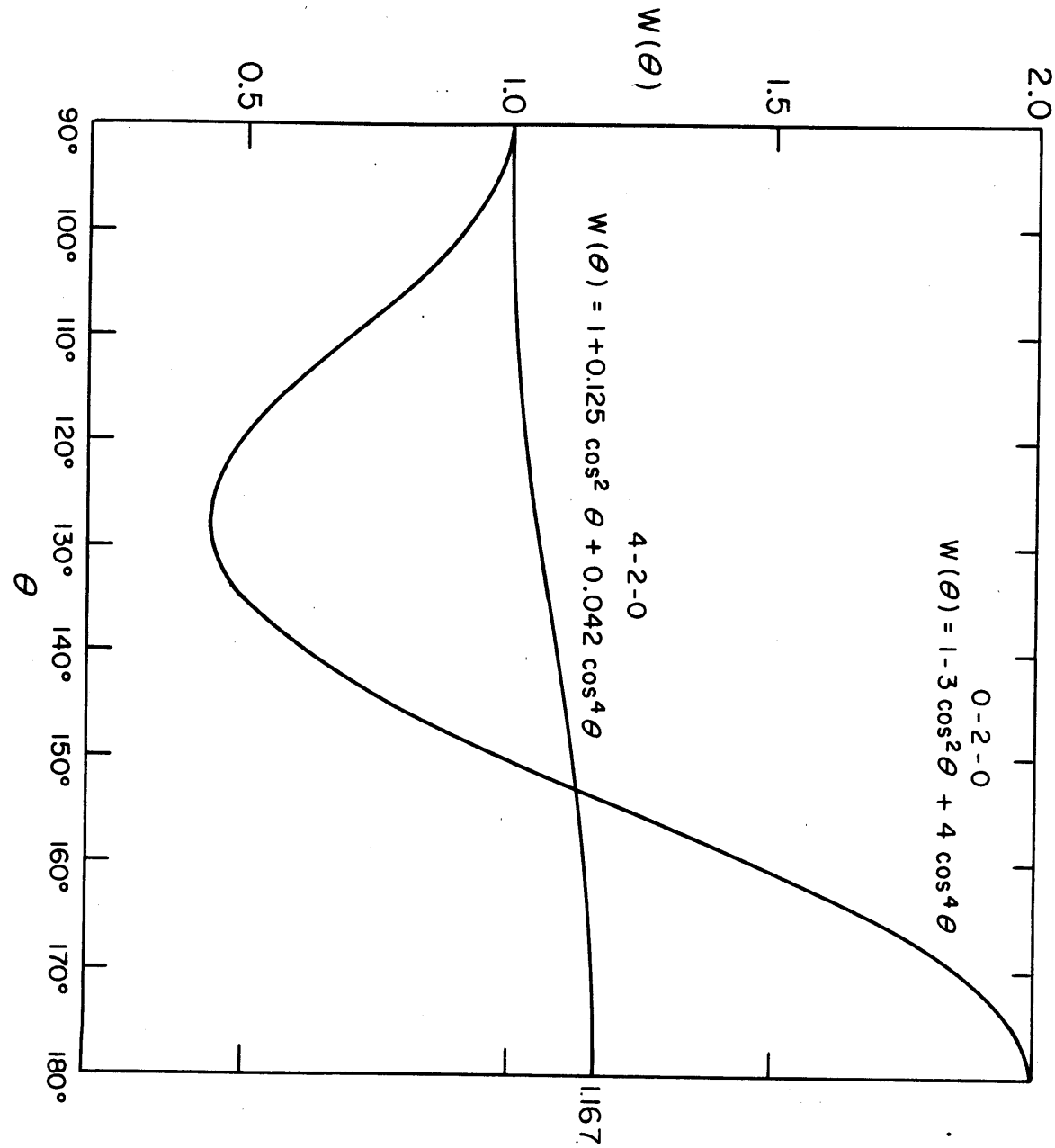
W(θ)
0.5
1.0
1.5
2.0
90°
100°
110°
120°
130°
140°
150°
160°
170°
180°
θ
W(θ) = 1+0.125 cos² θ + 0.042 cos⁴ θ
4-2-0
W(θ) = 1-3 cos²θ + 4 cos⁴ θ
0-2-0
1.167

If a magnetic field is applied perpendicular to the plane determined by the two gamma rays the correlation becomes:

$$W(\theta, H, t) = W(\theta - wt, H = 0)$$

Intergrated over time this gives:

$$W(\theta,H) = b_o + \frac{b_2}{1 + 4 w^2\tau^2} \cos 2(\theta - \Delta\theta_2) + \frac{b_4}{1 + 16w^2\tau^2} \cos 4(\theta - \Delta\theta_4)$$

where $\tan n\,\Delta\theta_n = nw\tau$

In practice, the magnetic interaction is most easily measured by observing the change in coincidence rate when the magnetic field is reversed. This effect is largest at the angle for which $\frac{dW}{d\theta}$ is a maximum. The field reversal effect is given by:

$$\frac{W(\uparrow) - W(\downarrow)}{W(\uparrow) + W(\downarrow)} = \frac{2w\ (G_2b_2 \sin 2\theta + 2G_4b_4 \sin 4\theta)}{b_o + G_2b_2 \cos 2\theta + G_4b_4 \cos 4\theta}$$

where $G_n = \frac{1}{1 + n^2w^2\tau^2}$. G_2 and G_4 are plotted as a function of $w\tau$ in Figure 30.

The attenuation of the correlation may also be used to measure the magnetic interaction. However this method is not sufficiently accurate to be practical unless $w\tau$ is at least 0.20. If a randomly oriented magnetic field is present, the correlation will not be rotated, but it will be attenuated.

The angular correlation is given by (CFW - 62; MRS - 65):

$$W(\theta) = 1 + G_2 A_2 P_2 (\cos\theta) + G_4 A_4 P_4 (\cos\theta) + \ldots\ldots$$

where $$G_n = \frac{1}{2n+1} \sum_{N=-n}^{+n} \frac{1}{1 + N^2 w^2 \tau^2} .$$

G_2 and G_4 for the case of a randomly oriented magnetic field are plotted in Figure 31. Such a field may be found, for example, at nuclei dissolved in iron when there is no external aligning field present.

Electric quadrupole fields also attenuate and rotate the correlation. The analysis becomes extremely complicated when both electric and magnetic perturbations are present and are of comparable magnitude. The problem has been examined both for the case of a unique orientation of the electrostatic field gradient with respect to the magnetic field direction (AMSS - 63) and for the case of randomly oriented field gradients (SMS -62). If, however, the quadrupole frequency $W_Q = \frac{e^2 Qq}{4I(2I-1)\hbar}$ is much smaller than the magnetic frequency $W_B = \frac{gHu_N}{\hbar}$, the main effect is a small decrease, $\Delta\theta_Q$, in the angle of rotation of the correlation. $\Delta\theta_Q$ for small quadrupole interactions varies linearly with W_B/W_Q. In this work, $\Delta\theta_Q$ is presumed negligible. (Section III - G).

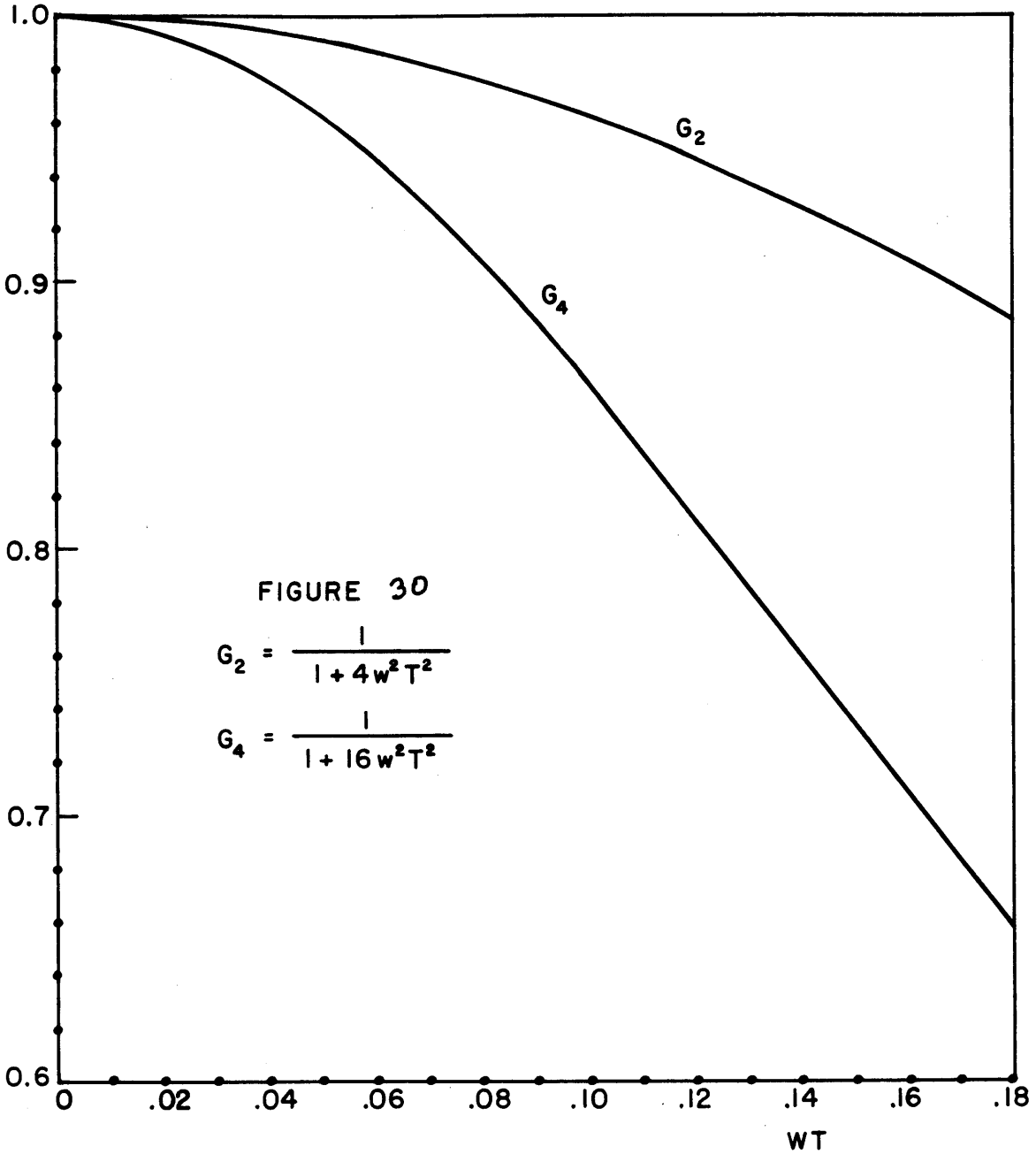

FIGURE 30

$$G_2 = \frac{1}{1 + 4w^2T^2}$$

$$G_4 = \frac{1}{1 + 16w^2T^2}$$

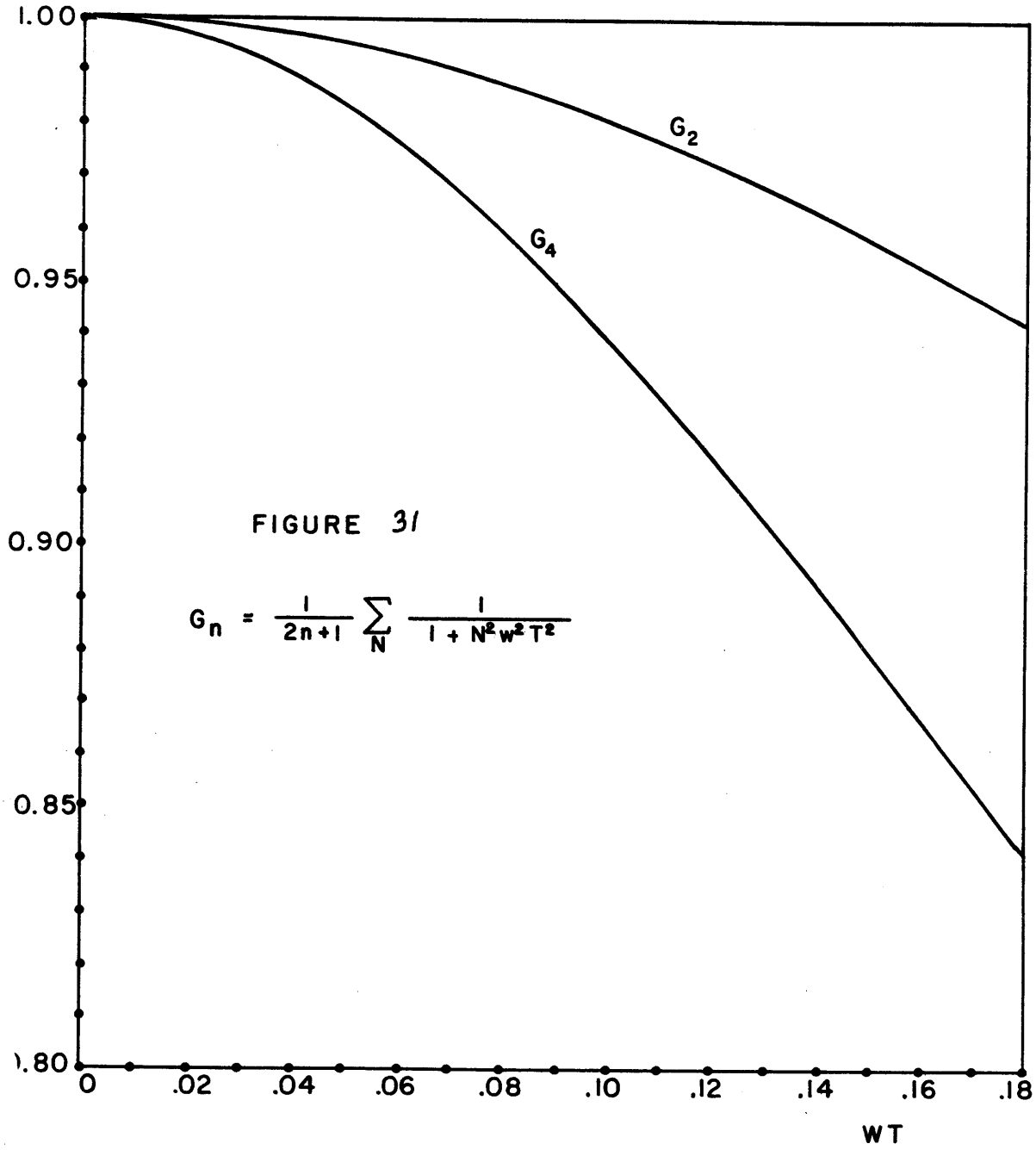

FIGURE 31

$$G_n = \frac{1}{2n+1} \sum_{N} \frac{1}{1 + N^2 w^2 T^2}$$

B EXPERIMENTAL TECHNIQUES

1. Angular Correlation Apparatus

Figure 32 shows the counting arrangement. Counter B and the source were fixed. Counter A could be automatically rotated around the source. Switches were placed at 15° intervals from 180° to 90° to stop the motor drive and reverse it at the end points. These switches also started the counting by the appropriate scalers and the corresponding quadrants of the four hundred channel multi-channel analyzer. Any combination of angles could be selected. However, if coincidences were counted at more than four angles, the multi-channel analyzer could not be used. In experiments described as 4 Angle Angular Correlation (Tables 6, 9, 10, ~~and~~) the angles 180°, 150°, 135°, and 90° were used. In 3 Angle Angular Correlation, the 150° point was omitted.

Both counters were 3x3 inch Na I (Tl) Harshaw Integral Line Detectors with 7.5% resolution for the 662 KeV Cs^{137} line. Lead cones shielded the crystals from background and scattered radiation, and defined the solid angle. The aperture of the cones was 0.75 inches in diameter and was 1.75 inches from the counter face. Thirty mils of cadmium was placed over the aperture of the cones when the Ir^{194} source was used, to stop the high energy β rays.

The aperture of the cones was usually 1.5 inches from the source; in several experiments the distance was slightly greater. This 1½" to ¾" arrangement, called 2/1 Geometry, provided an acceptance angle of $\pm$ 14°. A finite solid angle attenuates the angular correlation: (R-53)

$$W(\theta) = 1+Q_2(\gamma_1)Q_2(\gamma_2)A_2P_2(\cos\theta)+Q_4(\gamma_1)Q_4(\gamma_2)A_4P_4(\cos\theta)$$

$$Q_n = \frac{\int_0^{\Delta\theta} P_n(\cos\beta)N(\beta)\,d(\cos\beta)}{\int_0^{\Delta\theta} N(\beta)\,d(\cos\beta)}$$

β is the angle between a gamma ray direction and the crystal axis. $\Delta\theta$ is the half-angle subtended on the front face or defined by a collimator; in this case $\Delta\theta = 14^{\circ}$. $N(\beta)$ is the photopeak efficiency at the angle β, and depends on the energy of the gamma ray. For $N(\beta) = 1.0$, (energy independent), $Q_2 = 0.956$ and $Q_4 = 0.858$. For our geometry, with 3x3 inch crystals, the energy dependence of $N(\beta)$ does not have much effect on Q_2 and Q_4. Herskind and Yoshizawa (HY-64) have experimentally determined $N(\beta)$ for a 3x3 crystal for several gamma-ray energies and source to counter distances. Taking their results for a 662 KeV gamma ray, we calculate $Q_2 = 0.960$ and $Q_4 = 0.867$. These were the values used for the Pt^{194} correlations. The energy independent values were used for the Pt^{192} and Pt^{196} correlations, which involved lower energy gamma-rays.

Two types of sources were used: alloy wire sources and liquid sources (see Section III-B-2). The alloy sources were placed between the pole pieces of a small electromagnet which provided an aligning field of about 1500 gauss. A pure iron sample requires only a few hundred gauss for saturation. The liquid sources were one-half inch long and were contained in sealed glass tubes of three millimeters outer diameter and one millimeter inner diameter. When a liquid source was being used, it was contained in a stainless steel tube with a screw cap. The wall thickness of the tube was seven mils.

For measurements of A_2 and A_4 with the alloy sources, the field of the magnet was not reversed during the experiment. For the measurement of WT by the Field Reversal Effect, the field was automatically reversed every five minutes. In this case the counter was held fixed. Counts for one field direction were fed into one-half of the multichannel analyzer; counts for the other field direction were fed into the other half. Normalizing singles and timing pulses were also counted for each field direction. The gain of the

photomultipliers did not depend on the field direction. A shift of the singles pulse height spectrum with field reversal was looked for on the multichannel analyzer, and was not detected. Moreover the field direction affected the singles counting rate in the scalers by about 0.1% at most.

Before each run, the source was centered by equalizing the singles counting rate at 180°, 150°, 135°, and 90°. A maximum variation of 1.5% was permitted. This was done both for the angular correlation and the field reversal experiments. In the angular correlation experiments, normalizing singles and timing pulses were counted at each angle.

Stabilizers were used to insure gains did not vary. Singles pulse height spectra were taken before and after each run to check stability.

The multichannel analyzer was a four hundred channel RIDL analyzer. The amplifiers and coincidence circuits were Cosmic plug in units.* The resolving time of the coincidence circuit was measured as fifty nanoseconds by counting accidental coincidences between two separate sources. The accidental to accidental plus true ratio for each experiment was measured by taking the ratio of coincidences with the built-in Delay in and out. The accidental rate was checked several times with the rate computed from the measured resolving time. The accidental rate rarely exceeded 15%, and was usually less.

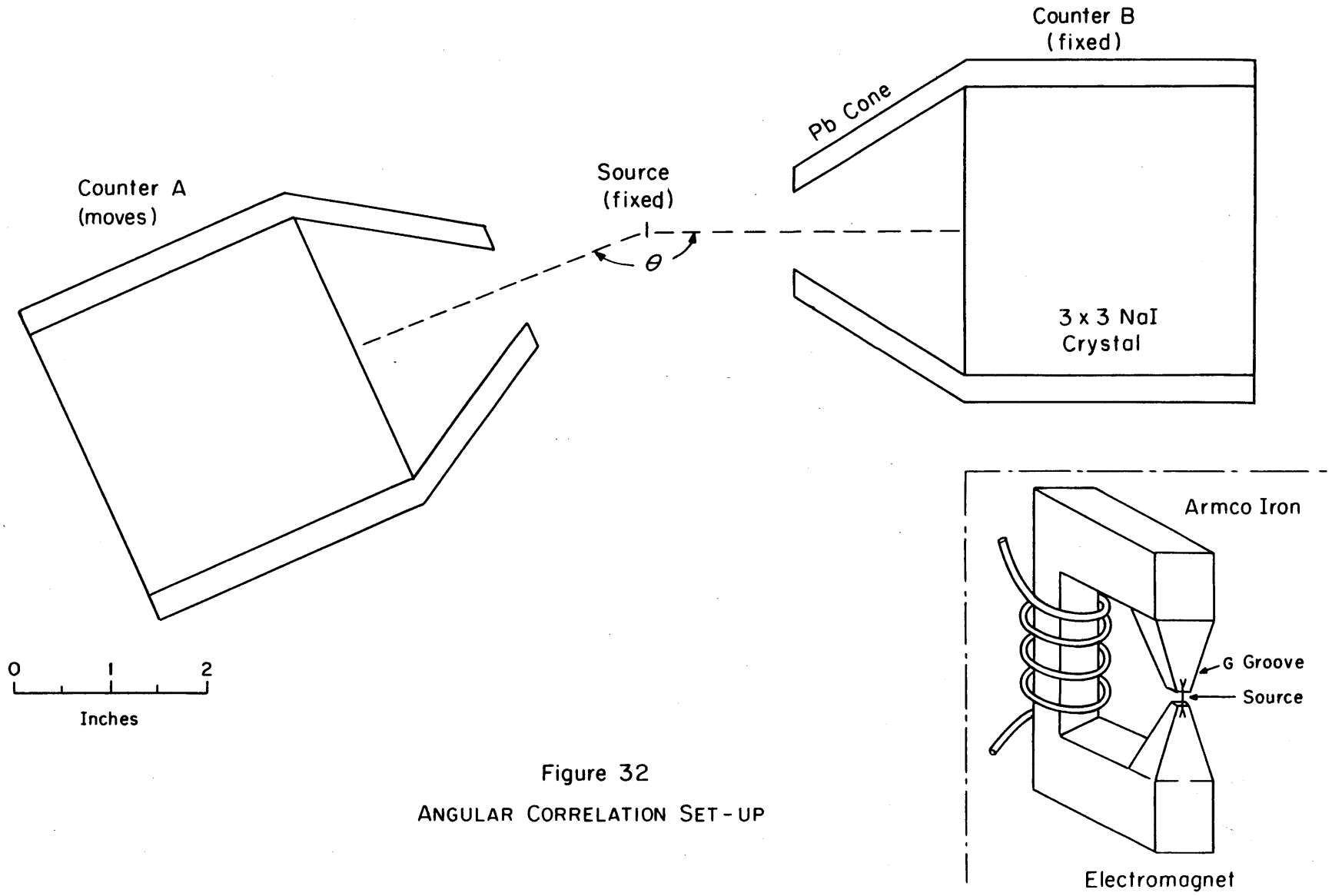

Figure 32

ANGULAR CORRELATION SET-UP

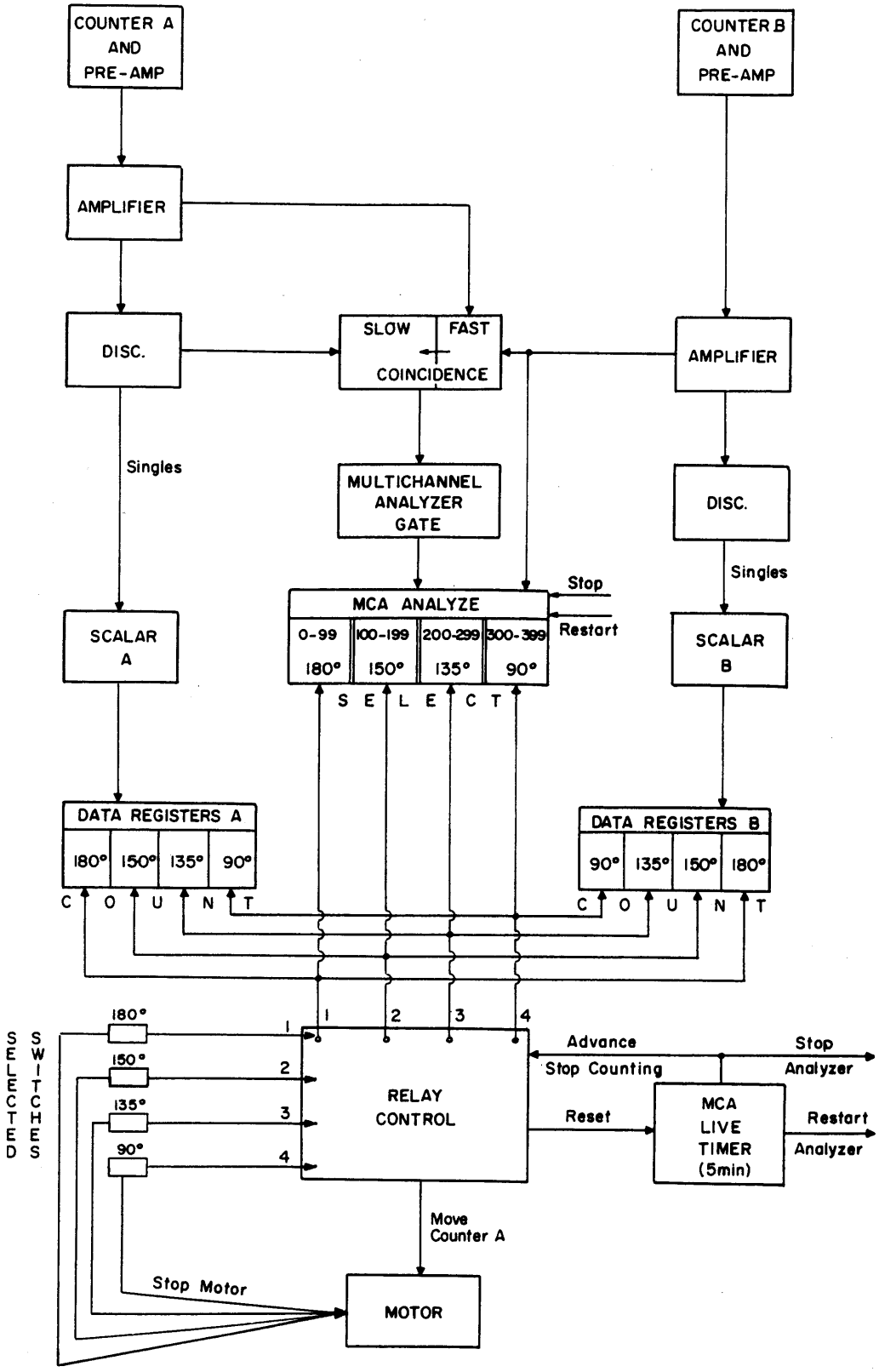

Figure 33

BLOCK DIAGRAM OF ELECTRONICS: MEASUREMENT OF A_2 AND A_4

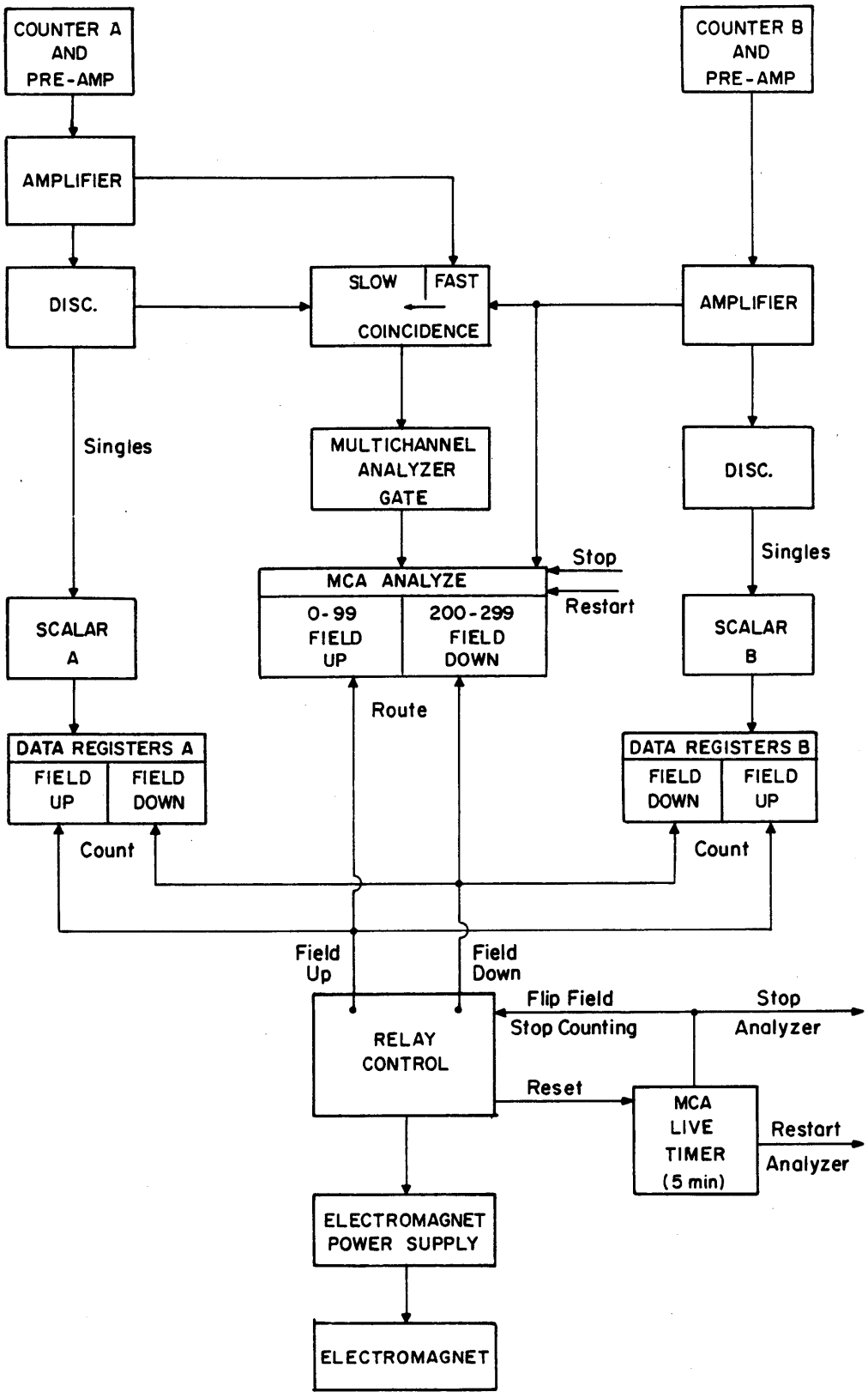

Figure 34

BLOCK DIAGRAM OF ELECTRONICS: FIELD FLIP EFFECT MEASUREMENT

2. Source Preparation

a. Ir^{192} and Ir^{194}

Ir - Fe alloy wire (3 at % Ir) was made by Prof. Wulff of the M. I. T. Metallurgy Department by the following procedure:

Iridium wire (~0.9992 pure) and iron wire (0.999 pure) were melted together ten successive times on a water cooled copper hearth argon arc furnace. The alloy was then encased in stainless steel and swaged cold to 0.070" diameter. The stainless steel was removed and the wire cleaned and swaged to 0.029" diameter ($\sim 1/34$"). The wire was cleaned by abrasion and with H Cl. It was then annealed in hydrogen, being heated up to 1300°C in two hours and slowly cooled in two hours to 600°C and in five hours from 600°C to 30°C. It came out bright and lead soft suggesting no hydrogen pickup.

Ir^{192} and Ir^{194} were produced at the M. I. T. Reactor by a neutron irradiation of the alloy wire.

The reactions are:

Ir^{191} (n,γ) Ir^{192}; 74 days; σ = 960 barns

Ir^{193} (n,γ) Ir^{194}; 19 hours; σ = 130 barns

A 1/8" long piece of wire, irradiated for three minutes at a flux of 8×10^{12} neutrons /cm^2-sec produces 100 u C of Ir^{194} and 4.7 u C of Ir^{192}. The Ir^{192} experiments were performed on sources at least ten days old. No Ir^{194} data was taken with a source over twenty four hours old. The only impurity activity noticed was the 845 KeV gamma ray of 2.6 hour Mn^{56} produced by Fe^{56} (fast n,p) Mn^{56}.

b. Au^{196}

Three types of Au^{196} sources were prepared. The first was Au^{196} in Fe Wire. 1.5 Mil natural platinum foil was bombarded for three hours by fifty microamperes of 14 MeV deuterons in the external beam of the M. I. T. cyclotron. Au^{196} was produced by (d,n) and (d,2n) reactions on Pt^{195} and Pt^{196} respectively. A variety of other isotopes were made; only two are important in this context. Au^{195} was produced by (d,n) and (d,2n) reactions on Pt^{194} and Pt^{195} respectively, and Au^{194} (39 hours) by (d,2n) on Pt^{194}. Au^{194}, decaying to Pt^{194}, emits 294 KeV and 328 KeV gamma rays. Therefore measurements on the Au^{196} 333-356 KeV correlation were not started until the source was eighteen days old, when the Au^{194} activity should have been $\sim$ 1.0% of the Au^{196} activity. Figures **35** and **36** show the pulse height spectra of the source shortly after bombardment and at the start of experiments, respectively. A measurement of the counting rate in the 333-356 KeV peak gave about two millicuries as the total amount of Au^{196} produced by the bombardment.

The bombarded platinum foil was given to Mr. Gruverman of the New England Nuclear Corporation. He separated the gold activity, carrier free, by a solvent extraction process, then plated 20% of the activity, carrier free, onto a 1/2" by 0.014" diameter iron wire and annealed the source for eight hours at 740°C in hydrogen. The recovery was 85%.

Because this source gave a very low value for the g-factor of the 356 KeV level, it was suspected that the magnetic field at the platinum nucleus might be low. (Sections **III-F** and **II-D**).

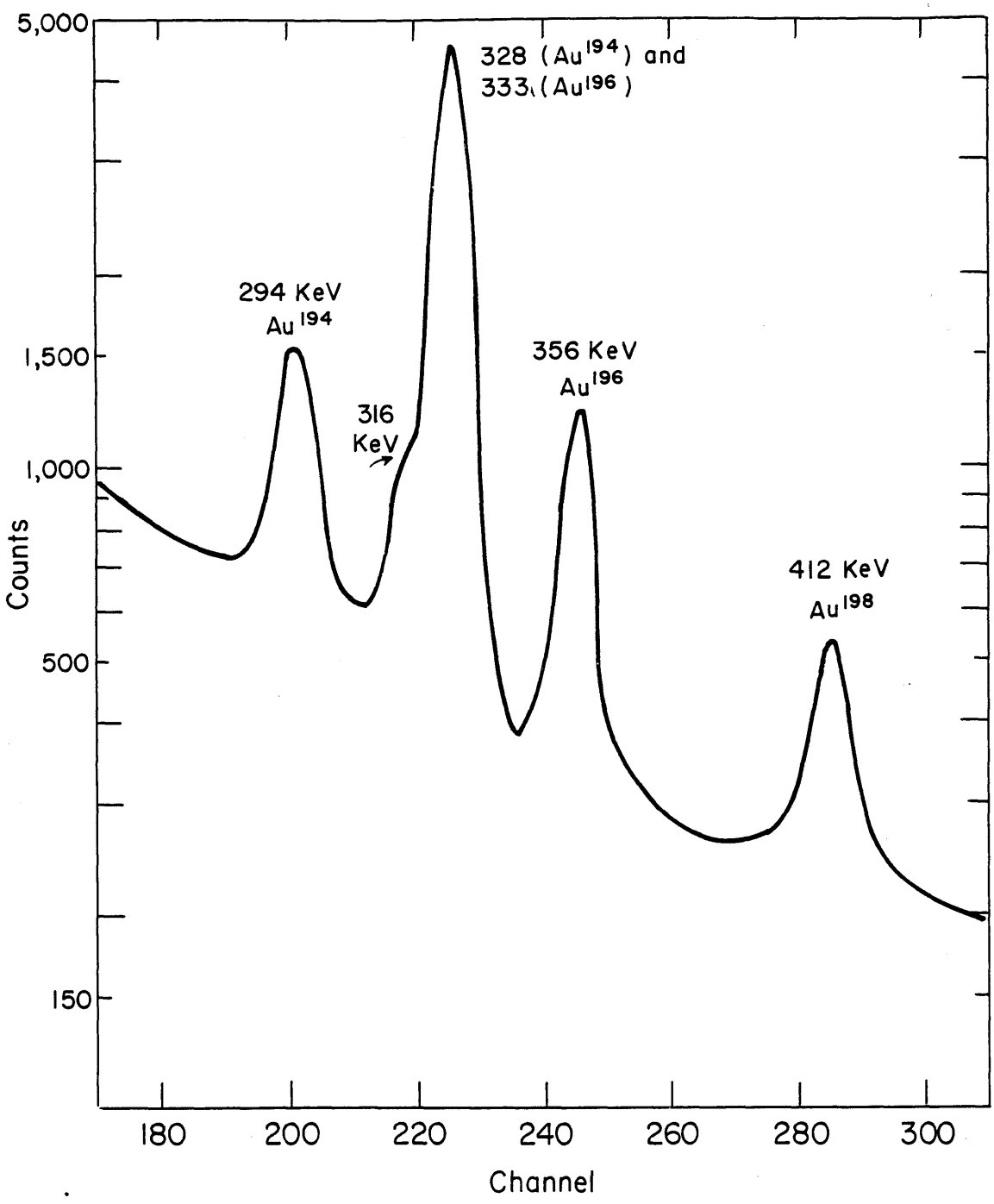

Fig. 35 (Pt foil + d) SOURCE : 10 HOURS OLD
Ge (Li) DETECTOR

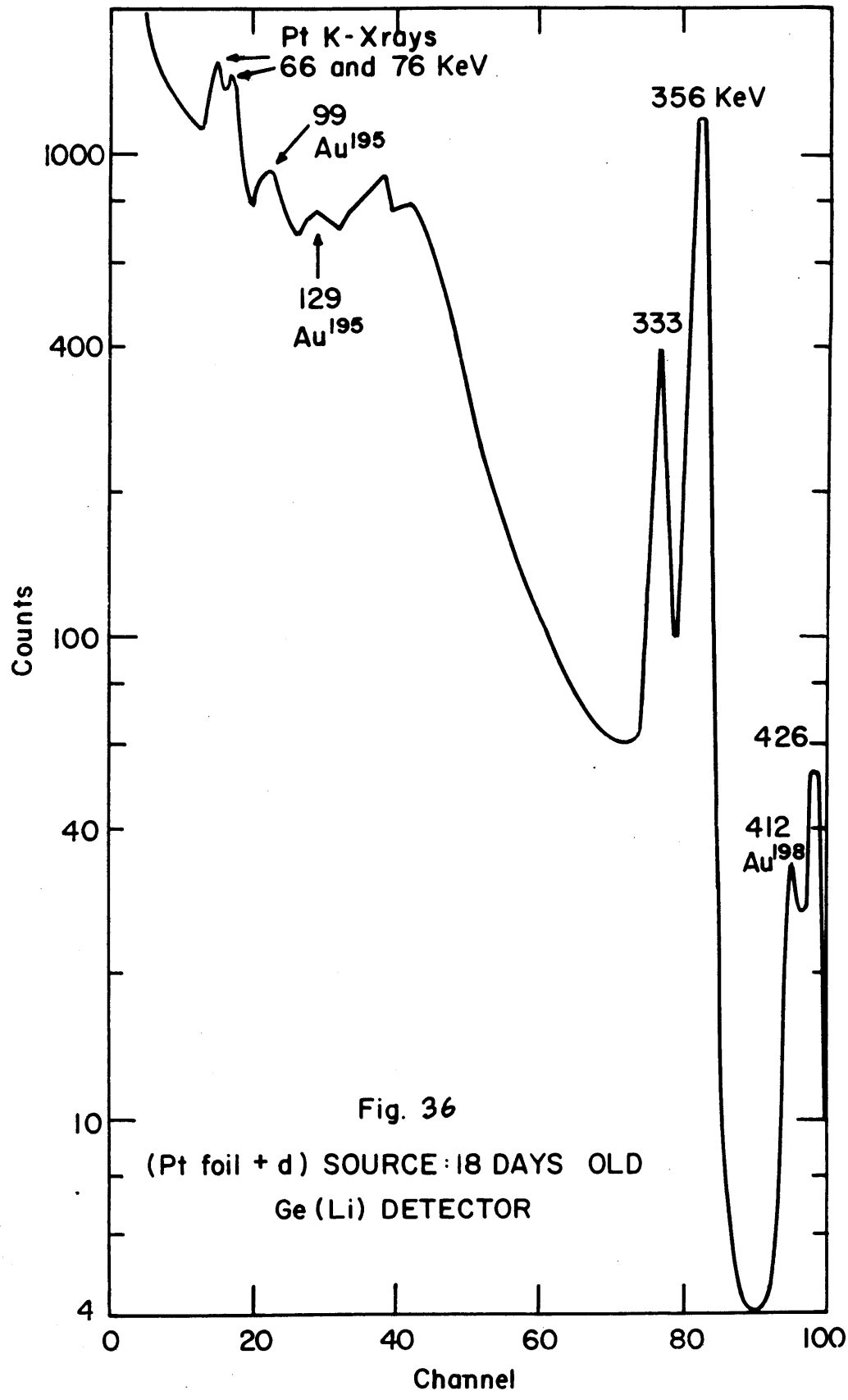

Fig. 36

(Pt foil + d) SOURCE: 18 DAYS OLD

Ge (Li) DETECTOR

Therefore the source was reannealed for fifty-eight hours at 720°C in argon. The source came out rusted, and was cleaned by abrasion and with dilute HCl. Before annealing the wire diameter was 0.014"; after cleaning 0.012". The strength of the source after cleaning was 65% of the strength before annealing, adjusted for decay. Since $\left(\frac{12}{14}\right)^2 = 0.73$, this indicates that the gold diffused deeply into the iron. This source is always referred to as Au^{196} in Fe Wire (Reannealed).

The second source was Au^{196} in Pt-Fe Alloy (3 at% Pt). A small strip of the thin 3 at% Pt Pt-Fe absorber (Section II-B-3) was bombarded with deuterons. This source was useless because of the high background at 333-356 KeV from β^+ emitting Co^{56} (77 days) made by $Fe^{56}(d,2n)\ Co^{56}$ (Figure 37).

The third source was Au^{196} in Pt-Fe Alloy (30 at% Pt). A strip 1/8" long by 1/32" wide was taken from the 0.017" thick 30 at% Pt Pt-Fe absorber (Section II-B-3). It was bombarded with deuterons, annealed for two hours at 1000°C in vacuum and furnace cooled. Figure 38 shows the singles spectrum of this source at the start of experiments, fourteen days after bombardment.

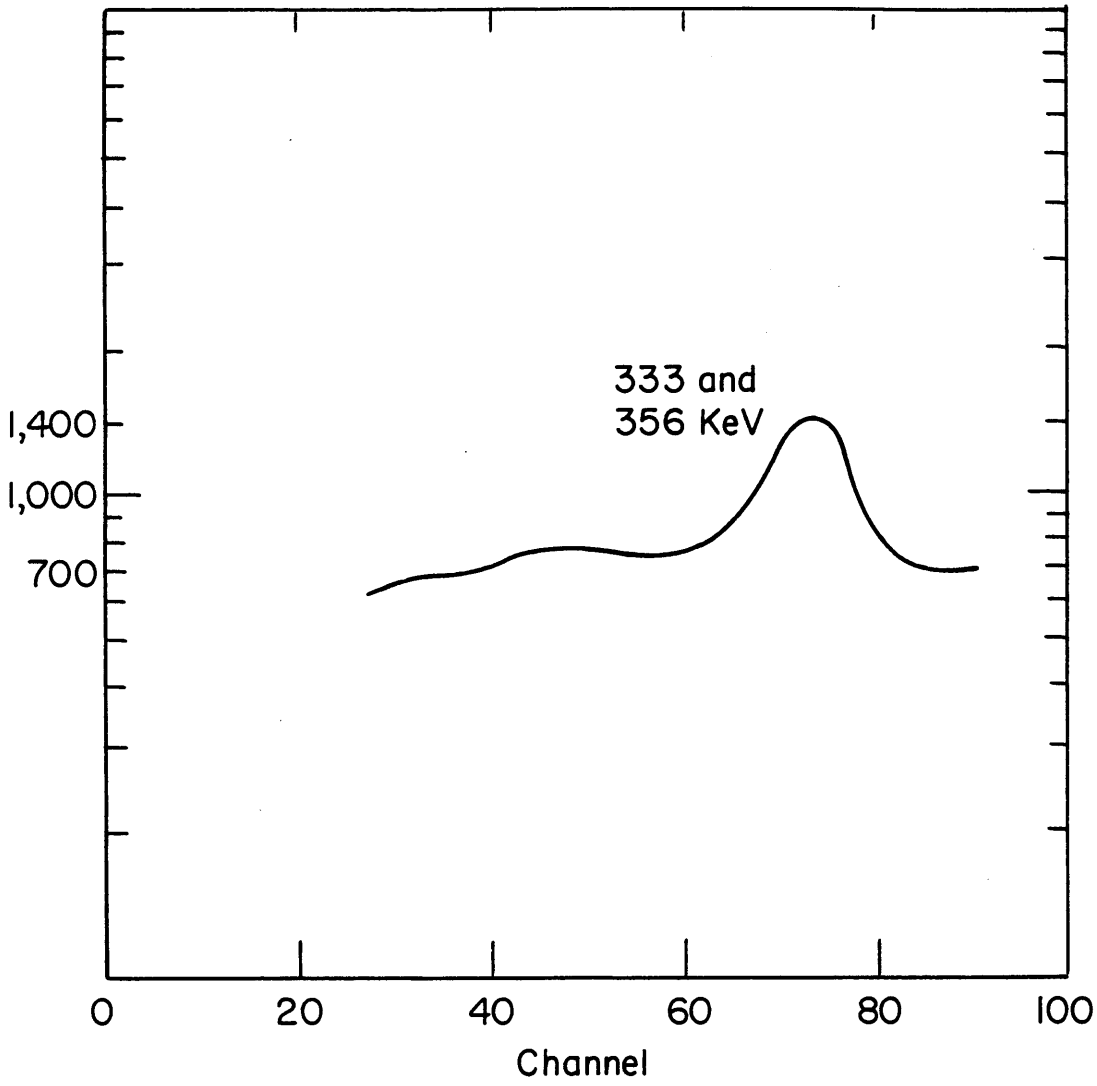

Fig. 37 Au^{196} in Fe - Pt Alloy (3 AT % Pt)

COINCIDENCE SPECTRUM: GATE 333 and 356 KeV

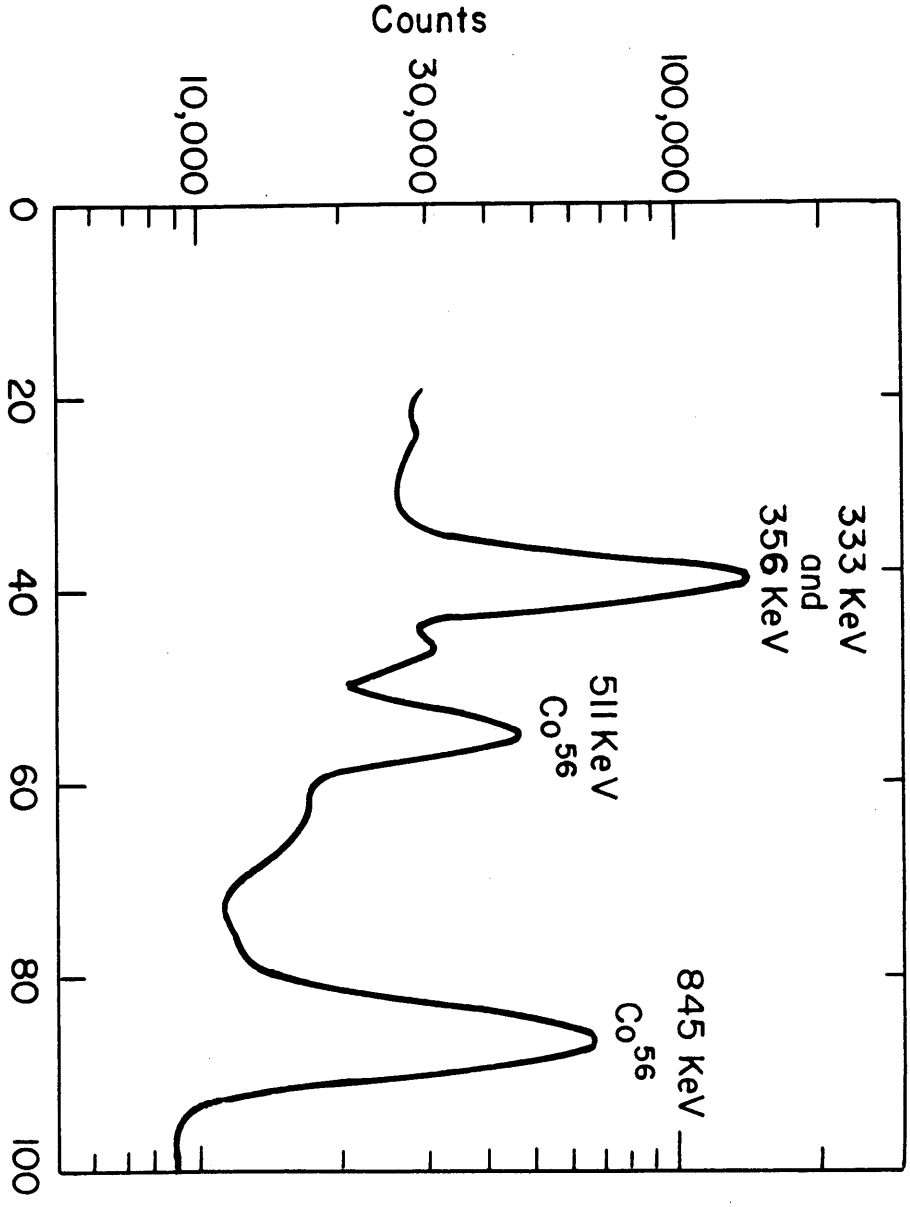

Fig. 38 Au^{196} in Fe-Pt Alloy (30 AT % Pt)
SINGLES SPECTRUM

C. Pt^{192}

1. Introduction

A partial decay scheme of Ir^{192} is shown in Figure 39. A number of weak transitions are left out, although no known level is omitted. The 4-2-0, 468-316 KeV correlation was used to measure the magnetic moment of the 2^+, 316 KeV state.

Figure 40 shows the singles spectrum of Ir^{192}. The arrows indicate the span of the 468 KeV gate. Figure 41 shows the coincidence spectrum obtained with the gate of Figure 40. The source preparation is described in Section III-B-2. Tables 6 and 7 present the results of the experiments.

All the data was taken with a source 1/8" long, at 2/1 Geometry. The accidental to (accidental plus true) ratio for Experiments 1 and 5 was 18%±2%; for Experiments 2 and 3 the ratio was only 6%±1% because the resolving time had been reduced from 100 ns to 60 ns and the source had decayed from 50 uC to 25 uC. Experiment 5 took three days to perform; the others took about one day apiece. The experimental procedure is described ~~in detail~~ in Section III-B-~~3~~.

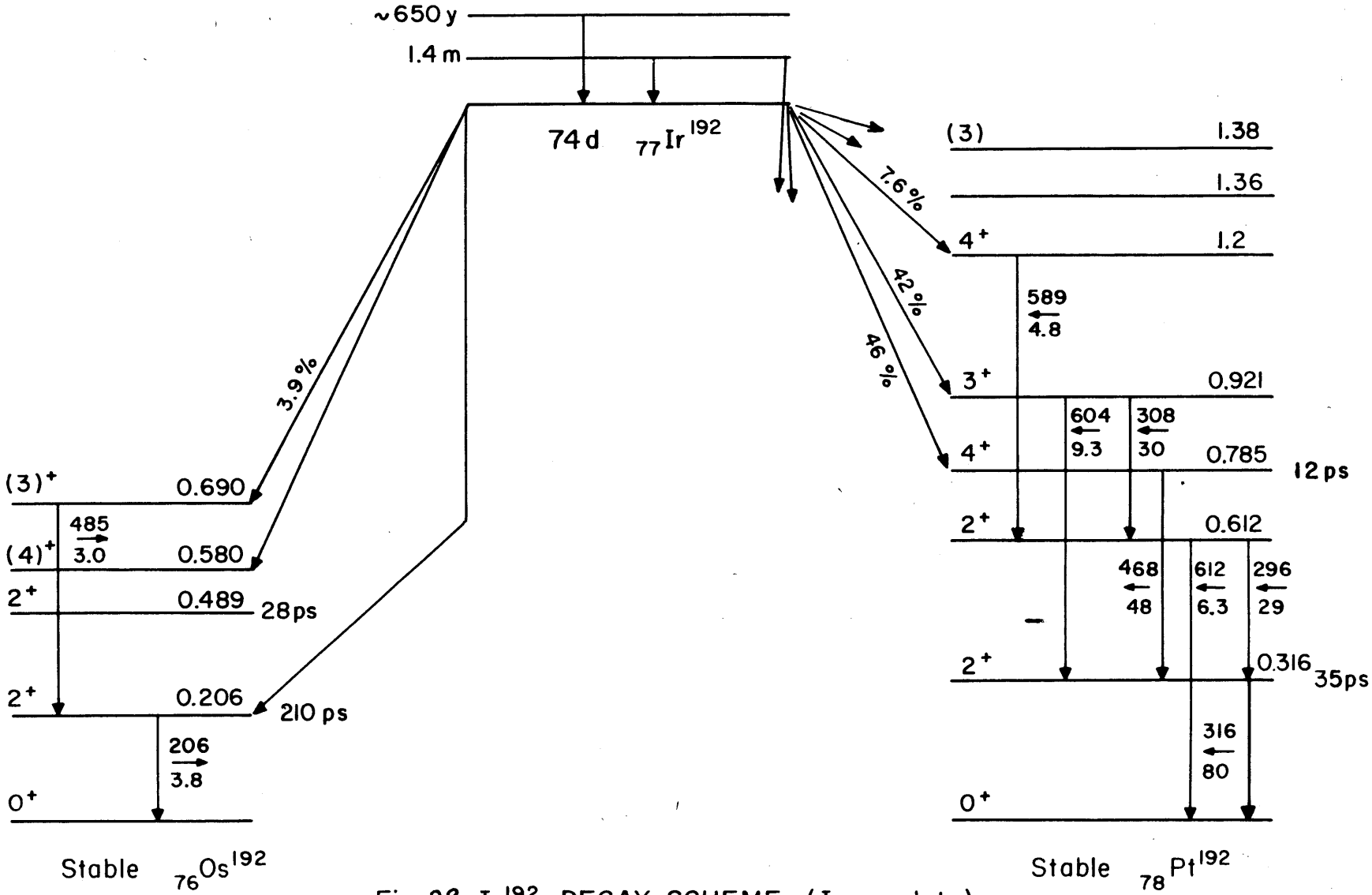

Fig. 39 Ir^{192} DECAY SCHEME (Incomplete)

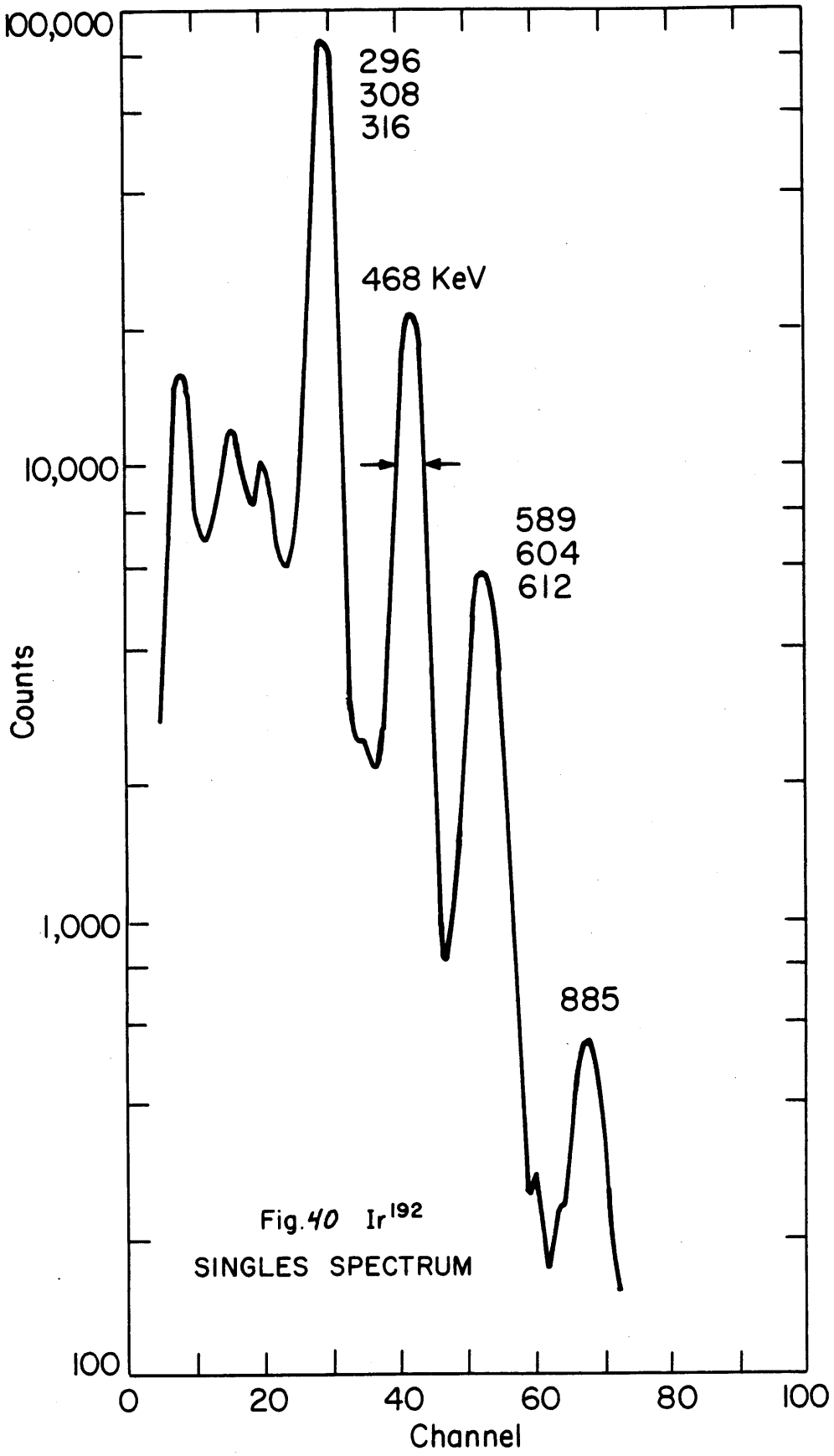

Fig. 40 Ir^{192}
SINGLES SPECTRUM

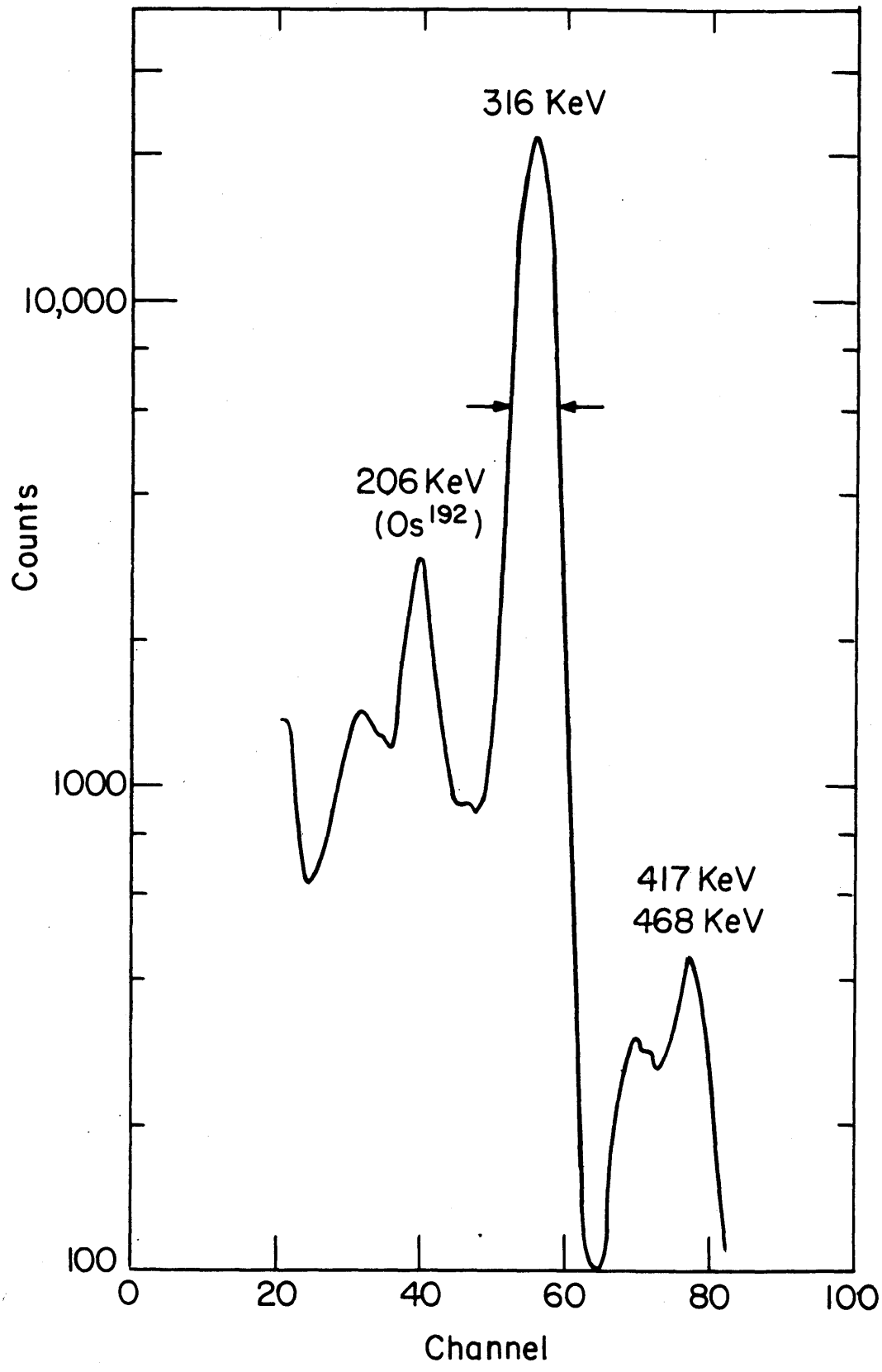

Fig. 41 Ir^{192} COINCIDENCE SPECTRUM: GATE 468 KeV

Table 6

Angular Correlation Coefficients of the

468-316 KeV Correlation in Pt^{192}

Source: Ir^{192} in Ir-Fe Alloy (3 at % Ir)

	Experiment	For 2/1 Geometry	Corrected for Solid Angle	
		G_2b_2/b_0 G_4b_4/b_0	G_2A_2 G_4A_4	A_2 A_4
1	3 Angle Angular Correlation No Aligning Field	-----	$0.094 \pm .003$ $0.008 \pm .004$	$0.096 \pm .003$ $0.008 \pm .004$
2	4 Angle Angular Correlation Aligning Field ↑	$0.064 \pm .003$ $0.002 \pm .002$	-----	-----
3	4 Angle Angular Correlation Aligning Field ↓	$0.062 \pm .003$ $0.002 \pm .002$	-----	-----
4	Average of 2 and 3	$0.063 \pm .002$ $0.002 \pm .001$	$0.092 \pm .003$ $0.005 \pm .003$	$0.095 \pm .003$ $0.006 \pm .004$

Theoretical Correlation Coefficients for

a 4-2-0 Correlation: $A_2 = 0.102$: $A_4 = 0.0091$

TABLE 7

WT for the 316 KeV Level of Pt^{192}

Field reversal experiment at 135° for the

468-316 KeV correlation gave:

$$\left| \frac{N(+)-N(-)}{N(+)+N(-)} \right|_{135^\circ} = 2.40\% \pm 0.15\%$$

WT, using correlation coefficients of Line 1, Table 6 :

0.093 ± 0.007

WT, using correlation coefficients of Line 4, Table 6 :

0.095 ± 0.007

---

3. Interpretation of Results

The decay scheme reveals two possible correlations to use to measure g(316 KeV): the 4-2-0, 468-316 KeV correlation and the 3-2-0, 604-316 KeV correlation. The first, which we have used, is very clean. As Table 8 shows, there is less than 1% contamination from unresolvable cascades. Moreover, this background is nearly isotropic. The background at the 316 KeV coincidence peak from Os^{192} (485-206 + X-ray) coincidences is less than 0.10%. However the 468 KeV gate does contain about 2% 600 KeV group. 40% of this (the 604 KeV gamma ray) is harmless and 35% (the 589 KeV gamma ray) gates nearly isotropic correlations. Thus the total contamination of the 316-468 KeV correlation is about 3%, and the non-isotropic impurity, not going through the 316 KeV level exclusively, is less than 1%.

The correction to $\omega\tau$ is negligible. The correction to the correlation coefficients makes $A_2 = 0.103 \pm .004$ and $A_4 = 0.008 \pm .004$.

In contrast, the 604-316 KeV correlation is very impure. As Table 8 shows, even with the most exclusive selection of gate and counting span, the counting rate in the 612-308 $3\text{-}2^2\text{-}0$ cascade is still nearly 25% that of the 604-316 $3\text{-}2^1\text{-}0$ cascade. The correlations gated by the 589 KeV gamma ray are much weaker than a 3-2-0 correlation (Section): they could be considered isotropic and corrected for. It was concluded that experiments with the 604-316 KeV correlation would be of little value compared to 468-316 results; none worth reporting were done.

Table 8

Purity of the 468-316 KeV and

604-316 KeV Correlations in Pt^{192}

Cascade	Coincidences per 100 Decays of Ir^{192}	Correlation	Percent of the Total Correlation	
468-316	48	4 - 2 - 0	99.1%	1.
417-316	1.4	4 - 4 - 2 - 0	~ 0.8%	
438-316	0.07	(Many Branches)	~ 0.1%	
604-316	9.3	$3 - 2^1 - 0$	55%	2.
589-316	3.9	$4-2^2 - 2^1 - 0$	23%	
589-296	3.9	$4 - 2^2 - 2^1$	8%	
612-308	5.3	$3 - 2^2 - 0$	13%	

1. Calculated from Column 2 and the gate of Figure 40.

2. Calculated from Column 2 and a gate on the low side of the "600" group peak and counting the high side of the "300" group peak.

D. Pt^{194}: 328 KeV Level

1. Introduction

The level scheme of Pt^{194} produced by the decay of Ir^{194} is shown in Figure 42. Figure 43 shows the gamma ray transitions important for this work. The 0-2-0, 939-328 KeV and the 0-2-0, 1151-328 KeV correlations were used to measure the magnetic moment of the 2^+, 328 KeV state. Both correlations are highly contaminated, but much of the background either goes through the 328 KeV level exclusively or is nearly isotropic. The background is analyzed in detail in Section III-D-3.

Figure 44 shows the singles spectrum of Ir^{194}. The arrows indicate the span of the "300" KeV group gate. Figure 45 shows the coincidence spectrum obtained with the gate of Figure 44. The arrows indicate the portions of the 939 KeV and 1151 KeV groups that were analyzed. The source preparation is described in Section III-B-2. Tables 9 to 11 present the results of the experiments.

All the data was taken at 2/1 Geometry. The wire sources were all 1/8" long. The liquid sources were sealed in 3mm OD glass tubing; the length of the sources was about 1/2". The average accidental to accidental plus true ratio varied between 6% and 12%; for each experiment the average ratio was known to $\pm$ 15%. The Ir^{194} source strengths varied between 50 and 100 uC at the end of irradiation. No source older than twenty-four hours was used. Experiment 1 took four days to perform; Experiments 2, 6, and 7 took two days each; and Experiments 3, 4, and 8 required one day apiece. The experimental procedure is described ~~in detail~~ in Section III-B-3.

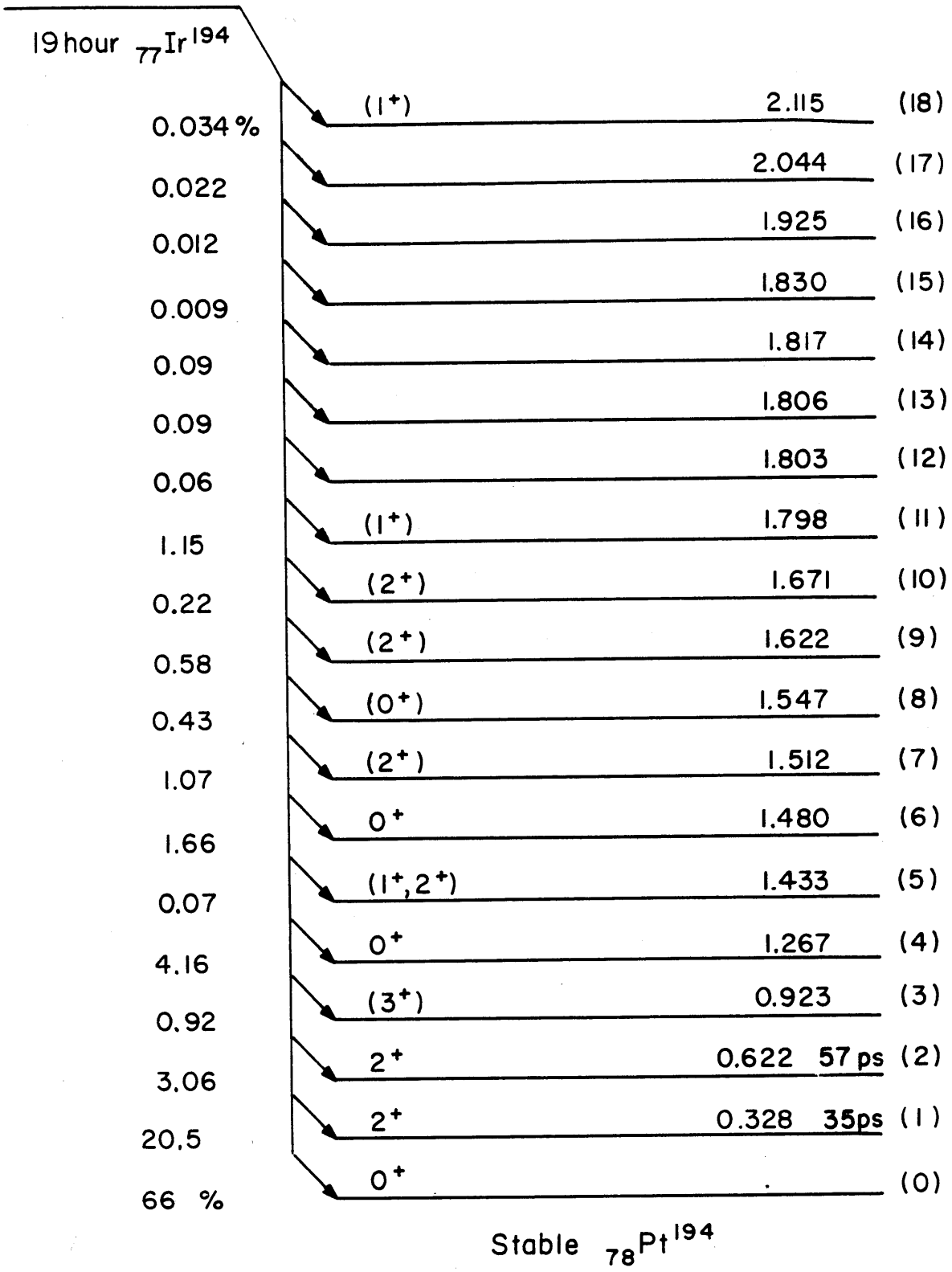

Fig. 42 LEVELS OF Pt^{194} (Fed from Ir^{194})

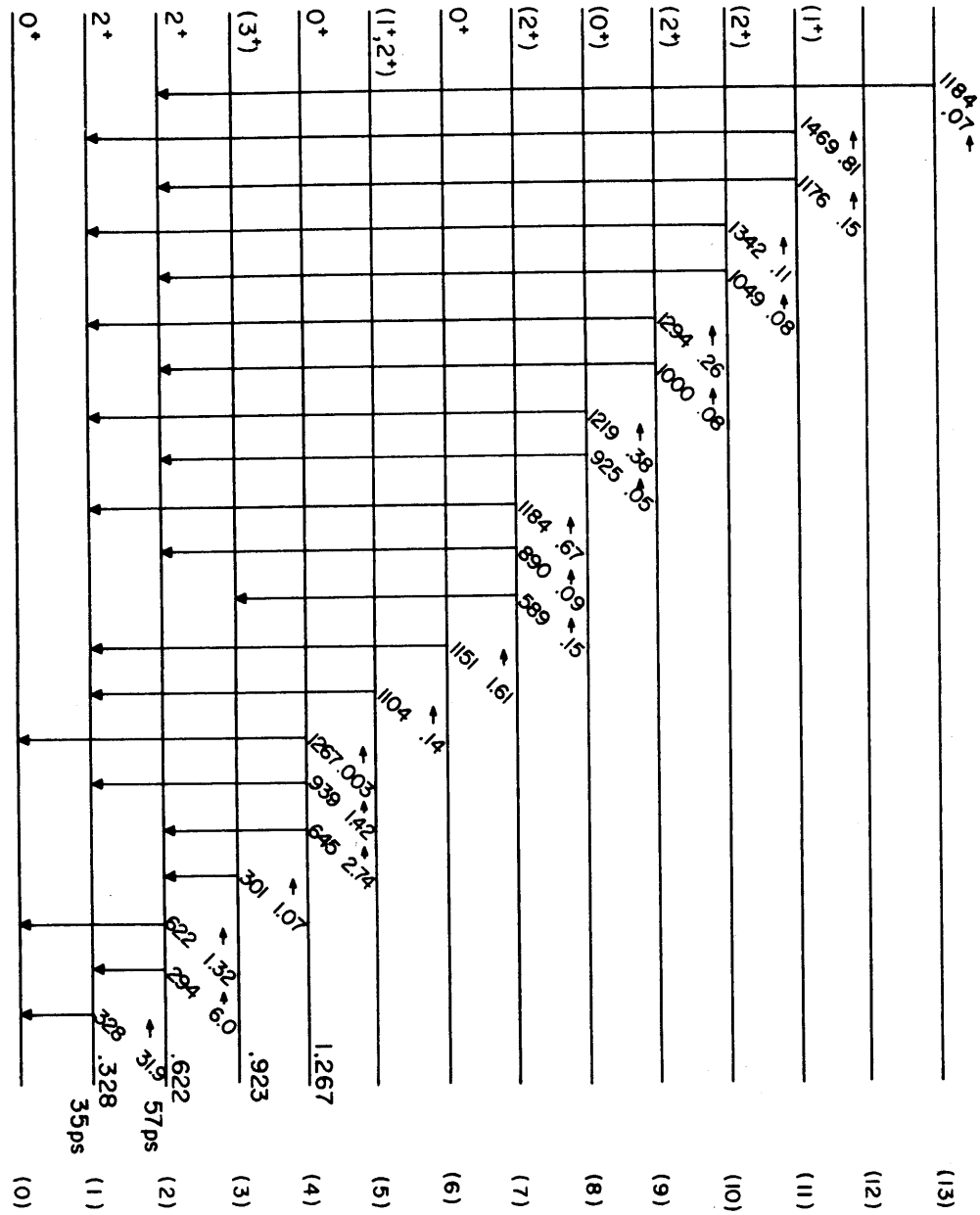

Fig. 43 TRANSITIONS OF Pt^{194} FED FROM Ir^{194} (Incomplete)

(Transitions to Ground State from Levels ≥ 5 Omitted)

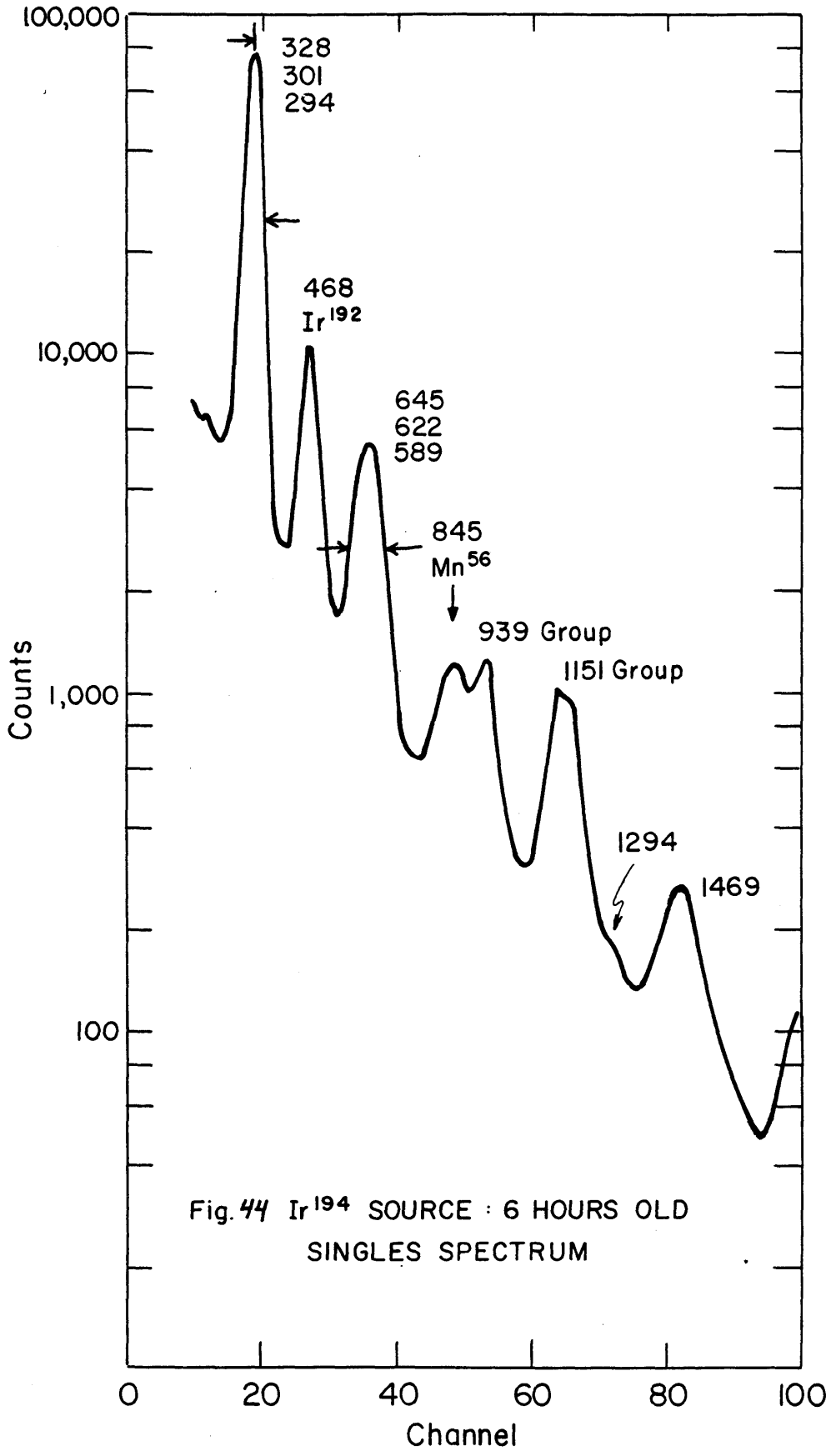

Fig. 44 Ir^{194} SOURCE : 6 HOURS OLD
SINGLES SPECTRUM

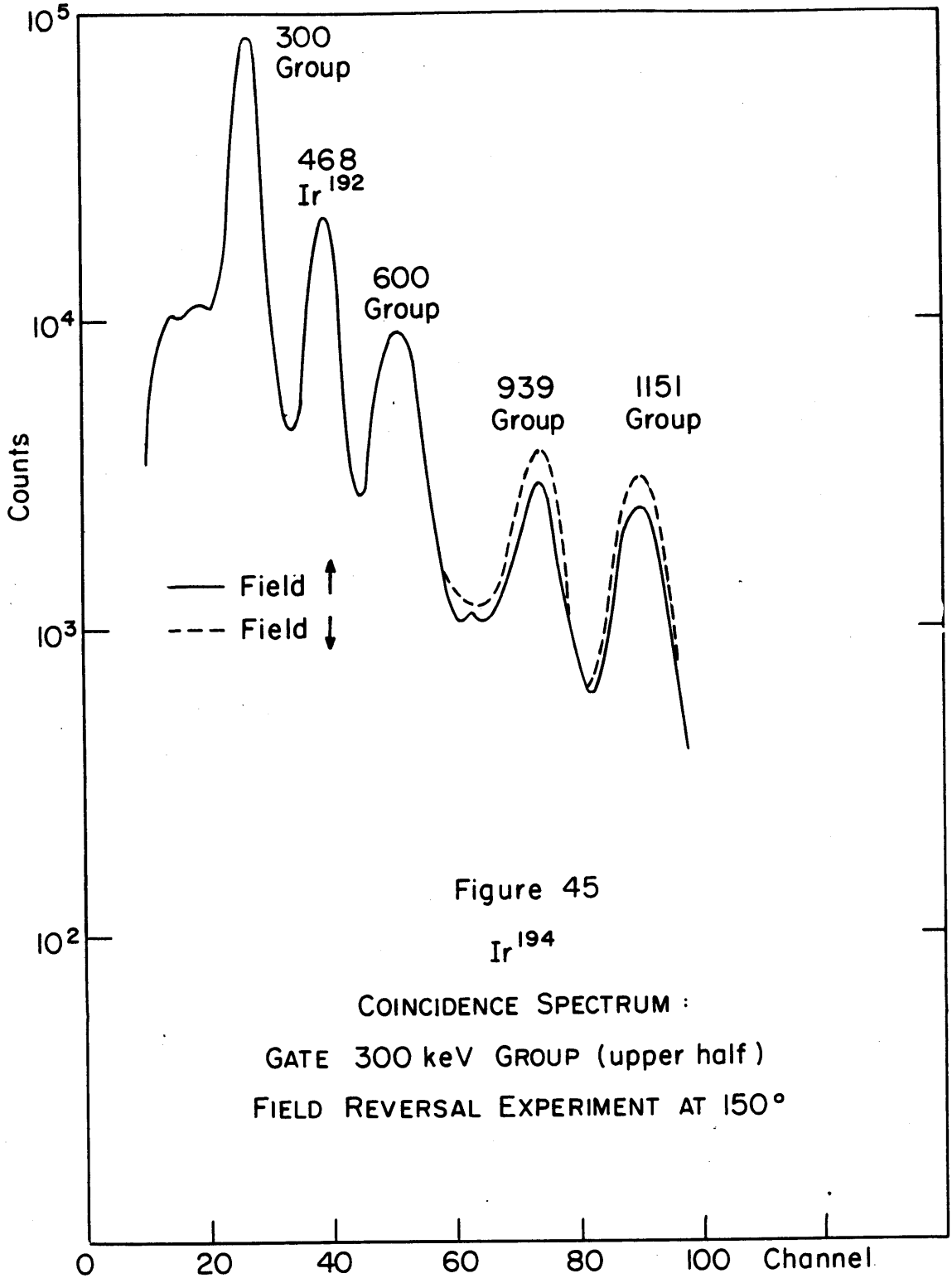

Figure 45

Ir^{194}

COINCIDENCE SPECTRUM :

GATE 300 keV GROUP (upper half)

FIELD REVERSAL EXPERIMENT AT 150°

Table 9

Angular Correlation Coefficients for the

328-939 KeV Group Correlation in Pt^{194}

	Experiment	For 2/1 Geometry G_2b_2/b_0 G_4b_4/b_0	Corrected for Solid Angle G_2A_2 G_4A_4	A_2 A_4
1	3 Angle Angular Correlation Liquid Source	-----	-----	$0.23\pm.02$ $0.81\pm.02$
2	3 Angle Angular Correlation Alloy Wire Source No Aligning Field	-----	$0.21\pm.02$ $0.79\pm.02$	$0.21\pm.02$ $0.83\pm.02$
3	4 Angle Angular Correlation Alloy Wire Source Aligning Field ↑	$0.319\pm.011$ $0.261\pm.010$	-----	-----
4	4 Angle Angular Correlation Alloy Wire Source Aligning Field ↓	$0.295\pm.011$ $0.240\pm.010$	-----	-----
5	Average of 3 and 4	$0.307\pm.008$ $0.250\pm.008$	-----	$0.25\pm.02$ $0.82\pm.02$

Theoretical Correlation Coefficients for a

Pure 0-2-0 Correlation: $A_2 = 0.357$: $A_4 = 1.143$

Table 10

Angular Correlation Coefficients for the

328-1151 KeV Group Correlation in Pt^{194}

	Experiment	For 2/1 Geometry G_2b_2/b_0 G_4b_4/b_0	Corrected for Solid Angle G_2A_2 G_4A_4	A_2 A_4
1	3 Angle Angular Correlation Liquid Source	-----	-----	$0.11\pm.02$ $0.70\pm.02$
2	3 Angle Angular Correlation Alloy Wire Source No Aligning Field	-----	$0.14\pm.02$ $0.59\pm.02$	$0.14\pm.02$ $0.63\pm.02$
3	4 Angle Angular Correlation Alloy Wire Source Aligning Field ↑	$0.224\pm.012$ $0.238\pm.012$	-----	-----
4	4 Angle Angular Correlation Alloy Wire Source Aligning Field ↓	$0.194\pm.012$ $0.213\pm.012$	-----	-----
5	Average of 3 and 4	$0.209\pm.010$ $0.226\pm.010$	-----	$0.10\pm.02$ $0.66\pm.03$

Table //

Results of Field Reversal Experiments

at 150° and 105° for the 328-939 KeV Group

and the 328-1151 KeV Group Correlations in Pt^{194}.

	Experiment	$2\left\lvert\frac{W(+)-W(-)}{W(+)+W(-)}\right\rvert$ 939 KeV Group	$2\left\lvert\frac{W(+)-W(-)}{W(+)+W(-)}\right\rvert$ 1151 KeV Group
6	Field Reversal at 150° Upper Half of "300" KeV Peak in Gate	$25.3\%\pm0.9\%$	$22.6\%\pm0.9\%$
7	Field Reversal at 150° Entire "300" KeV Peak in Gate	$25.6\%\pm1.5\%$	$20.6\%\pm1.6\%$
8	Field Reversal at 105° Upper Half of "300" KeV Peak in Gate	$12.6\%\pm1.6\%$	$13.7\%\pm1.7\%$

TABLE 12

WT for the 328 KeV Level of Pt^{194}

	Correlation Coefficients of	Field Reversal at	WT
939 KeV Group	Liquid Source	150°	.093±.006
	see Row 1, Table 9	105°	.094±.013
	Aligned Alloy Wire Source	150°	.093±.006
	see Row 5, Table 9	105°	.097±.013
1151 KeV Group	Liquid Source	150°	.099±.008
	see Row 1, Table 10	105°	.120±.017
	Aligned Alloy Wire Source	150°	.098±.008
	see Row 5, Table 10	105°	.111±.015

3. Interpretation of Results

The variation of G_2 and G_4 as a function of WT, assuming only a magnetic interaction, is plotted in Figure 30 for an aligned field, and in Figure 31 for the nonaligned case. The angular distribution experiments (Experiments 2, 3, and 4 in Tables 9 and 10) performed with aligned and non-aligned alloy wire sources yield values of A_2 and A_4 consistent with those obtained with a liquid source (Experiment 1), for WT = 0.10 ± 0.02.

The values of WT in Table 12 were calculated using the observed angular correlation coefficients (row 5 of Tables 9 and 10) and the observed field reversal effects (Table 11) without making any corrections for background. The accidentals were, however, subtracted out. The value of WT from these field reversal experiments agrees well with the above numbers.

It is obvious that there is a large background under the 939 KeV and 1151 KeV coincidence photopeaks since A_2 and A_4 are much lower than their theoretical values of 0.357 and 1.143 respectively. For the 328-939 KeV correlation, $A_2 = 0.23 \pm 0.03$ and $A_4 = 0.82 \pm 0.02$, so that $\frac{A_2(\text{EXP})}{A_2(\text{THEOR})} = 64.5\% \pm 8.4\%$ and $\frac{A_4(\text{EXP})}{A_4(\text{THEOR})} = 71.7\% \pm 1.8\%$. If the background is isotropic these two ratios are equal. (The reverse is not necessarily true.) Within the rather large error bracket they are equal so that as a first approximation we could consider the background as isotropic. If we subtract an isotropic background equal to 25% of the counting rate at 90°, $A_2(\text{EXP})$ becomes 0.320 and $A_4(\text{EXP})$ becomes 1.133. If we then subtract 25% from the denominator of the expression $\left|\frac{N(+) - N(-)}{N(+) + N(-)}\right|_{150^\circ}$ and solve for WT, we find that WT = 0.093 ± 0.007. Thus even a fairly large

unsubtracted isotropic background has little effect on the value of WT. (Possibly this is true for all correlations if the appropriate angle for observing the Field Reversal Effect is selected.) Is the background isotropic? Probably not. The background is composed of many parts. There are negligble contributions ($\sim$0.1%) to the counting rates in the 939 KeV and 1151 KeV coincidence peaks from the three lower energy peaks. In the 328 KeV gate there is about 1.5% of the "600" KeV group and roughly 3.0% of the 468 KeV peak. The 468 KeV contamination of the gate can be ignored because the 468 KeV gamma ray is not in coincidence with any gamma ray near 939 KeV or 1151 KeV. The 1.5% "600" KeV contamination of the gate causes a negligble contamination of the 939 KeV and 1151 KeV coincidence peaks because "600" KeV--"1000" KeV coincidences are extremely rare. Therefore essentially 100% of the background comes from cascades which have one gamma ray in the "300" KeV group and the other in the "1000" KeV group. Table 13 lists all such cascades and their strengths. The data for the table was obtained from the decay scheme presented in the Nuclear Data Sheets.

The second column of Table 13 tells us that the intensity of the 328-939 KeV cascade is at least 84% of the 328-939 KeV Group. When the discrimination of the gate against the 294 KeV gamma ray is taken into account (fourth column of the table) the intensity of the 328-939 KeV cascade is raised to 89% of the Group total. The background under the 939 KeV Group coincidence peak from the 1151 KeV Group is about 14% of the total; from the 1049 KeV Group the background is about 3%, and from the High Energy Group, about 8%. Using these percentages, if we take $A_2 = 0.12$ and $A_4 = 0.66$ for the 328-1151 KeV Group (Table 10), and assume the remaining background correlations are isotropic, we find $A_2 = 0.26$ and $A_4 = 0.86$ for the measured 328-939 KeV Group. These values are very close to our experimental limits. Of course the individual background correlations

TABLE 13

Contamination of the 328-939 KeV and 328-1151 KeV Correlations in Pt^{194}

Cascade	Coincidences per 100 Decays of Ir^{194}	Correlation	Number of Coincidences Adjusted for Gate of Figure	
328-939	1.42	$0 - 2^1 - 0$	1.42	
328-890	.07	$2-2^2-2^1-0$	.07	
328-925	.04	$0-2^2-2^1-0$	.04	
294-890	.07	$2 -2^2 -2^1$	.023	939 KeV Group
294-925	.04	$0 - 2^2 -2^1$	.013	
(316-885)*	(.045)	(4 - 2 - 0)	(.027)	
(316-945)*	(.006)	(? - 2 - 0)	(.004)	
328-1000	.07	$2-2^2-2^1-0$	.07	
328-1049	.07	$2-2^2-2^1-0$	.07	
294-1000	.07	$2 - 2^2 -2^1$	.023	1049 KeV Group
294-1049	.07	$2 - 2^2 -2^1$	.023	
(316-1063)*	(.004)	(3 - 2 - 0)	(.002)	
328-1151	1.61	$0 - 2^1 - 0$	1.61	
328-1104	.14	$(1,2)- 2^1 - 0$	.14	
328-1176	.12	$1-2^2-2^1-0$	.12	
328-1184	.67	$2 - 2^1 - 0$	.67	1151 KeV Group
328-1184	.06	$?-2^2-2^1-0$	.06	
294-1176	.12	$1 - 2^2 -2^1$	.04	
294-1184	.06	$? - 2^2 -2^1$	.02	
328-1219	.38	$0 - 2^1 - 0$	.38	
328-1294	.26	$2 - 2^1 - 0$	.26	HIGH ENERGY GROUP
328-1342	.11	$2 - 2^1 - 0$	.11	
328-1469	.81	$1 - 2^1 - 0$	.81	

* From the decay of Ir^{192}.

listed in Table 13 are not isotropic; however all but one (328-1219 KeV) are weaker than a 0-2-0 correlation, some are much weaker, and some will have negative A_2 or A_4. Altogether, they seem sufficient to account for the experimental values of A_2 and A_4 for the 328-939 KeV correlation.

The background under the 1151 KeV coincidence peak is definitely not isotropic: there must be a large negative A_2 term to account for the very low experimental value of $A_2 = 0.12 \pm 0.03$.

From column 4 of Table 13 we can calculate that correlations which go through only the first 2^+ state of Pt^{194} should compose about 90% of both the 939 KeV and the 1151 KeV coincidence peaks. The remaining 10% is composed of correlations going through either the second 2^+ state or both the first and second 2^+ states.

How will these impurity correlations affect our value of WT? The expression we have used to calculate WT is: (See Section III -A).

$$WT = 0.577 \left| \frac{N(+)-N(-)}{N(+)+N(-)} \right|_{150^o} \frac{b_o + \frac{1}{2}(G_2 b_2 - G_4 b_4)}{G_2 b_2 + 2G_4 b_4}$$

The term $\left[b_o + \frac{1}{2}(G_2 b_2 - G_4 b_4)\right]$ is dominated by a constant; for G_2 and G_4 equal to one, the expression may be written as $1 + 0.625A_2 + 0.023A_4$, which for a pure 0-2-0 correlation equals 1.26. We will consider several types of impurity correlations.

1. Isotropic Background

If the isotropic background is composed of individually isotropic correlations or of several non-isotropic correlations which are rotated through the same angle by a magnetic field, then WT will not be much affected by even a fairly large unsubtracted background. The reason for this is that the numerator of the above expression for WT will be only slightly decreased by the background, while $|N(+)+N(-)|_{150^o}$ will be

increased by nearly the same fraction that $(G_2b_2 + 2G_4b_4)$ is decreased. However, if the isotropic background is composed of several non-isotropic correlations which are rotated through different angles by a magnetic field, then the value of WT will be in error. If all the impurity correlations rotate in the same direction (all the rotating magnetic moments have the same sign), then the error will at worst be caused by half the background. This case can be treated in the manner of Case 3, below.

2. Non-Isotropic Background, Not Rotated by a Magnetic Field

In this case, and Case 3, let us define f, the impurity fraction, as $\frac{N(IMP)}{N(PRIMARY)}$, averaged over θ. PRIMARY refers to all coincidences which go only through the level whose g-factor we want to measure; IMP refers to all coincidences which go through other states. Obviously the error will depend on the strength of the impurity correlations; therefore let us consider two cases which for a predominantly O-2-O primary correlation are reasonable limiting cases. Firstly, if the impurity correlation has coefficients of the same magnitude and sign as the primary correlation, the fractional correction to the measured value of WT will nearly equal f, and the corrected value will be larger than the measured value. Secondly, if the impurity correlation has coefficients of the same magnitude but opposite sign as the primary, the fractional correction to WT will be again nearly f, but the corrected value will be the smaller. The variation of the nearly constant term $[b_o + \frac{1}{2}(G_2b_2 - G_4b_4)]$ will decrease the correction slightly. For impurity correlation coefficients smaller in magnitude than the primary coefficients, the corrections will be smaller in magnitude than these two extremes.

3. Non-Isotropic Background, Rotated by a Magnetic Field

We will assume that the magnetic moments of all the intermediate states have the same sign. We will also assume that WT is small so that the

precession angle, θ, varies linearly with $w\tau$. Then if the impurity correlation has coefficients of the same magnitude and sign as the primary, the correction to the measured value of $w\tau$ will be $+f\left(1-\theta_{IMP}/\theta_{PRIM}\right)$. If the impurity correlation has coefficients of the same magnitude but opposite sign as the primary, the correction to $w\tau$ will be $-f\left[1-\theta_{IMP}/\theta_{PRIM}\right]$.

This analysis applied to the cases of the 328-939 KeV and the 328-1151 KeV correlations suggests that the correction to the values of $w\tau$ in Table 12 will be small. The contamination of both correlations is about 10%. All the contaminating correlations are considerably weaker than the 0-2-0 primaries, so that the correction to $w\tau$ must be less than 10%. Those correlations which go through only the second 2^+ state will have very little effect, because $w\tau$ for the second 2^+ level is not very different from $w\tau$ for the first 2^+ level (see Table 21).

E. Pt^{194}: 622 KeV Level

1. Introduction

The level scheme of Pt^{194} produced by the decay of Ir^{194} is shown in Figure 42. Figure 43 shows the gamma ray transitions important for this work. The 0-2-0, 645-622 KeV correlation was used to measure the magnetic moment of the 2^+, 622 KeV state.

Figure 44 shows the singles spectrum of Ir^{194}. The arrows indicate the span of the "600" KeV group gate. Figure 46 shows the coincidence spectrum obtained with the gate of Figure 44. The arrows indicate the portion of the "600" KeV coincidence peak that was analyzed. Exclusive of background, this portion of the coincidence peak contained 91% 645 KeV gamma ray and 9% 622 KeV gamma ray. These percentages were determined by analyzing a peak constructed of two Cs^{137} peaks (661 KeV) of equal intensity, separated by 24 KeV, and counted in the same geometry.

All the data was taken at 2/1 Geometry. The wire sources were all 1/8" long. The average accidental to accidental plus true ratio at 180° varied between 8% and 16%; for each experiment the average ratio was known to ±15%. The Ir^{194} source strengths varied between 50μC and 100μC at the end of irradiation. No source older than 24 hours old was used. The source preparation is described in Section III-B-2; the experimental procedure in Section III-B-1. The results of the experiments are presented in Table 14. Each experiment took three days to perform. Several experiments were tried with aligned alloy wire sources; the results were inconclusive because of gain drifts.

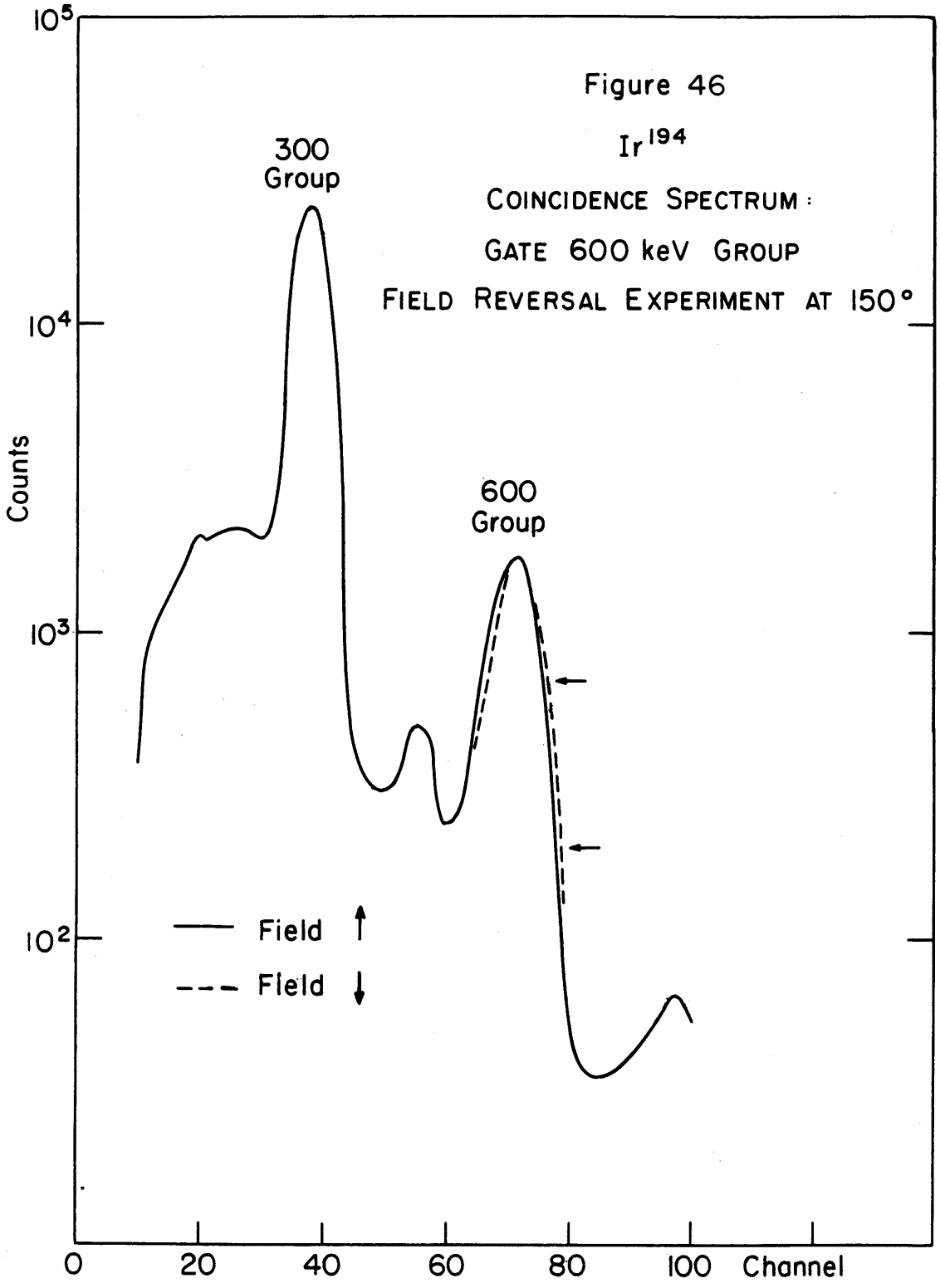
Figure 46
Ir 194
COINCIDENCE SPECTRUM:
GATE 600 keV GROUP
FIELD REVERSAL EXPERIMENT AT 150°
300 Group
600 Group
Counts
10^5
10^4
10^3
10^2
Field ↑
Field ↓
0
20
40
60
80
100
Channel

TABLE 14

Angular Correlation Coefficients for the
622-645 KeV Correlation in Pt^{194}
WT for the 622 KeV Level of Pt^{194}

	Experiment	Correlation Coefficients Corrected for Finite Solid Angle	
		G_2A_2	A_2
		G_4A_4	A_4
1	3 Angle Angular Correlation Liquid Source	----	$0.19 \pm .02$ $0.88 \pm .03$
2	3 Angle Angular Correlation Alloy Wire Source No Aligning Field	$0.27 \pm .03$ $0.84 \pm .04$	$0.27 \pm .04$ $0.88 \pm .05$

Field Reversal Effect: $2\left|\frac{N(+)-N(-)}{N(+)+N(-)}\right|_{150^\circ} = 27.3 \pm 3.7\%$

WT, using coefficients of Experiment 1 = $0.096 \pm .014$

WT, using coefficients of Experiment 2 = $0.093 \pm .015$

A_2 (THEOR) = +0.357

A_4 (THEOR) = +1.143

3. Interpretation of Results

In Figure 31, G_2 and G_4 are plotted as a function of $\omega\tau$, for a non-aligned field, assuming only a magnetic interaction. For $\omega\tau = 0.10 \pm 0.02$ the results of Experiment 2 (Table 14) using a non-aligned alloy source agree with the A_2 and A_4 found from Experiment 1, using a liquid source. The value of $\omega\tau$ obtained from the Field Reversal Experiment and the average value of the correlation coefficients agrees with the above number. The values of $\omega\tau$ in Row 4 of Table 14 were calculated using the observed values of the correlation coefficients and the observed field flip effect, without correcting for background. The accidentals were, however, subtracted out. The measured field flip effect also was corrected for the lack of resolution between the 622 KeV and 645 KeV gamma rays. The effect quoted in Table 14 contains this correction.

There must be considerable background under the "600-600" coincidence photopeak since the experimental A_2 and A_4, 0.22 ± 0.03 and 0.88 ± 0.03 respectively, are much lower than the theoretical values of 0.357 and 1.143. If we calculate $\frac{A_2(EXP)}{A_2(THEOR)}$ and $\frac{A_4(EXP)}{A_4(THEOR)}$, we find $62 \pm 8\%$ and $77 \pm 3\%$. If the background were isotropic, these two ratios would be equal. The reverse is not necessarily true.

It is difficult to account for such a large background from the decay scheme presented in the Nuclear Data Sheets. From Figure 44, we calculate that the "600" KeV Group gate contains $< 0.1\%$ "300" KeV Group, about 1.5 % 468 KeV gamma ray, and roughly 8% from higher energy gamma rays. The first is negligible, and the second is also negligible, since there are no "600"--"400" coincidences in the decay of Ir^{194}, and practically none in the decay of Ir^{192}. The third is also inconsiderable since "600"-"1000" coincidences are about 1/10 as numerous as "600"-"600" coincidences. (See Table 15). From

TABLE 15

Purity of the 645-622 KeV Correlation in Pt^{194}

Cascade	Number of Coincidences per 100 Decays of Ir^{194}	Correlation	Relative Number of Coincidences Adjusted for the Selected Span of Figure
645-622	0.49	$0\text{-}2^2\text{-}0$	0.05
622-645	0.49	$0\text{-}2^2\text{-}0$	0.49
622-589	0.027	$2\text{-}3\text{-}2^2\text{-}0$	< 0.003
589-622	0.027	$2\text{-}3\text{-}2^2\text{-}0$	< 0.003
612-589*	0.08*	4-2-0*	< 0.008*
589-612*	0.08*	4-2-0*	< 0.008*
622-811	0.001	$(1,2)\text{-}2^2\text{-}0$	--
622-890	0.016	$2\text{-}2^2\text{-}0$	--
622-925	0.009	$0\text{-}2^2\text{-}0$	--
622-1000	0.014	$2\text{-}2^2\text{-}0$	--
622-1049	0.014	$2\text{-}2^2\text{-}0$	--

* From the Decay of Ir^{192}

For a 4-2-0 Correlation: $A_2 = +0.1020$ $A_4 = +0.0091$

For a 2-2-0 Correlation: Depending on the multipolarity mixture of the first gamma ray, A_4 can have any value between 0 and +0.326, and A_2 any value between -0.315 and +0.485. See Figure 28.

For a 0-2-0 Correlation: $A_2 = +0.357$ $A_4 = +1.143$

the coincidence spectrum of Figure 46, we calculate that the "300" KeV group and the 468 KeV peak contribute insignificantly to the counting rate under the "600" KeV coincidence photopeak. From Figure 46, we also calculate that the "1000" KeV group contributes about 5% of the counts in the analyzed portion of the "600" KeV peak. Thus, the analyzed portion of the "600" KeV coincidence peak is composed of about 94% "600"-"600" coincidences, 1% "1000"(Gate)-"600" coincidences, and 5% "600"(Gate)-"1000" coincidences. From Table 15, we see that all the "600"-"1000" coincidences are 622-"1000" coincidences going through the second 2^+ state only. From Table 15 we also see that the 589-612 KeV correlation from the decay of Ir^{192} is the most important contaminating correlation in the "600"-"600" group. However, we have strongly discriminated against this correlation by choosing to count only the high side of the "600" KeV coincidence peak. In fact, all four contaminating correlations together contribute only about 5% of the counts in the analyzed portion of the "600" peak. Thus we can amass, at most, a background of about 11%. However we need at least a 23% background with $A_4=0$ to account for our experimental value of A_4. We need a 38% background with $A_2=0$, or a 19% background with $A_2=-0.357$ to account for our experimental value of A_2. We must conclude that we cannot completely account for the low values of our correlation coefficients. Our correlation coefficients are consistent with those measured by Johns and MacArthur (JM-59) for the "600"-"600" KeV correlation: $A_2=+0.10$ and $A_4=+0.71$.

In this context, it is interesting to examine several Ir^{192} and Ir^{194} singles pulse height spectra obtained with a lithium drifted germanium detector (see Figures 48-51). The Ir^{192} source was a few weeks old; the Ir^{194} source had been made only a few hours before the spectra were taken. The intensities of the Ir^{192} peaks relative to the Ir^{194} peaks in Figures 49 and

51 are about twice as great as would be predicted on the basis of the isotopic abundances, the neutron capture cross-sections, the decay schemes presented in the Nuclear Data Sheets, the half lives, and the age of the source. For example, in Figure 49, the theoretical intensities, based on the criteria just mentioned should be:

Ir^{194}	328 KeV	32 = 32
Ir^{192}	308 KeV + 316 KeV	~2 + ~6 = ~8
Ir^{194} + Ir^{192}	294 KeV + 296 KeV	6 + ~2 = ~8

However, after subtracting out suitable backgrounds from the peaks, the experimental intensities in Figure 49 are:

328 KeV	2.6
308 KeV + 316 KeV	1.4
294 KeV + 296 KeV	1.0

Similarly, in Figure 51, we find that the intensity of the Ir^{192} (589+612+604) relative to the Ir^{194} (622+645) is more than twice the predicted value. However the intensity of the 622 relative to the 645 is close to the expected value. In Figures 48 and 50 (pure Ir^{192} source), the relative intensities are about what one would predict from a consideration of the Ir^{192} decay scheme. Thus we seem to have about twice as much Ir^{192} in our Ir^{194} sources as we would expect. This helps to account for the low values of A_2 and A_4 in the "600"-"600" correlation, but it does not offer a complete explanation. The extra Ir^{192} may come from Ir^{191}(fast n, γ)Ir^{192}. However, although there are several resonances in the Ir^{191} neutron capture cross section, they do not seem high and wide enough to account for the enhancement of Ir^{192} activity.(HS-58)

How will the background affect our value of $\omega\tau$? The 622(Gate)-"1000" portion of the background should have no effect on the value of $\omega\tau$, since the only intermediate level in all those correlations is the second 2^+ state of

Pt^{194}.(Table 15). The other background correlations listed in Table 15 are all much weaker than a 0-2-0 correlation, and to first approximation they could be considered isotropic. We concluded in Section III-D-3 that even a large unsubtracted isotropic background had very little effect on the measurement of $\omega\tau$. Our value of $\omega\tau$ could be in error by about $\pm 5\%$ because of unsubtracted background correlations.

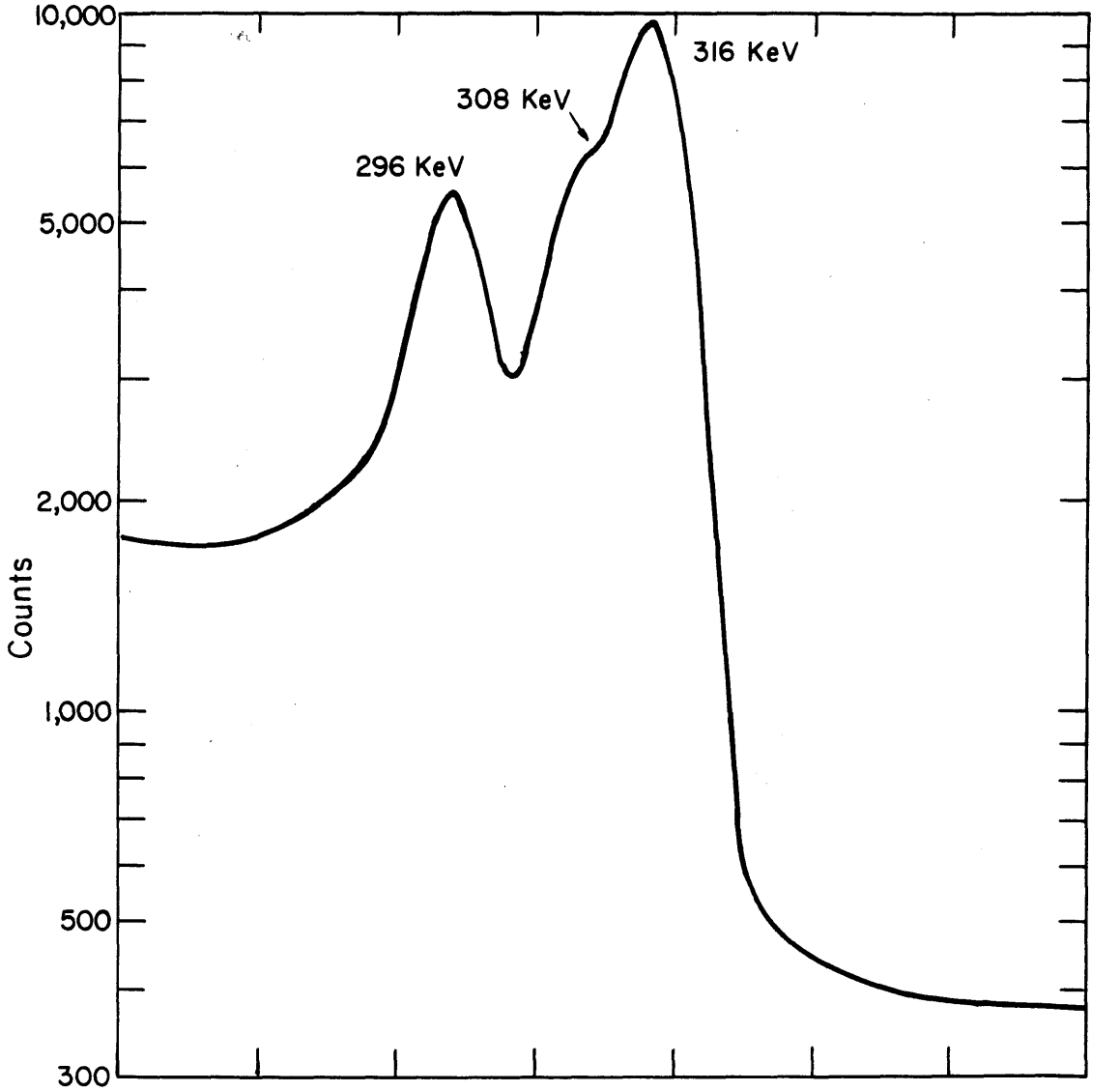

Fig. 48 Ir^{192}
Ge (Li) DETECTOR

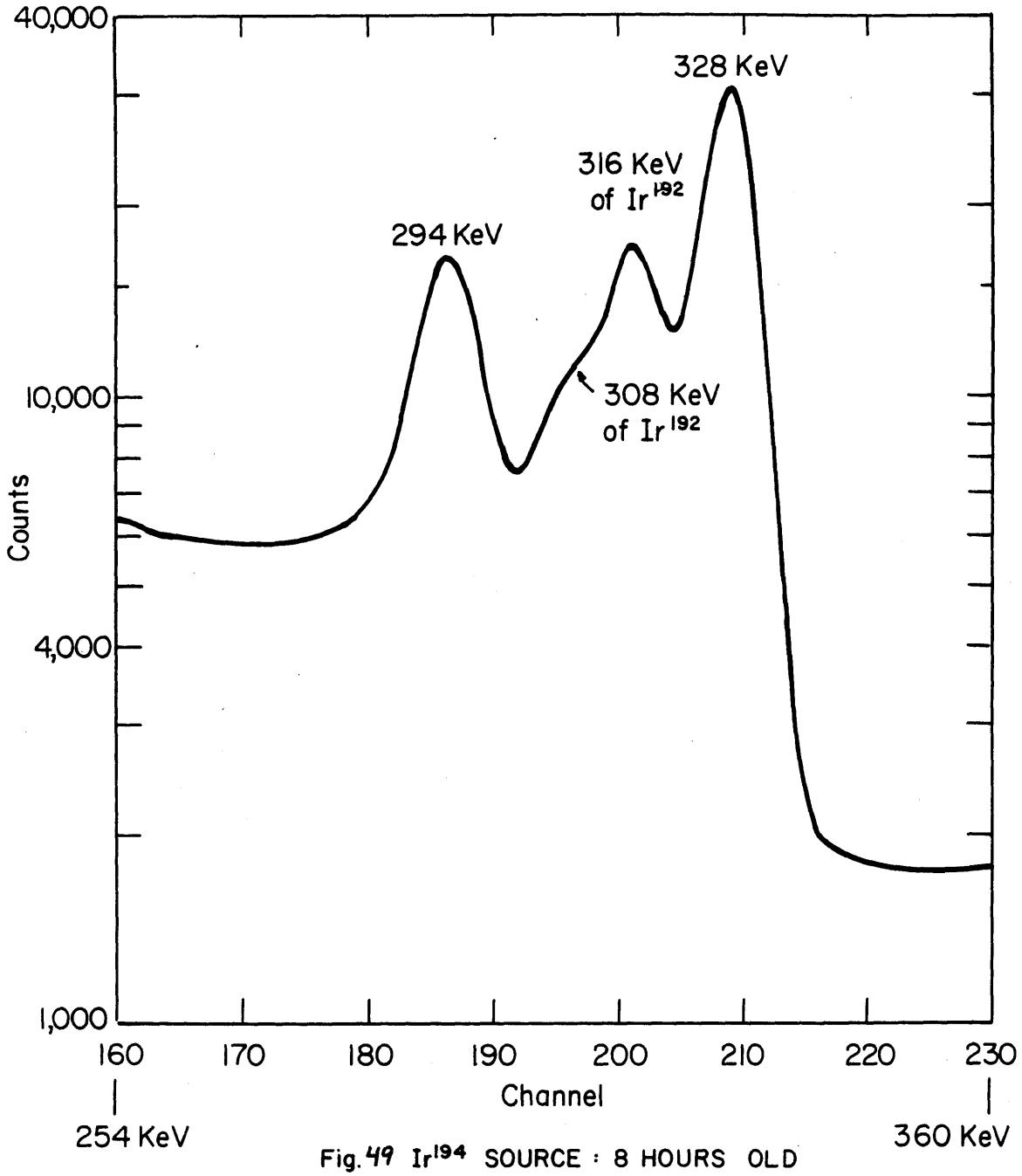

Fig. 49 Ir^{194} SOURCE : 8 HOURS OLD
Ge (Li) DETECTOR

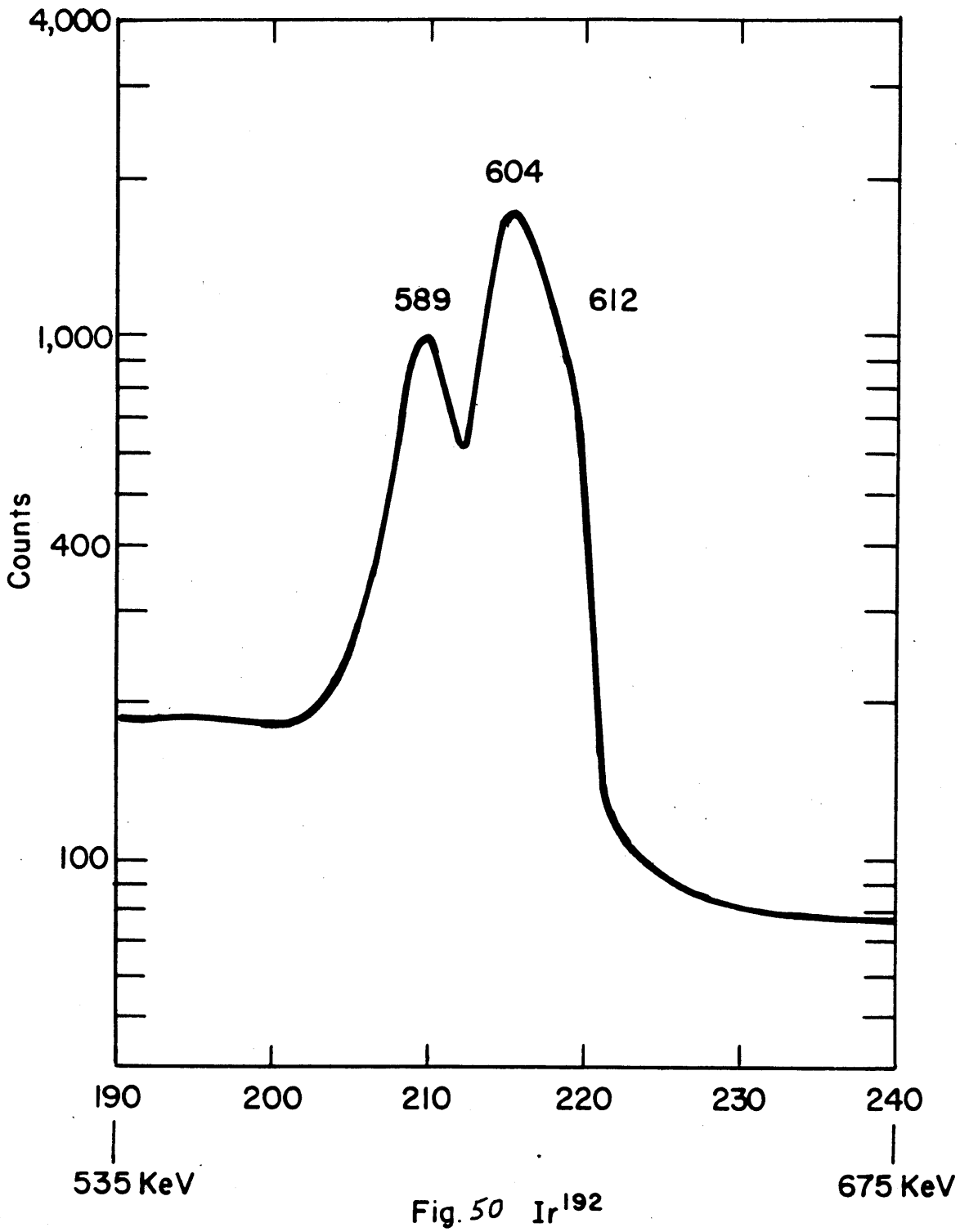

Fig. 50 Ir^{192}

Ge (Li) DETECTOR

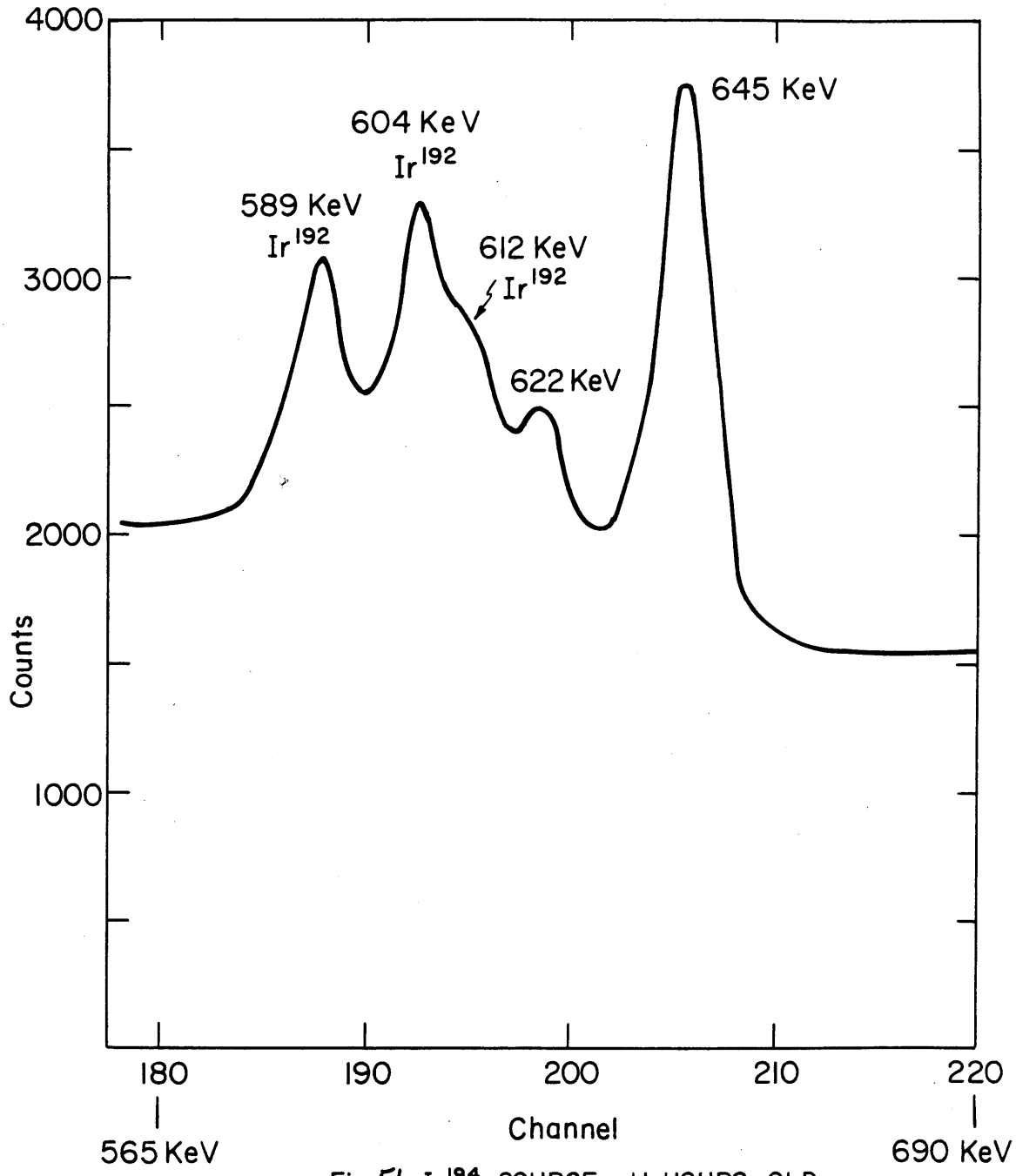

Fig. 51 Ir^{194} SOURCE : 11 HOURS OLD
Ge (Li) DETECTOR

F. Pt^{196}

1. Introduction

A partial decay scheme of Au^{196} is shown in Figure 52. Although no known level of Pt^{196} is omitted, no details of the four highest levels are shown. These levels are very weakly populated by the decay of Au^{196}. The 2-2-0, 333 KeV-356 KeV correlation was used to measure the magnetic moment of the 2^+, 356 KeV state.

The source preparation is described in Section III-B-2. The most reliable results were obtained with the Au^{196} in Fe Wire source. Figure 53 shows the singles spectrum of this source. The arrows indicate the span of the gate. Figure 54 shows the coincidence spectrum obtained with the gate of Figure 53. In order to spread the 333-356 KeV peak over a large number of channels the low energy portion of the spectrum was eliminated by raising the window threshold of the analyzer. The 333-356 KeV coincidence peak, composed of equal parts 333 KeV and 356 KeV gamma ray was analyzed in three parts: Region 1 contained 89.5%±2.0% 333 KeV gamma ray, Region 3 contained 94.5%±1.0% 356 KeV, and Region 2, 50.0%±0.5% 356 KeV gamma ray. These percentages were determined by analyzing a peak constructed of two In^{115m} peaks (335 KeV) of equal intensity separated by 23 KeV. The In^{115m} peak was obtained from the Gamma-Ray Spectrum Catalogue (H-64). The validity of using the Catalogue's "300" KeV peak was checked by comparing its Cs^{137} pulse height spectrum with ones taken by our detectors.

The results of the measurements on the Au^{196} in Fe Wire source are given in Tables 17 and 18. Data was taken at 2/1 Geometry for Counter B, and at 2.33/1 Geometry for Counter A. (See Section III-B-3 for the details of the experimental procedure.) The geometry factors then are: $Q_2 = 0.924$ and $Q_4 = 0.765$. For the measurement of A_2 and A_4 data was taken for five

days, with a source 1/16" long, of average strength 9 uC. The accidental to accidental plus true ratio was 4.0%±1.0%, measured at 180°. For measurement of the Field Reversal Effect, data was taken for three days, with a source 1/4" long, of average strength 20uC. The accidental to accidental plus true ratio was 10.0%±1.0%, measured at 150°. For Regions 1 and 3, the Field Reversal Effect is corrected for the lack of resolution; for Region 2, of course, this correction cannot be made. The results from the Au^{196} in Fe Wire (Reannealed) source are given in Table 18.

Data was also taken for the 30 at% Pt Fe-Pt Alloy source. Figure 55 shows the coincidence spectrum for this source. After subtraction of background, this coincidence peak was also analyzed in three parts. Table 18 presents the results of experiments on this source. The Geometry was 2/1 for both counters.

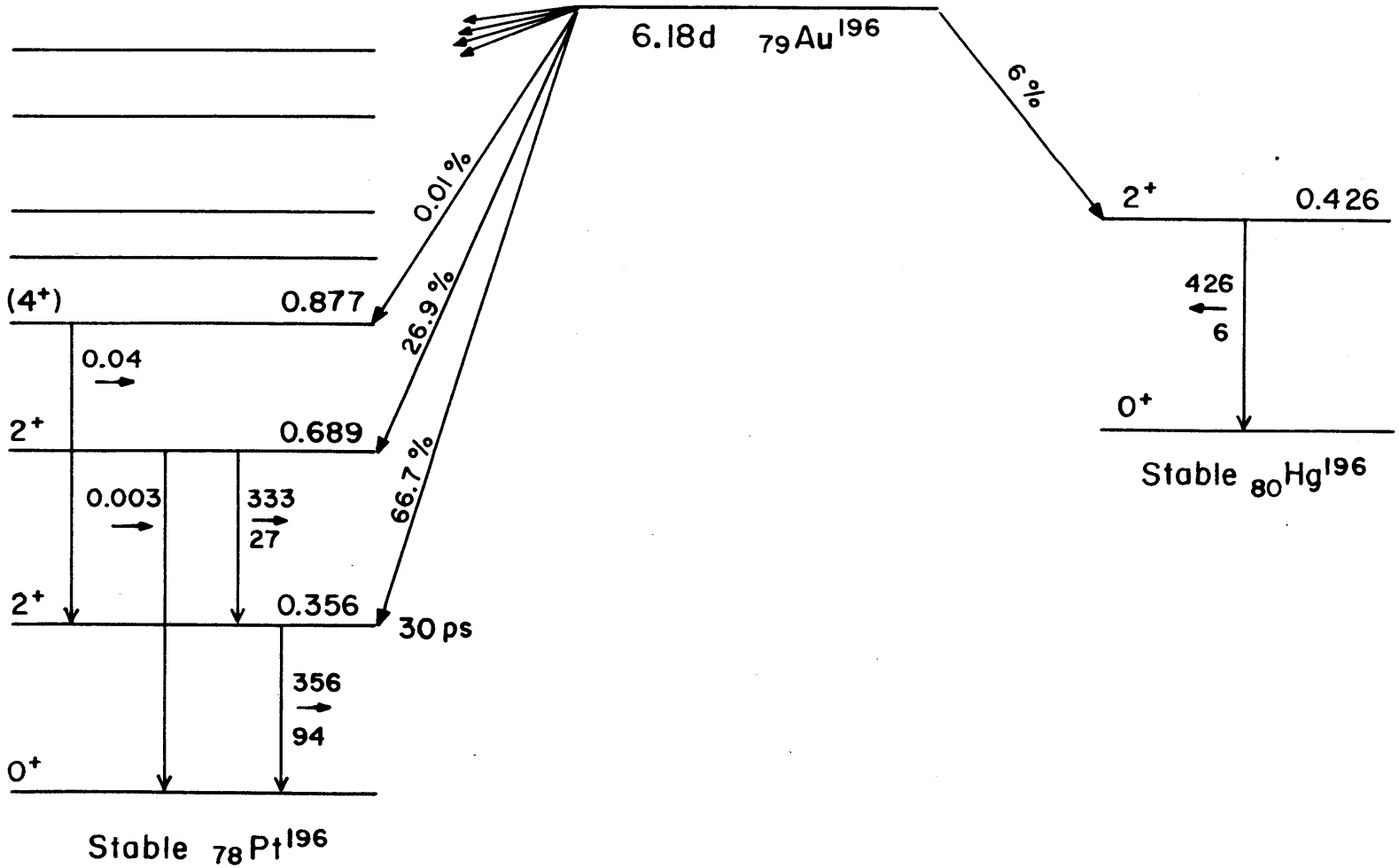

Fig. 52 DECAY SCHEME OF Au^{196} (Simplified)

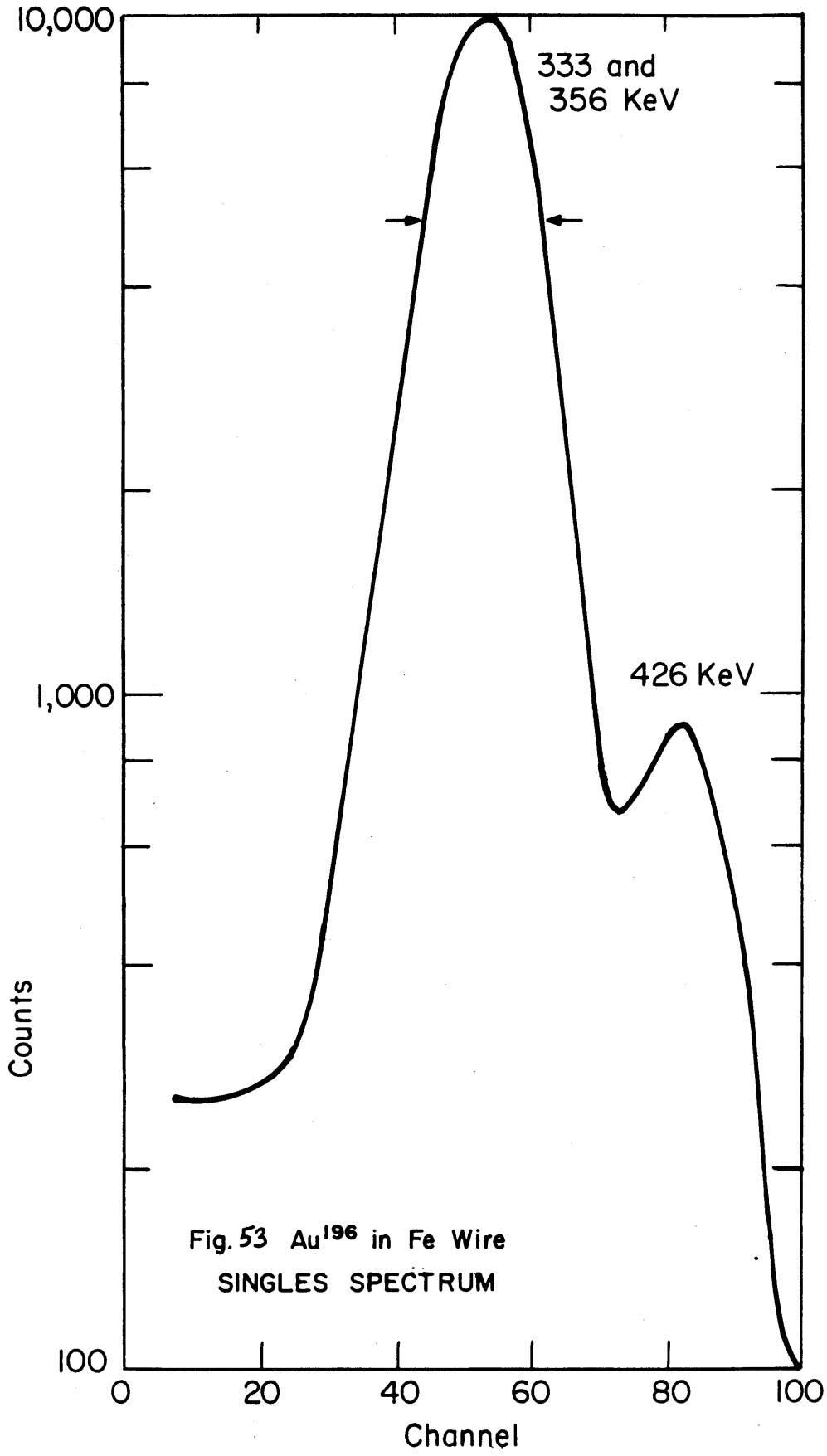

Fig. 53 Au^{196} in Fe Wire
SINGLES SPECTRUM

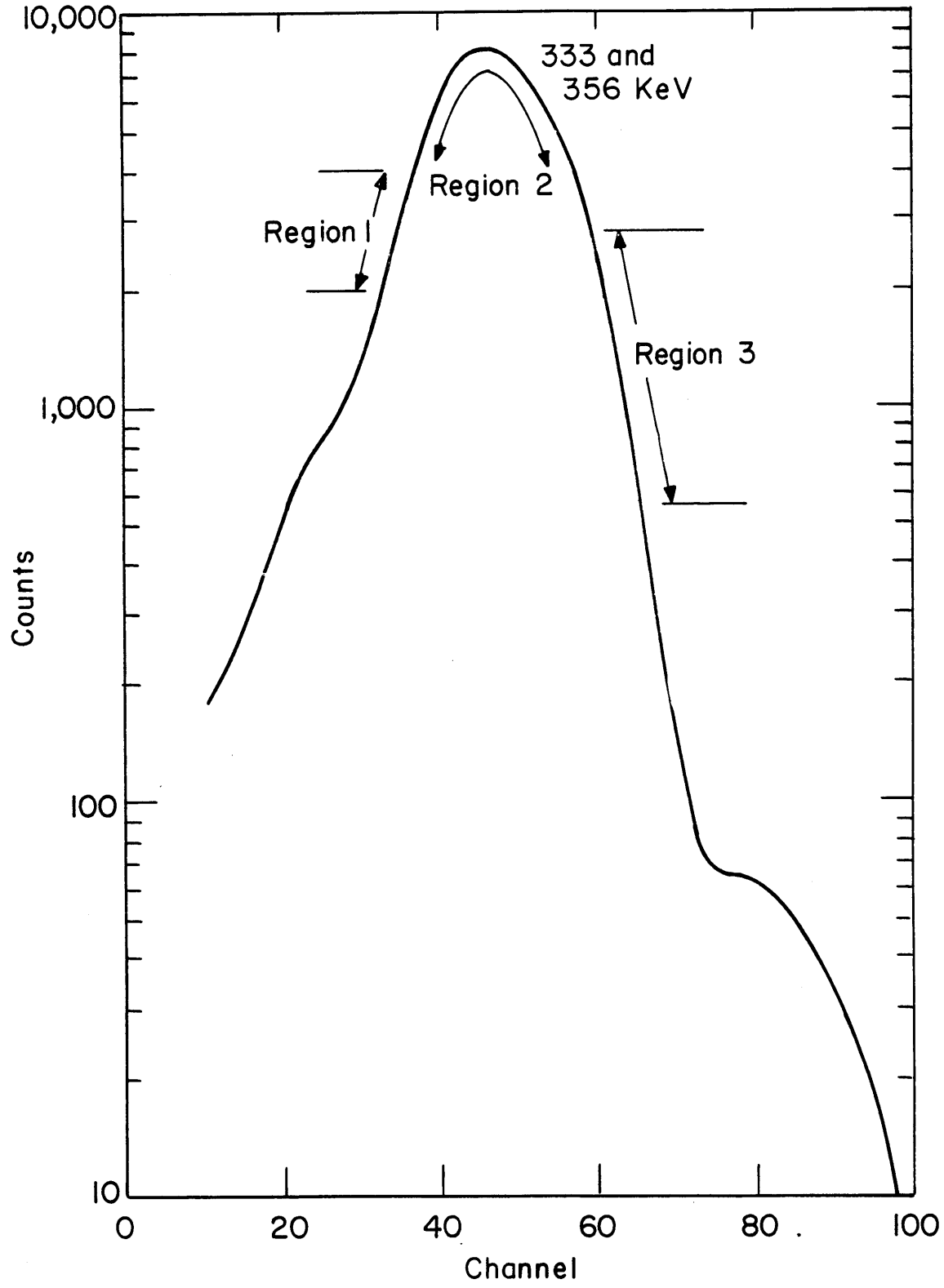

Fig. 54 Au^{196} in Fe Wire
COINCIDENCE SPECTRUM: GATE 333 and 356 KeV

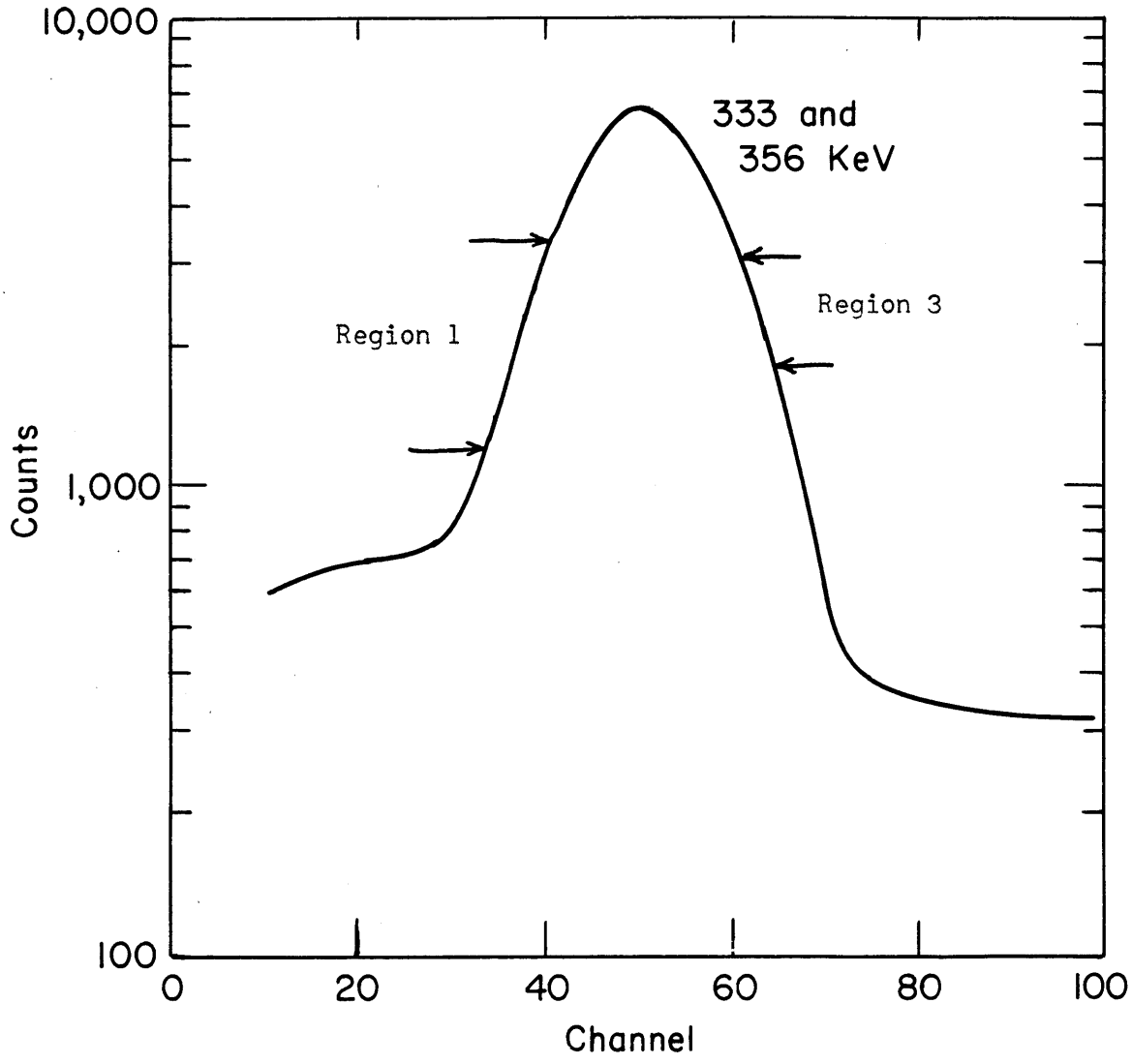

Fig. 55 Au^{196} in Fe - Pt Alloy (30 AT % Pt)
COINCIDENCE SPECTRUM : GATE 333 and 356 KeV

Table 17

Angular Correlation Coefficients for the 2-2-0, 333-356 KeV Correlation in Pt^{196}. Source: Au^{196} in Fe Wire

	Before Solid Angle Correction		After Solid Angle Correction	
	A_2	A_4	A_2	A_4
Region 1	0.052±.006	0.228±.006	0.056±.007	0.298±.008
Region 2	0.071±.002	0.243±.003	0.077±.002	0.318±.003
Region 3	0.064±.006	0.248±.006	0.069±.006	0.325± .008

Table 18

Results of Field Reversal Experiments

at 150° for the 333-356 KeV Correlation in Pt^{196}

Source	$2\left(\frac{N(+) - N(-)}{N(+) + N(-)}\right)$ in %		
	Region 1	Region 2	Region 3
Au^{196} in Fe Wire	-4.68 ± 0.65	-0.44 ± 0.17	$+4.82 \pm 0.68$
Au^{196} in Fe Wire (Reannealed)	-----	-0.36 ± 0.26	$+4.77 \pm 1.04$
Au^{196} in Fe-Pt Alloy 30 at % Pt	-9.56 ± 1.34	-1.11 ± 0.23	$+9.84 \pm 1.25$

3. Interpretation of Results

Table 19 presents the three values of g calculated from the field flip effects of the three sources (Table 18). In all three cases, the values of A_2 and A_4 from Region II in the coincidence spectrum of the Au^{196} in Fe Wire source were used. (Table 17, Row 2). Our correlation coefficients agree with those obtained by Steffen (S-53). He used a liquid Au^{196} source in dilute $AuCl_3$ and obtained $A_2 = +0.08$ and $A_4 = +0.33$.

The internal field at the platinum nucleus in the Au^{196} in Fe Wire source and the Au^{196} in Fe Wire (Reannealed) source was found by using the sources as Au^{195} Mossbauer sources after all the Au^{196} had decayed (see Section III-B-2). Figure 57 shows the Mossbauer velocity spectrum obtained with the $Au^{195,(196)}$ in Fe Wire source and a 5.6 mil platinum foil absorber. The spectra were then compared with computer simulated six line spectra. Since we know the g-factors of both the ground state (PY-51) and the 99 KeV state (Section II-D) of Pt^{195}, we could determine $H_{INT}(Pt)$ from the width of the curve. Because the resolution of the curve was zero, our value of $H_{INT}(Pt)$ has a rather large error. The reason for the low internal field in these sources is not understood. However, gold diffused in iron has an affinity for grain boundaries, and our low field may reflect such positions.

The values of g obtained with the Au^{196} in Fe Wire source and the Au^{196} in Fe Wire (Reannealed) agree within the rather large statistical errors. However, the value of g obtained with the Au^{196} in Fe-Pt Alloy source is definitely higher. The value of $H_{INT}(Pt)$ for this source is somewhat in doubt for several reasons.

Although the value of $H_{INT}(Pt)$ at $4^{o}K$ for this alloy was reliably measured as $(1.38 \pm 0.12) \times 10^6$ gauss, the Curie temperature of the alloy is

TABLE 19

$\omega\tau$ and g for the 356 KeV Level of Pt^{196}

Source	$\omega\tau$	H_{INT} (Pt) at 4° K H_{INT} (Pt) at 300° K (gauss)	g
Au^{196}		$(0.85 \pm 0.12) \times 10^6$	
	0.037 ± 0.004		0.22 ± 0.05
in Fe Wire		$(0.83 \pm 0.12) \times 10^6$	
Au^{196}		$(0.72 \pm 0.12) \times 10^6$	
in Fe Wire	0.037 ± 0.009		0.26 ± 0.08
(Reannealed)		$(0.70 \pm 0.12) \times 10^6$	
Au^{196}		$(1.38 \pm 0.12) \times 10^6$	
in Fe-Pt Alloy	0.082 ± 0.009		~ 0.32
(30% at % Pt)		$\sim 1.24 \times 10^6$	

FIG. 57

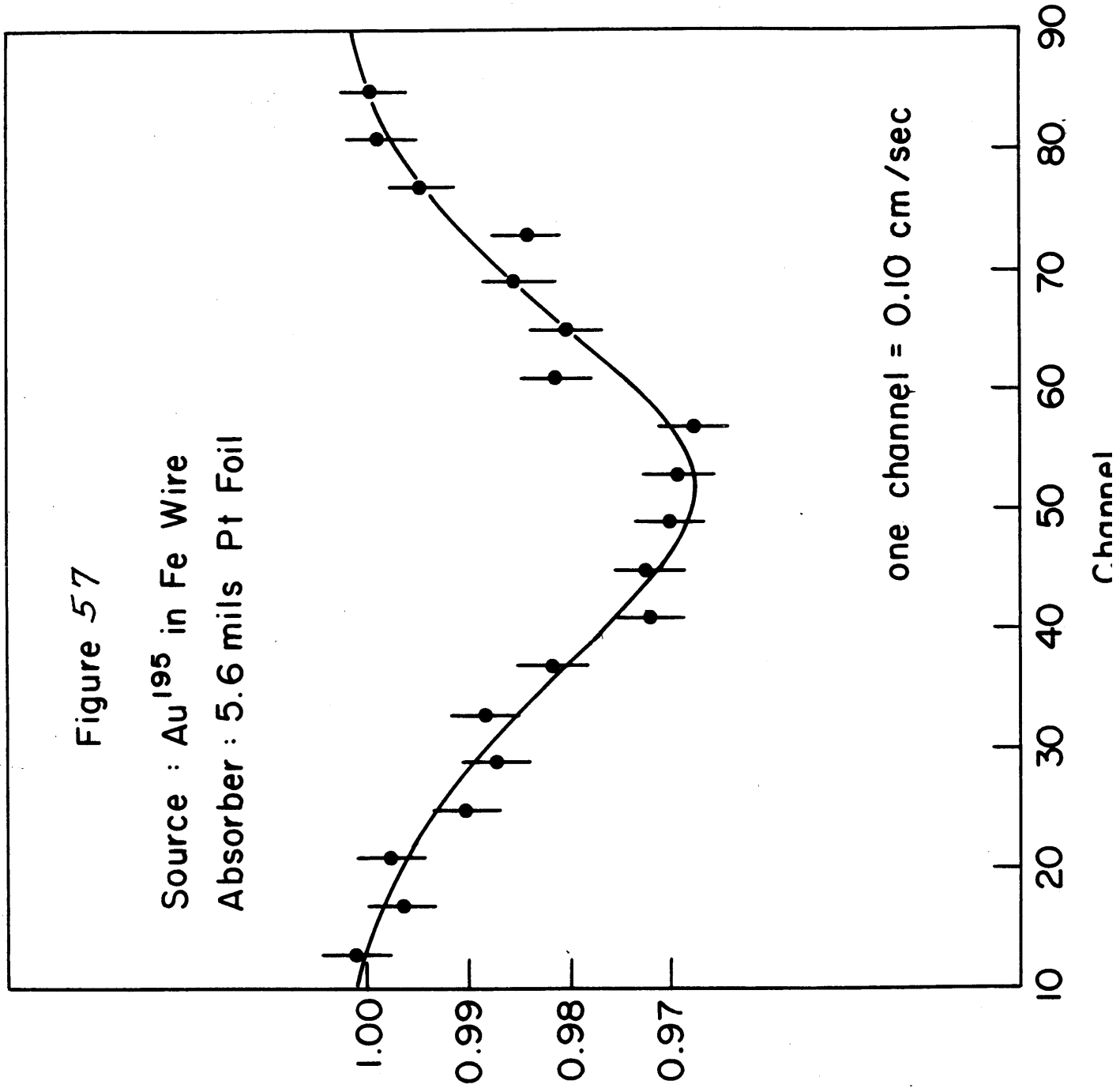
Figure 57
Source : Au^{195} in Fe Wire
Absorber : 5.6 mils Pt Foil
one channel = 0.10 cm/sec
1.00
0.99
0.98
0.97
10
20
30
40
50
60
70
80
90
Channel

in doubt. Therefore, H_{INT}(Pt) at room temperature is uncertain.

Berkowitz et al (BDFS-57) have conducted an extensive investigation into the properties of Fe-Pt alloys in the composition range 10 at% Pt to 30 at% Pt. They found that the heat treatment of the alloys drastically affected many properties of the alloys including Curie temperature and γ - α transition temperatures. A 30 at% Pt alloy, furnace cooled from 1000°C had a Curie temperature of 502°K. Our source was furnace cooled from about 900°C, and therefore could be expected to have a Curie temprature of about 500°K. For this Curie temperature, an internal field at 4°K of 1.38×10^6 gauss would reduce to 1.24×10^6 gauss at room temperature. If the Curie temperature of our sample were much higher than 500°K-if it were, in fact the 769°C of pure iron, the g-factor given by this source would still be as high as 0.30. There is another uncertainty: the phase of the 30 at% Pt alloy at room temperature after the heat treatment described above is, according to Berkowitz, entirely ordered face-centered cubic γ-phase. He did not determine at what temperature the transition to body-centered cubic α-phase took place, if in fact it did at all. The alloy remained completely γ-phase down to 78°K. Their magnetization curves for a 27.1 at% Pt alloy showed a decrease in magnetization at the γ - α transition: i.e. the magnetization decreased upon the transformation to α-phase. Moreover, it is not known how closely the behavior of H_{INT}(Pt) follows the magnetization.

If the Mossbauer experiment could have been done at liquid nitrogen temperature, or if the angular correlation experiment could have been done at liquid helium temperature, this uncertainty would not have arisen. However, the Mossbauer effect at 78°K is too small (Table 2) to detect changes in apparent splitting of the order of 0.5 cm/sec. At the time this work was done, we did not have the equipment to do angular correlation experiment at low temperatures. The magnetic behavior of low Pt Pt-Fe alloys is

simpler; below about 15 at% Pt the Curie temperatures are high, and the γ-α phase transformation takes place above room temperature. Unfortunately, Au^{196} sources made from such alloys would have too much Co^{56} background.

Because of the uncertainty in the internal field for the alloy source, our final number for the g-factor of the 356 KeV level of Pt^{196} (see Table 21) is taken from the results of the iron wire sources.

G. The Sign of $H_{INT}(Pt)$

Spehl et al (SKR-65) have determined the $g(2^+)$ value for the 328 KeV state of Pt^{194} by precessing a Coulomb excitation angular distribution with an external magnetic field. They found that $g(2^+)$ is positive. In our work we measured the precessions of the 939-328 KeV, 0-2-0 and 1151-328 KeV, 0-2-0 gamma-gamma angular correlations through this same state using the internal field at the platinum nucleus in a 3at% Ir Ir-Fe alloy wire. A small electromagnet provided a small aligning field. From Spehl's result, and our observation of the direction of rotation of the correlation pattern for a known orientation of the external aligning field, we can determine the sign of the internal field.

Frauenfelder states on page 577 of Reference S-55:

" The correlation pattern rotates in the same direction as would a magnetic dipole in the applied field, if the FIXED counter detects the FIRST gamma ray."

From the top drawing in Figure 56, we see that the fixed counter B does detect the first gamma ray. Counter A can move in the first quadrant of the x-y plane.

A compass was used to determine which pole of the electromagnet was the north pole for the switch position arbitrarily called Field "up". The north pole of a compass points towards the north, and is itself a north magnetic pole. We found (see middle drawing of Figure 56) that for the switch position Field "up" the top pole was the north pole; therefore the field applied by the electromagnet pointed down. For this switch position

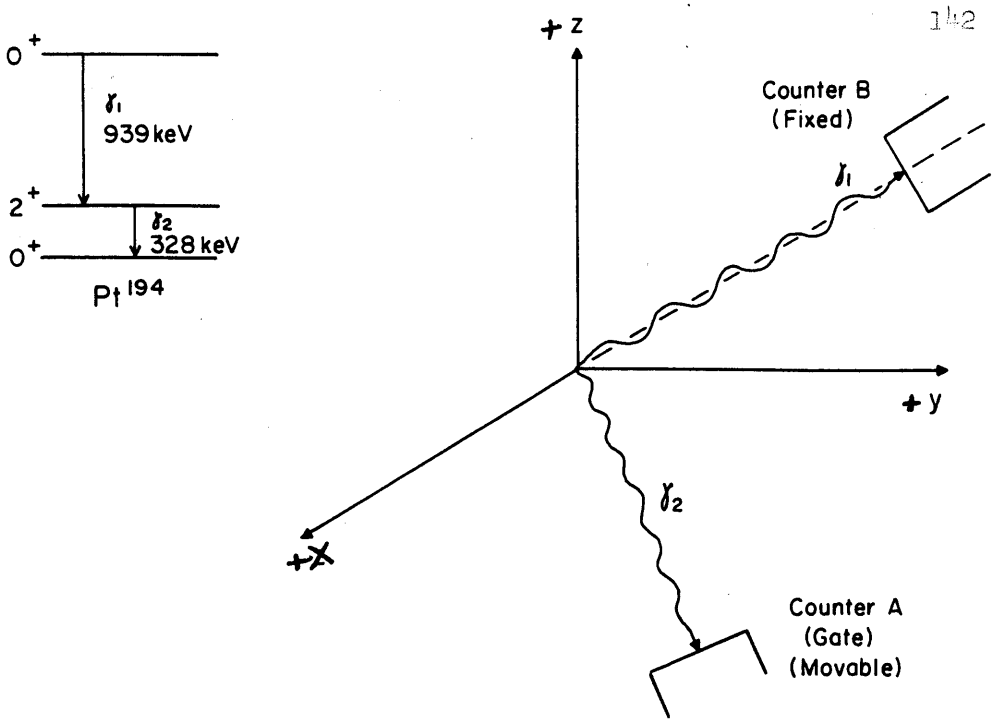

When field is "UP", there are fewer coincidences at 150°

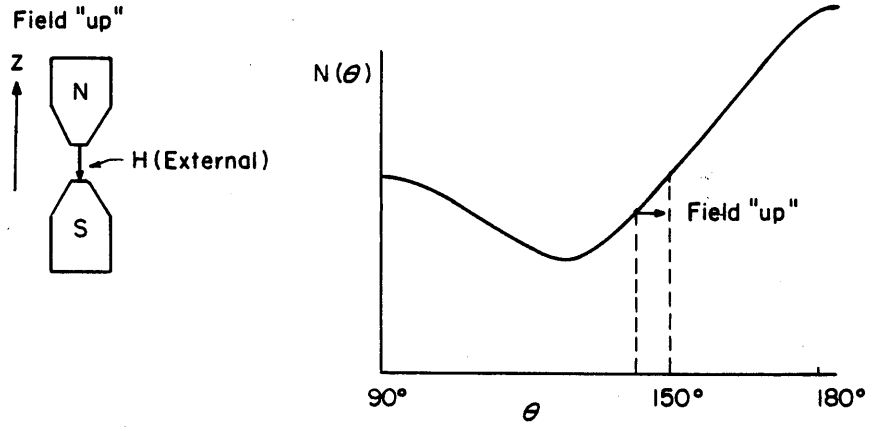

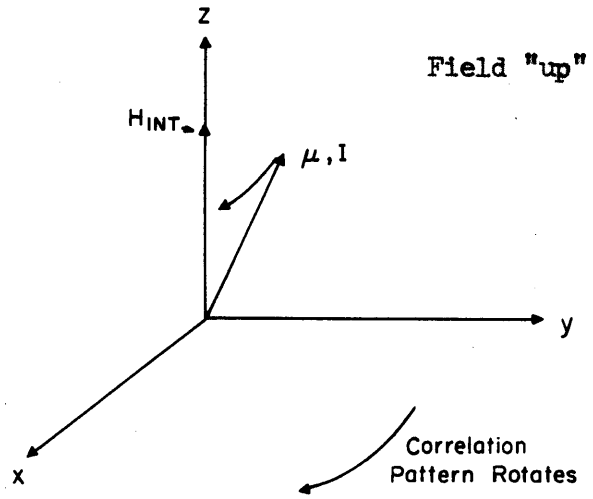

Figure 56
THE SIGN OF $g(2^+)\, H_{INT}(Pt)$

and Counter A at 150°, there were fewer coincidences. Consequently, our correlation pattern, whose shape we measured, must have rotated in the clockwise direction. If the internal field were pointing up, then a positive magnetic dipole would also rotate clockwise. Since the magnetic dipole moment of the 2^{+} state is positive, and since the aligning field was pointing down, $H_{INT}(Pt)$ is negative.

From the signs of the field flip effects, and the measured shapes of the correlation patterns, it was easily seen that all the 2^{+} moments measured in this work had the same sign.

H. Comparison of Results with Other Experimental Work

Table 20 lists the values of $w\tau$ of the 2^+ levels of Pt^{192}, Pt^{194}, and Pt^{196} measured in this work, and by two other groups. All the values for $w\tau$ for both the 2^+ states of Pt^{194} agree within experimental errors. All agree that the g-factor of the second 2^+ state is definitely smaller than the g-factor of the first 2^+ state. This result indicates that the structure of the 328 KeV and 622 KeV levels of Pt^{194} are significantly different.

Our value for $w\tau$ of the 316KeV level of Pt^{192} is much higher than that obtained by the Hungarian group (KBDP-65) and slightly higher than the number of the Indian group (ABB-66). Both these groups obtained correlation coefficients for the 468-316 KeV, 4-2-0, correlation far below the theoretical values, but our coefficients agree with theory. Both groups had large contributions from (600-300)KeV coincidences in their 468-316 KeV correlation, which they did not correct for.(see Table 8). A 4-2-0 correlation is very weak; practically any contaminating correlation not going through the 316 KeV level exclusively would affect the value of $w\tau$ measured by the 4-2-0 correlation. However, the Hungarian group's value of $w\tau$ for this level is not so easily explained.

TABLE 20*

Experimental Values of $\omega\tau$ of 2^+ Platinum Levels Obtained by Several Authors

Level	$\omega\tau$		
	This Author	(ABB-66)	(KB DP-65)
Pt^{192}: 316 KeV	0.094 ± 0.007	0.080 ± 0.005	0.063 ± 0.009
Pt^{194}: 328 KeV	0.096 ± 0.007	0.099 ± 0.009	0.0916 ± 0.0067
Pt^{194}: 622 KeV	0.089 ± 0.013	0.083 ± 0.020	0.078 ± 0.013
Pt^{196}: 356 KeV	See Table 19	-----	-----

* See Section IV

I. Effect of Quadrupole Interaction

The quadrupole interaction has been assumed to be negligble throughout this work. If the quadrupole interaction frequency

$$\hbar w_Q \doteq \frac{e^2 Qq}{4I(2I-1)}$$

is small compared to the magnetic interaction frequency

$$\hbar w_B = gHg_N$$

its main effect is to decrease the angle of rotation of the correlation by a small angle $\Delta\theta_Q$. It is shown in the Karlsson, Matthias and Siegbahn article (KMS-64), that if $w_B\tau$ is $\lesssim 0.10$, $\Delta\theta_Q$ is completely negligble for $y = w_B/w_Q$ greater than about 10. For our magnetic moments and internal field, $\hbar w_B$ is about 10^{-6} ev. For a quadrupole moment of 3×10^{-24} cm^2 and an electric field gradient of 3×10^{17} volts/cm^2, $\hbar w_Q$ is about $1/27\times10^{-6}$ ev. One would not expect an electric field gradient as large as this in a cubic alloy of low impurity content such as 3 at% Ir Ir-Fe alloy. We are therefore justified in ignoring quadrupole effects.

IV. DISCUSSION OF MAGNETIC MOMENT RESULTS

Table 21 lists all our final values of $\omega\tau$ and g. Several different models for explaining the experimental numbers are discussed.

A. Pt^{195}

The g-factor of the $3/2^-$ state in $_{78}Pt^{195}$ is far from the Schmidt limit of -1.27. We consider a particle-core coupling model which could account for the two $3/2^-, 5/2^-$ doublets at 99,129 KeV and 211,239 KeV (see Figure 10). In the simplest version of this model, the 99,129 KeV doublet would be formed by the coupling of the odd p(1/2) ground state neutron to only the first 2^+ excited core state of Pt^{194} (de-S-61); the higher doublet is ignored. This model predicts the g-factors of the $3/2^-$ and $5/2^-$ states as:

$$g(3/2^-) = 1.2(\, g_c - 0.20)$$

$$g(5/2^-) = 0.4(2g_c + 0.60)$$

where +0.60 is the magnetic moment of the ground state of Pt^{195} (PY-51) and g_c the g-factor of the first 2^+ state of Pt^{194}. However, as Figure 58 shows, the measured g-factors of the first 2^+ state of Pt^{194} and the $3/2^-$ state of Pt^{195} are far from agreeing with this prediction.

A. Gal (G-66) has recently considered the model in more realistic terms by coupling the neutron to both of the first two 2^+ excited states of Pt^{194} and adding a small mixing of single particle state. Then the Pt^{195} states would be described by a sum of three terms; the first two represent the particle-core coupling and the third gives the single particle contribution.

TABLE 21*

Final Values of $\omega\tau$ and g

H_{INT} (Pt) = (1.23±0.10) x 10^6 gauss at 300° K

Level	τ in ps	$\omega\tau$	g
Pt^{192} 316 KeV; 2^+	51 ± 4 (S-66)	0.094±0.007	0.31± 0.04
Pt^{194} 328 KeV; 2^+	51 ± 5 (SG-65) (McGS-61)	0.096±0.007	0.32± 0.05
Pt^{194} 622 KeV; 2^+	83 ± 19 (McGS-61)	0.089±0.013	0.18± 0.05
Pt^{196} 356 KeV; 2^+	43± 5 (GBH-66)	See Table 19	0.23± 0.05
Pt^{195} 99 Kev; $3/2^-$	219± 18 (This work)	------	- (0.04±0.10)

* See Section V.

Fig. 58

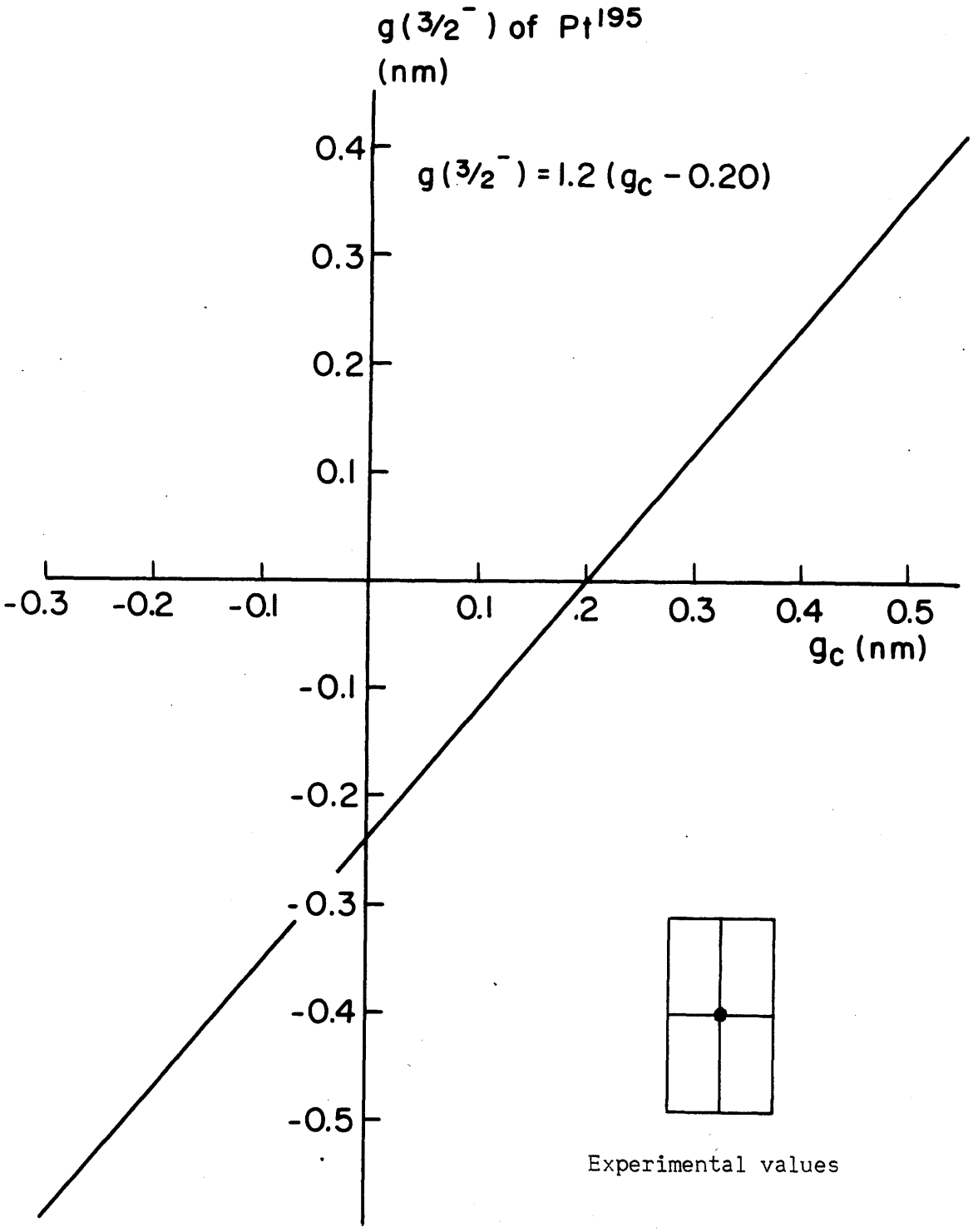
g(3/2⁻) of Pt¹⁹⁵
(nm)
g(3/2⁻) = 1.2 (gc - 0.20)
0.4
0.3
0.2
0.1
-0.1
-0.2
-0.3
-0.4
-0.5
-0.3
-0.2
-0.1
0.1
.2
0.3
0.4
0.5
gc (nm)
Experimental values

$$|J^-\rangle_E = a_E |2^+, 1/2^-; J^-\rangle + a_{E'}|2^{+'}, 1/2^-; J^-\rangle + \gamma_E|0^+, J^-; J^-\rangle$$

J and E refer to the spin and energy of the Pt^{195} state. The amplitudes a_E and γ_E are determined by the experimental values of

$$\frac{B(E2;\ J^- \longrightarrow 1/2^-)_d}{B(E2;\ 2^+ \longrightarrow 0^+)_d}$$

and $B(M1)_d$. In this approximation the g-factors become:

$$g(3/2^-) = \gamma_E^2 g_{SP}(3/2^-) + 1.2\left[a_E^2(g_c - 0.2) + a_{E'}^2(g_c' - 0.2)\right]$$

$$g(5/2^-) = \gamma_E^2 g_{SP}(5/2^-) + 0.4\left[a_E^2(2g_c + 0.6) + a_{E'}^2(2g_c' + 0.6)\right]$$

If we use Gal's choice of $B(E2;\ 2^+ \rightarrow 0^+)_d$ for Pt^{196}, $2.53\times10^{-49}\,cm^4$ (McGS-61), we get $a_E^2 = 40\%$. Substituting in $\gamma^2 = 5\%$, our experimental values of g_c and g_c', and the Schmidt limits $g_{SP}(3/2^-) = -1.27$, $g_{SP}(5/2^-) = +0.544$, we get $g(3/2^-) = -0.02$ and $g(5/2^-) = +0.44$. If we use $B(E2;\ 2^+ \rightarrow 0^+)_d$ for Pt^{194}, $3.89\times10^{-49}\,cm^4$ (McGS-61), we get $a_E^2 = 26\%$, $g(3/2^-) = -0.04$, and $g(5/2^-) = +0.42$. The predicted value of $g(3/2^-)$, -0.04, differs considerably from the measured value, $-(0.40 \pm 0.10)$, but it is an improvement over the single particle estimate of -1.27. The predicted value of $g(5/2^-)$ is close to the single particle estimate of +0.544. With our measured values of g_c and g_c', both $g(3/2^-)$ and $g(5/2^-)$ are quite insensitive to variations of a_E^2 if γ_E is kept fixed. However, $g(3/2^-)$ is sensitive to the addition of higher configurations. Gal has calculated that 5% of the $|2^+, 3/2^-; 3/2^-\rangle$ configuration would cause a change of $\Delta g(3/2^-) = |0.30|$. He could not determine the sign of the change. This contribution is an

off-diagonal term caused by the mixing of the $|2^+, 3/2^-; 3/2^-\rangle$ and $|2^+, 1/2^-; 3/2^-\rangle$ states by the magnetic moment operator.

Arima and Horie (AH-54), by configuration mixing, were able to account for the magnetic moment of the $3/2^-$ ground state of ${}_{80}Hg^{201}_{121}$ (u = -0.5567 nm). The zeroth order configuration of the Hg^{201} nucleus is:

$$\text{Protons:} \quad (1h_{\frac{11}{2}})^{12}$$
$$\text{Neutrons:} \quad (1i_{\frac{13}{2}})^{12}(3p_{3/2})^3$$

There are three configurations which contribute to the deviation of the magnetic moment from the Schmidt limit:

1. $\text{Protons:} \quad (1h_{\frac{11}{2}})^{11}(1h_{\frac{9}{2}})^1$
2. $\text{Neutrons:} \quad (1i_{\frac{13}{2}})^{11}(1i_{\frac{11}{2}})^1(3p_{3/2})^3$
3. $\text{Neutrons:} \quad (1i_{\frac{13}{2}})^{12}(3p_{3/2})^2(3p_{1/2})^1$

If the $3/2^-$, 99 KeV state of ${}_{78}Pt^{195}_{117}$ is assumed to have the configuration:

$$\text{Protons:} \quad (1h_{\frac{11}{2}})^{10}$$
$$\text{Neutrons:} \quad (1i_{\frac{13}{2}})^{8}(3p_{3/2})^3$$

the correction to the magnetic moment would be nearly the same as the Hg^{201} correction, since the coefficients of mixing depend only on A, the angular momenta, the numbers of nucleons in the configurations involved in the mixing, and constant terms. If the configuration is assumed to be:

$$\text{Protons:} \quad (1h_{\frac{11}{2}})^{10}$$
$$\text{Neutrons:} \quad (1i_{\frac{13}{2}})^{10}(3p_{3/2})^1$$

the Arima-Horie prediction would be $u(3/2^-)$ = -1.03 nm. This model fails utterly to account for the $3/2^-$ ground state of ${}_{76}Os^{189}$, u = +0.65 nm. It predicts a magnetic moment of about +0.08 nm (NAH-58).

Freed and Kisslinger (FK-61) were also able to account for the Hg^{201} magnetic moment. They assumed a pairing interaction admixing seniority one states and considered seniority three states as perturbations. The determination of the deviation of a magnetic moment from the Schmidt limit then becomes the summing of the contributions of the seniority three configurations weighted by the coefficients obtained from the pairing force calculation. Since they did not consider the details of the actual single particle states, and varied parameters smoothly, their result should be applicable to the excited state in Pt^{195}.

B. The 2^+ State of Pt^{196} and the Core Model for Au^{197}

The core-excitation model has also been applied to Au^{197}, for which Pt^{196} is the core. (Bde-S-62; de-S-65). The ground state of $_{79}Au^{197}$ is $3/2^+$. By coupling the odd d(3/2) proton of Au^{197} to the excited 2^+ core of Pt^{196}, the quadruplet of spins $1/2^+$, $3/2^+$, $5/2^+$, and $7/2^+$ is formed. From this model, one can predict the value of g_c using two essentially independent pieces of data:

1. From the magnetic moment of the ground state of Au^{197} and several M1 transition probabilities within the multiplet, g_c is calculated to be (0.64 ± 0.04). This value is far from our measured value of (0.23 ± 0.05) for the g-factor of the 2^+ state of Pt^{196}.

2. From the magnetic moment of the $1/2^+$, 77 KeV first excited state of Au^{197}, 0.37 nm, and the Schmidt g-factor of the d(3/2) proton, 0.083, g_c is calculated to be 0.41.

These two methods yield different g_c, and neither agrees very well with our experimental result. In conclusion, it seems that the successes of the

core-particle coupling model lie in predicting parameters within a multiplet, but that this model is not very accurate in accounting for magnetic moments of one isotope in terms of the parameters of the other.

C. Pt^{192}, Pt^{194}, and Pt^{196}

If we look at the g-factors of the first 2^+ states of Pt^{192}, Pt^{194}, and Pt^{196}, we see that they are far below the g = Z/A prediction of the simple hydrodynamical model of uniform charge distribution (Figure 59). Nor is the trend of the moments that which would be predicted for collective motion involving only valence particles. In this picture, the rotational gyromagnetic ratio g_R, is given by

$$g_R = \frac{I_p}{I_p + I_n} = \frac{z}{z + n}$$

where z and n are the number of protons and neutrons outside a major closed shell. In this model, the addition of two neutrons in this region of more than half-filled major shells lowers I_n and hence increases g_R : similarly the addition of two protons decreases g_R. This model is not too bad in accouting for the measured Os 2^+ moments.

If the I's are calculated assuming a stronger pairing force (G_p) for protons than for neutrons (G_n), as in the work of Nilsson and Prior (NP-60), g_R is reduced below z/z+n. This model does very well in accounting for the moments of 2^+ first excited states in the deformed region.

Kisslinger and Sorenson (KS-66) have recently calculated the g-factors of the first excited 2^+ states of many even-even isotopes. They assume a pairing force, plus a quadrupole interaction, and adjust their force parameters so that their predictions for the single particle levels of odd-A nuclei and the energies of 2^+ states of even-even nuclei agree with experiment. They use their wave functions thus obtained to calculate

Fig. 59

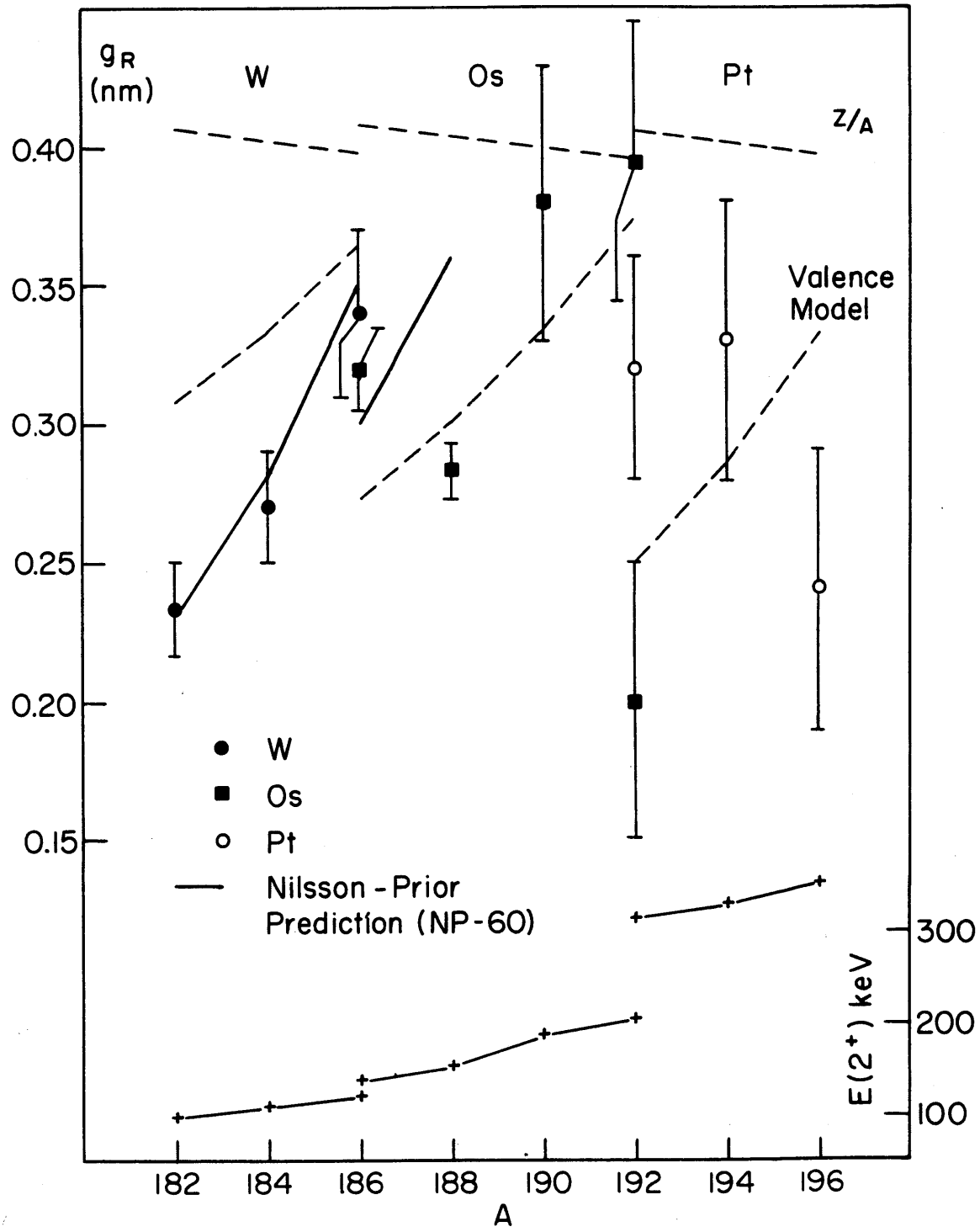
g_R (nm)
W
Os
Pt
Z/A
0.40
0.35
0.30
0.25
0.20
0.15
Valence Model
W
Os
Pt
Nilsson - Prior Prediction (NP-60)
300
200
100
E(2⁺) keV
182
184
186
188
190
192
194
196
A

B(E2)'s and magnetic moments. Their B(E2)'s agree with experiment remarkably well. They get the following g-factors for the first 2^+ excited states of the platinum isotopes:

Pt-190	g = 0.46
192	0.46
194	0.47
196	0.50
198	0.56

These g-factors are considerably higher than our experimental values.

V. ADDENDUM

After most of the thesis was typed, a more recent Ir^{194} decay scheme was brought to my attention. (MJ-65). Figures 60 and 61 present some of the additions and modifications of Macarthur and Johns to the decay scheme presented in the Nuclear Data Sheets. The decay scheme in Figure 61, although incomplete, contains all the transitions of importance in this work.

The first thing we note is that the absolute intensities of the 328, 294, 622, and 645 KeV gamma rays are down by factors of 3.3, 2.8, 2.6, and 2.3 respectively. Although recent work has also been done on the Ir^{192} decay scheme (JK-65), the intensities of the important gamma rays in the decay of Ir^{192} remain unchanged. (See Figure 39). We mentioned in Section III-E-3 that Ir^{192} and Ir^{194} pulse height spectra obtained with a lithium drifted germanium counter showed anomalously large amounts of Ir^{192} relative to Ir^{194} activity. (Figures 48-51). On the basis of this new decay scheme, the anomaly disappears.

In Section III-E-3, we were discussing the results of the 0-2-0 645-622 KeV correlation in Pt^{194}. We noted the low values of A_2 and A_4 for the correlation. If the new decay scheme is accepted, the contamination of the 622-645 KeV correlation by the 612-589 KeV correlation of Pt^{192} is increased by a factor of 2.1. This still cannot explain the low values of A_2 and A_4 because we strongly discriminate against this impurity correlation by counting only the high side of the 600-600 coincidence peak. We have analyzed the composition of the 600-600 coincidence peak by constructing a singles peak from five Cs^{137} 661 KeV peaks representing the 645, 622, 612, 604, and 589 KeV gamma rays. The relative intensities were determined from

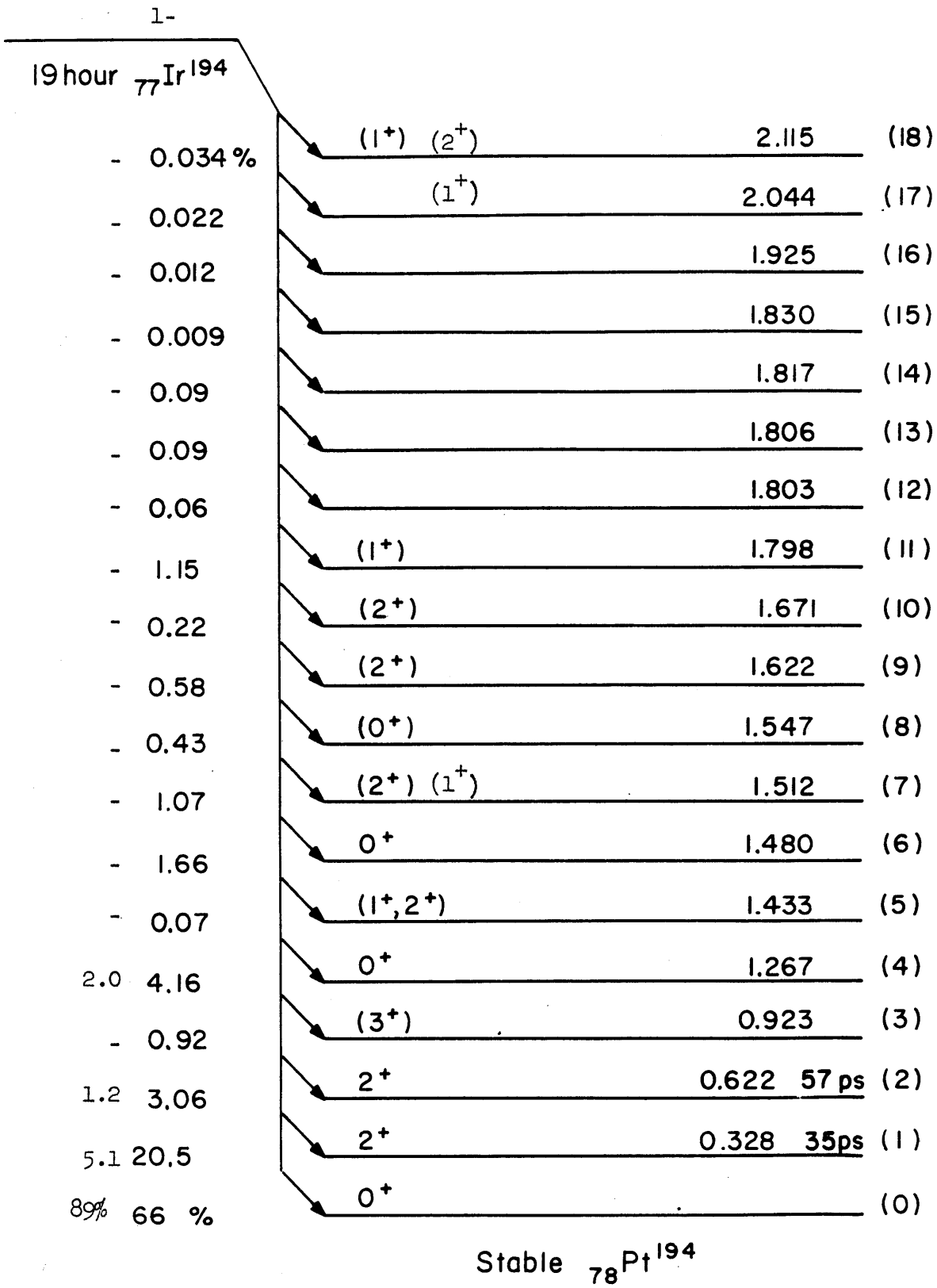

Fig. 60 LEVELS OF Pt^{194} (Fed from Ir^{194})

Inked Numbers: From Nuclear Data Sheets

Typed Numbers: MacArthur and Johns (MJ-65) modifications or additions

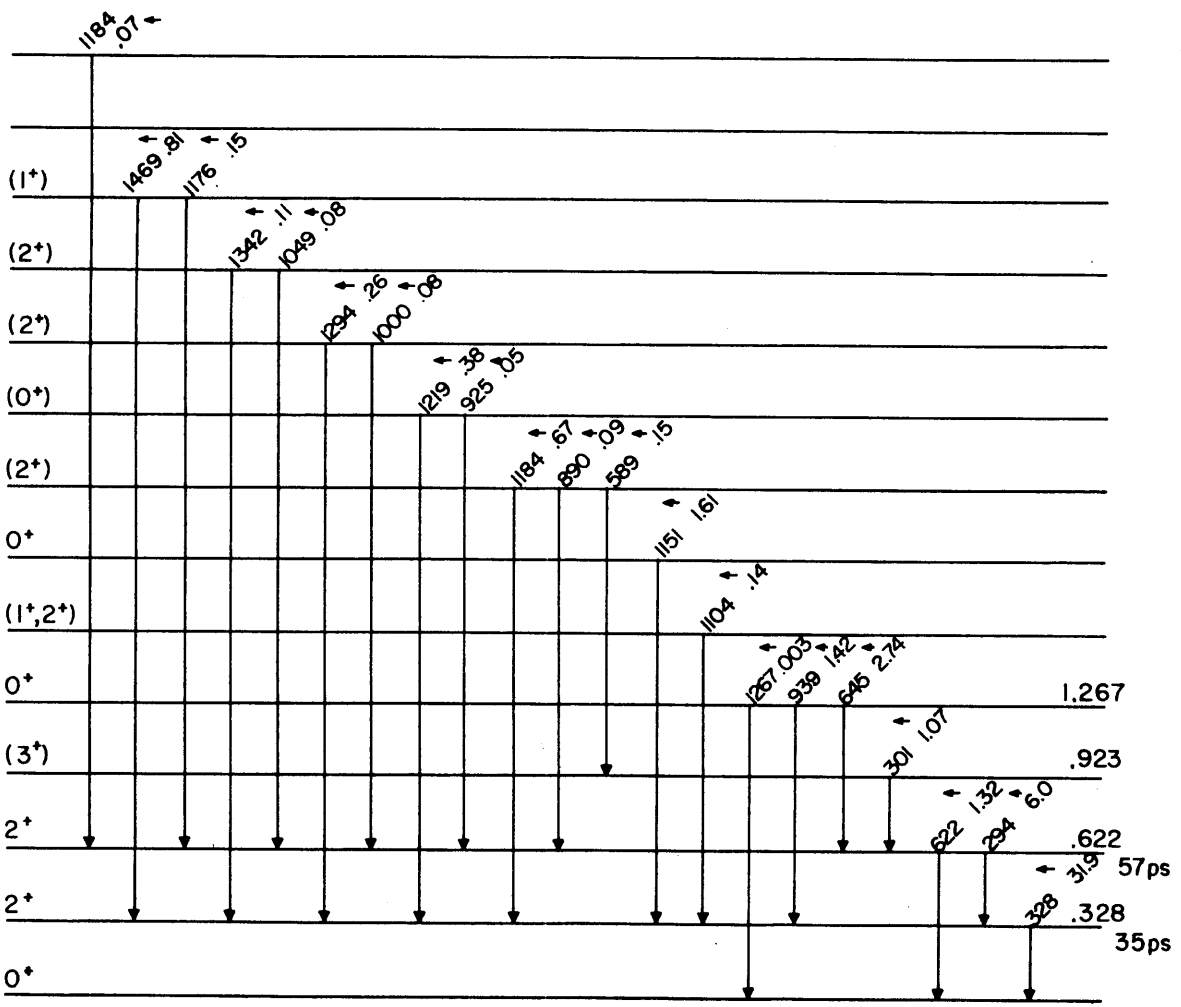

Stable $_{78}Pt^{194}$

Fig. 61 TRANSITIONS OF Pt^{194} FED FROM Ir^{194} (Incomplete)

(Transitions to Ground State from Levels ≥ 5 Omitted)

MJ-65

Modifications

Number of γ's per 100 Decays of Ir^{194}

328	9.6
294	2.1
622	0.5
301	0.4
645	1.2
939	0.85
1104	0.03
1151	0.7
890	0.07
1184	0.4
925	0.05
1219	0.08
1000	0.06
1294	0.07
1049	0.04
1342	0.03
1176	0.08
1469	0.2

the new decay schemes. We then applied the 600 gate of Figure 44 to this synthetic peak and constructed the 600-600 coincidence peak. The selected portion of the coincidence peak (Figure 46) contained 7% 622 KeV, 93% 645 KeV, and less than 1% of other $\lambda^{600\ KeV}$ gamma rays. The high background manifested in the low correlation coefficients remains a mystery.

Our value of W_T in Table 14 was calculated assuming 9% 622 KeV and 91% 645 KeV, but in the Abstract and Tables 20 and 21, the newer proportion was assumed.

In Section III-D-3, we calculated from the decay scheme and our singles and coincidence pulse height spectra that the contamination of the 939-328 and 1151-328 KeV correlations was about 10%. The new decay scheme would raise the contamination to about 15% for the 939-328, and to about 20% for the 1151-328.

REFERENCES

ABB-66 Y. K. Agawal, C. V. K. Baba, and S. K. Bhattacherfee, Nucl. Phys. 79, 437 (1966)

G-66 A. Gal, Physics Letters 20, 414 (1966)

GC-66 L. Grodzins and Y. W. Chow, Phys.Rev. 142, 86 (1966)

HP-65 J. M. Ho and N. E. Phillips, Phys. Rev. 140, A648 (1965)

S-66 Arthur Schwarzschild, Phys. Rev. 141, 1206 (1966)

BDGHP-65 A. E. Blaugrund, Y. Dar, G. Goldring, J. Hess, and I. Pleaner, Nucl. Phys. 69, 423 (1965)

BGH-65 R. Borschers, L. Grodzins, and G. B. Hagemann (To be Published)

B-K, HR-65 N. Benczer-Koller, J. R. Harris, and G. M. Rothberg, Phys. Rev. 140, B547 (1965)

de-S-65 A. de-Shalit, Physics Letters, 15, 170 (1965)

GTH-65 S. R. de Groot, H. A. Tolhoek, and W. J. Huiskamp, Chapter XIX-B in Reference S-65

H-65 & HB-KR-65 J. R. Harris, N. Benczer-Koller, and G. M. Rothberg, Phys. Rev. 137, A1101 (1965)

HRB-K-65 J. R. Harris, G. M. Rothberg, and N. Benczer-Koller, Phys. Rev. 138, B554 (1965) (Decay of Au-195: Branching Ratios from Au and)

JK-65 M. W. Johns and M. Kawamura, Nucl. Phys. 61, 385 (1965)

KBDP-65 L. Keszthelyi, I. Berkes, I. Dezsi, and L. Pocs Nucl. Phys. 71, 662

M-65 P. Mukherjee, Nucl Phys. 64, 65 (1965)

MJ-65 J. D. Macarthur and M. W. Johns, Nucl. Phys. 61, 394 (1965)

MRS-65 E. Matthias, S. S. Rosenblum, and D. A. Shirley, Phys. Rev. Lett., 14 46 (1965)

NS-65 O. B. Nielson and P. Salling (private communication)

S-65 Kai Siegbahn; Alpha- Beta- and Gamma-Ray Spectroscopy; Volume 2, Chapter XIX; North Holland Publishing Co. (1965)

SG-65 Paul H. Stelson and Lee Grodzins, Nuclear Data 1, 21 (1965)

SKR-65 H. Spehl, O. Klepper, and H. Ropke, Nucl. Phys. 63, 477 (1965)

SW-65 D. A. Shirley and G. A. Westenbarger, Phys. Rev. 138, A170 (1965)

B-64 Norman Allen Blum, High Field Mossbauer Study of Localized Magnetic Moments in Metals (National Magnet Laboratory Report NML 64-2)

GMKB-64 W. Goedbloed, E. Mastenbroek, A. Kemper and J. Block, Physica 30, 2041 (1964)

H-64 R. L. Heath, Scintillation Spectrometry, Gamma-Ray Spectrum Catalogue, 2nd Edition (Phillips Petroleum Company 1964)

HY-64

KMS-64 E. Karlsson, E. Matthias, K. Siegbahn, Perturbed Angular Correlations (North-Holland Publishing Company, 1964)

AMSS-63 K. Adler, E. Matthias, W. Schneider, and R. M. Steffen, Phys. Rev. 129, 1199 (1963)

G-63 Dwight E. Gray, Coordinating Editor; American Institute of Physics Handbook, Second Edition; Mc Graw-Hill (1963)

L-63 H. J. Lipkin, Ann. Phys. 23, 28 (1963)

PSW-63 F. M. Pipkin, J. Sanderson, and W. Wehymann, Phys. Rev. 129, 2626 (1963)

B-62 Audrey B. Buyrn, M. S. Thesis (MIT) (Unpublished) (1962)

Bde-S-62 A. Braunstein and A. de-Shalit, Physics Letters, 1, 264 (1962)

CFW-62 M. E. Caspari, S. Frankel, and G. T. Wood, Phys. Rev. 127, 1519 (1962)

KI-62,63 Yu. Kagan and Ya. Iosilevskii Zhur. Eksp I Theoret. Fig. 42, 259 (1962)/ Soviet Physics JETP 15, 182 (1962) and Ibid 44, 284 (1963) / 17, 195 (1963)

SMS-62 R. M. Steffen, E. Matthias, and W. Schneider, Tables of Directional Correlation Attenuation Coefficients for Combined Magnetic Dipole and Randomly Oriented Electric Quadrupole Interactions. USAE C. Report TID-17089. October 1962

SSW-62 Lennart Simons, Erik Spring, and Gerhard Wendt Nucl. Phys. 31, 452 (1962)

B-60 A. E. Blaugrund, Phys. Rev. Letters 3, 226 (1959)

de-S-61 A. de-Shalit, Phys. Rev. 122, 1530 (1961)

L-61 G. W. Leddicotte, The Radiochemistry of Platinum, National Academy of Sciences National Research Council, Nuclear Science Series (NAS-NS 3044), October 1961

M-61 Seymour Margulies, Technical Report No. 28, Research in Nuclear Physics at the University of Illinois under Contract ONR 1834 (05), October 1961

McGS-61 F. K. McGowan, P. H. Stelson, Phys. Rev. 122, 1274 (1961)

NP-60 S. G. Nilsson and O. Prior, Kgl Danske Videnskat. Selshab, Mat. - Fys. Medd. 32, No. 16 (1960)

JM-59 M. W. Johns and J. D. MacArthur, Can. J. Phys. 37, 1205 (1959)

McGs-59 F. K. McGorvan and P. H. Stelson, Phys. Rev. 116, 154 (1959)

AW-58 R. G. Arns and M. L. Wiedenbeck, Phys. Rev. 111, 1631 (1958)

C-58 C. F. Coleman, Nucl. Phys 5, 495 (1958)

HS-58 Donald J. Hughes and Robert B. Schwartz, Neutron Cross Sections (Commonly Called BNL 325, Second Edition) 1958

BDFS-57 A. E. Berkowitz, F. J. Donahoe, A. D. Franklin, and R. P. Steyn, Acta Metallurgica, 5, 1 (1957)

P-56 Paul M. Parker, J. Chem. Phys. 24, 1096 (1956)

S-55 Beta and Gamma-Ray Spectroscopy edited by Kai Siegbahn (North Holland 1955)

AH-54 Akito Arima and Hisashi Horie, Prog. Theor. Phys. 12, 623 (1954)

R-53

S-53 Rolf M. Steffen, Phys. Rev. 89, 665 (1953)

de-SHS-52 A. de-Shailt, O. Huber, and H. Schneider, Helv. Acta 25, 279 (1952)

PY-51 W. G. Proctor and F. C. Yu, Phys. Rev. 81, 20 (1951)

Wh-49 Geoffrey Wilkinson, Phys. Rev. 75, 1019 (1949)

Mossbauer Effect References

1. K. G. Malmfors and R. L. Mossbauer, Chapter XXI in Reference S-65

2. Third International Conference on the Mossbauer Effect reported in Reviews of Modern Physics 36, 333 (1964)

3. The Mossbauer Effect: Proceedings of the Second International Conference on the Mossbauer Effect (Wiley & Sons, 1962)

4. Hans Frauenfelder, The Mossbauer Effect, W. A. Benjamin (1962)